

Dissertation zur Erlangung des Doktorgrades
der Fakultät für Chemie und Pharmazie
der Ludwig-Maximilians-Universität München

Herpesvirus Capsid Dynamics in Living Cells



Jens-Bernhard Bosse
(geb. Lösing)

aus

Vreden

2011

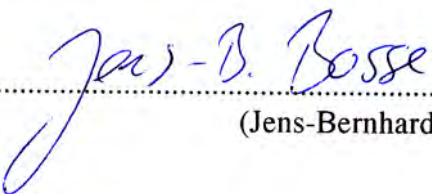
Erklärung

Diese Dissertation wurde im Sinne von §13 Abs. 3 bzw. 4 der Promotionsordnung vom 29. Januar 1998 (in der Fassung der sechsten Änderungssatzung vom 16. August 2010) von Herrn Prof. Koszinowski betreut und von Herrn Prof. Beckmann von der Fakultät für Chemie und Pharmazie vertreten.

Ehrenwörtliche Versicherung

Diese Dissertation wurde selbständig, ohne unerlaubte Hilfe erarbeitet.

München, 11.08.2011


.....
(Jens-Bernhard Bosse)

Dissertation eingereicht am:	11.08.2011
1. Gutachter:	Prof. Beckmann
2. Gutachter:	Prof. Koszinowski
Tag der mündlichen Prüfung:	14.09.2011

Für meinen Großvater

Contents

1	Introduction.....	1
1.1	Light Microscopy.....	1
1.1.1	Light microscopy and the invention of microbiology	1
1.1.2	History of light microscopes	1
1.1.3	Optical resolution	2
1.1.4	The discovery of fluorescence.....	3
1.1.5	The quest for contrast.....	4
1.1.6	The advent of fluorescence microscopy	4
1.1.7	The discovery of green fluorescent protein	5
1.1.8	Basic structure of modern fluorescence microscopes.....	6
1.1.9	Fluorescence live cell imaging	8
1.2	Diffusion theory and single particle tracking	9
1.2.1	Cellular transport processes.....	9
1.2.2	Methods to study particle mobility in a cellular environment.....	9
1.2.3	Determination of particle positions in SPT	10
1.2.4	The mean square displacement as a measure of particle behavior	10
1.3	Herpesviruses.....	11
1.3.1	The Order Herpesvirales	11
1.3.2	General structure of herpesvirus particles	12
1.3.3	The herpesvirus lifecycle.....	13
1.3.4	Entry of herpesviruses	13
1.3.5	Viral gene expression cascade.....	14
1.3.6	Nuclear steps of morphogenesis.....	15
1.3.7	Cytoplasmic steps of morphogenesis	16
1.3.8	Herpesvirus capsids.....	16
1.4	Murine models of human beta and gamma-herpesviruses.....	17
1.4.1	MCMV as an animal model for HCMV pathogenesis	17
1.4.2	Murine gamma-herpesvirus 68 as model for EBV and KSHV pathogenesis.....	18
1.4.3	Fluorescent herpesvirus particles uncover the dynamics of herpesvirus morphogenesis.	19
1.5	Aims of this thesis	20
2	Materials and Methods.....	22
2.1	Cells and viruses	22
2.2	Analysis of viral growth in vitro.....	23
2.3	Measurement of plaque sizes.....	23
2.4	Plasmid construction.....	23

2.5	Construction of recombinant MCMV and MHV-68 BACs.....	25
2.6	Yeast two hybrid analysis.....	26
2.7	Density gradient purification of virus particles	26
2.8	Analytical polymerase chain reactions (PCRs)	27
2.9	Immunoblotting	27
2.10	Immobilization of virions on glass coverslips	28
2.11	Immunostaining for microscopy.....	29
2.12	Fluorescence microscopy.....	29
2.13	Single Particle Tracking	30
2.14	Transmission electron microscopy	31
3	Results	32
3.1	Construction of capsid-tagged fluorescent beta- and gamma-herpesviruses	32
3.1.1	Construction of capsid-tagged MCMV recombinant	32
3.1.2	Reconstitution and basic characterization of recombinant MCMVs.....	34
3.1.3	Construction of fluorescent, capsid-tagged MHV-68 recombinants.....	36
3.1.4	Reconstitution and basic characterization of recombinant MHV-68s.....	39
3.2	Characterization of Labeled Particles	40
3.3	MCMV S-GFP-SCP interacts with MCP	44
3.4	Assessment of the genetic stability of capsid-tagged recombinant viruses	46
3.4.1	MCMV S-GFP-SCP and S-HA-SCP labeled virus mutants are genetically stable.....	46
3.4.2	MHV-68-D2-ORF65-FP viruses express less SCP-FP isoforms	47
3.4.3	MHV-68 capsid-tagged viruses are not stable over extended passages	48
3.5	Normal morphogenesis of S-FP-SCP tagged recombinant MCMV	49
3.6	MCMV and MHV-68 fluorescent capsids are transmitted between cells	50
3.7	Labeled MHV-68 particles can be visualized throughout the infection cycle.....	52
3.8	Labeled MCMV capsids allow insights into beta-herpesvirus entry	54
3.9	Quantification of cytoplasmic movement paths in herpesvirus egress.....	56
4	Discussion.....	61
5	Primer Sequences.....	70
6	List of Abbreviations	71
7	References.....	73
8	List of Figures and Tables.....	80
9	Danksagung	81
10	Curriculum Vitae	84

Summary

Herpesviruses are clinically and economically important pathogens that establish life-long persistence in their animal or human hosts. Despite considerable efforts, up to now vaccines which protect against disease are not available, emphasizing the central role of antiviral chemotherapy in the control of herpesvirus infections. However, most approved anti-herpesvirus drugs target solely viral genome replication. These drugs are often associated with considerable side effects and cross-resistant strains can occur under therapy. Therefore, the comparative study of herpesvirus morphogenesis is important to define new common drug targets for herpesviruses.

One of the least understood aspects of viral morphogenesis are the dynamics of viral particle transport. Trafficking during infection is studied best by fluorescently labeled virus particles in combination with live cell fluorescence microscopy. In recent years, recombinant viruses which express fusions of structural proteins to fluorescent proteins (FPs) widely extended our understanding of virus morphogenesis. However, studies on beta- and gamma-herpesviruses by this method were limited. This was due to the lack of replication competent, capsid-tagged fluorescent virus mutants representing these subfamilies.

This thesis reports on the construction and characterization of viable recombinants of Murine Cytomegalovirus (MCMV) and Murine Gamma-Herpesvirus 68 (MHV-68) carrying ectopic insertions of the small capsid protein (SCP) fused to FPs.

To tag SCPs, their coding sequences were first rated as either conserved or variable domains by sequence alignments. Then the fluorescent proteins were inserted into variable linker sequences flanking conserved domains. Subsequently, the new fusion constructs were inserted ectopically as a second copy into the viral genomes in the presence of the wild type (WT) SCP allele and viruses were reconstituted. This way, inhibitory or dominant negative properties of the fusion proteins could be assessed. Most resulting recombinant viruses replicated with WT kinetics in cell culture. Their bright fluorescence allowed studies on particle dynamics by live cell microscopy including single particle tracking during entry and egress with high spatial as well as temporal resolution.

In summary, Virus recombinants described here will enable the comparative study of alpha-, beta- and gamma-virus capsid dynamics throughout herpesvirus morphogenesis.

Zusammenfassung

Herpesviren sind bedeutende humane Pathogene, die eine lebenslange Persistenz in ihren Wirten induzieren. Trotz vieler Versuche ist es bisher nicht gelungen, Impfstoffe zu entwickeln. Aus diesem Grund sind anti-herpesvirale Wirkstoffe umso wichtiger. Jedoch haben die meisten zugelassenen Wirkstoffe die virale Genom-Replikation als Ziel. Diese Beschränkung auf eine Funktion im Replikationszyklus erleichtert das Auftreten von kreuz-resistenten Stämmen bei länger dauernder Therapie. Darüber hinaus ruft diese Klasse von Inhibitoren erhebliche Nebenwirkungen hervor. Um neue Wirkstoffziele aufzudecken, sind vergleichende Studien über generelle Prinzipien der Herpesvirus-Morphogenese wichtig.

Die Prinzipien Viruspartikel-Transportes gehören zu den bisher weniger verstandenen Aspekten der Herpesvirus-Morphogenese. Diese dynamischen Prozesse lassen sich am besten mit Hilfe der Fluoreszenzmikroskopie in lebenden Zellen verfolgen und analysieren. In den letzten Jahren haben rekombinante Viren, die für Fusionen zwischen Strukturproteinen und fluoreszierenden Proteinen kodieren, unser Verständnis für die dynamischen Prozesse der Morphogenese stark erweitert.

Jedoch konnten bisher im Gegensatz zu den alpha-Herpesviren, beta- und gamma-Herpesviren kaum mit dieser Methode analysiert werden. Dies ist vor allem dem Fehlen replikations-kompetenter, Kapsid-markierter, fluoreszierender Virusmutanten in diesen Sub-Familien zuzuschreiben.

Diese Arbeit beschreibt die Konstruktion, Charakterisierung und Anwendung von fluoreszenzmarkierten Mutanten des Murinen Cytomegalovirus (MCMV) und des Murinen Gammaherpesvirus 68 (MHV-68), die ektopische Insertionen des kleinen Kapsidproteins (SCP) fusioniert zu verschiedenen Fluoreszenzproteinen (FPs) tragen.

Um lebensfähige SCP-FP-tragende Mutanten zu konstruieren, wurde ein mehrstufiges Mutageneseverfahren entwickelt. Zuerst wurden potentiell konservierte Proteindomänen mit Hilfe von multiplen Aminosäureabgleichen definiert. Die Gene der FPs wurden dann in potentielle Verknüpfungssequenzen zwischen konservierten Domänen eingefügt. Daraufhin wurden die Fusionssequenzen ektopisch in die viralen Genome eingefügt. Dies hatte zur Folge, dass funktionsbestimmende SCP Sequenzen nicht unterbrochen wurden. Dabei konnten die Fusionsproteine auf etwaige hemmende oder dominant-negative Eigenschaften untersucht werden. Die resultierenden Virusmutanten wuchsen mit Wildtyp-Kinetik in Zellkultur und helle Fluoreszenzsignale konnten sowohl in infizierten Zellen, als auch in aufgereinigten Viruspräparationen nachgewiesen werden. Diese rekombinanten Viren eigneten sich dazu, orientierte Partikelbewegungen mit hoher zeitlicher Auflösung aufzunehmen und per *single particle tracking* räumlich zu beschreiben.

Die hier beschriebenen Virusmutanten ermöglichen zum ersten Mal vergleichende Studien zur alpha-, beta- und gamma-Herpesvirus Kapsid-Dynamik.

1 Introduction

1.1 Light Microscopy

1.1.1 Light microscopy and the invention of microbiology

The term microscope comes from the Greek words μικρός, mikrós, "small" and σκοπεῖν, skopeîn, "to look" or "see". Therefore, a microscope is literally an apparatus to see small things.

The first (light-) microscopes were built in the 16th century, however it took until the last quarter of the 17th century that microscopes were used in biomedical research. A huge impact had the work of Antoni van Leeuwenhook. He reported on the discovery of protists in 1674 and bacteria in 1676 (40). He therefore became the founder of microbiology, the science dealing with "unseen life on earth" (undertitle of *This week in Microbiology*, a podcast by Prof. Vincent Racaniello). Since then, microbiology and microscopy are strongly connected.

1.1.2 History of light microscopes

Antoni van Leeuwenhook mostly used very simple microscopes consisting of just one lens that were more similar to magnifying glasses. His skill in grinding lenses as well as his good eyesight enabled him to build and use some lenses with 200 fold magnification. However, compound microscopes that consist of more than one lens were already known at that time and, for example, used by Robert Hooke. The disadvantage of this early compound microscopes was their strong chromatic aberration, an effect that is caused by the failure of a lens to focus all colors to the same convergence point. This problem resulted in a drastic decrease in resolution. Therefore, higher magnifying lens combinations could not be used and the microscopes, for example used by Robert Hooke, did not magnify more than 20-30 times. This physical problem was solved in the 1730s by Chester More Hall with the invention of achromatic lenses that employed different types of glass to realign the different wavelengths. However, it took until 1827 when Giovanni Battista Amici introduced the first achromatic microscope (85).

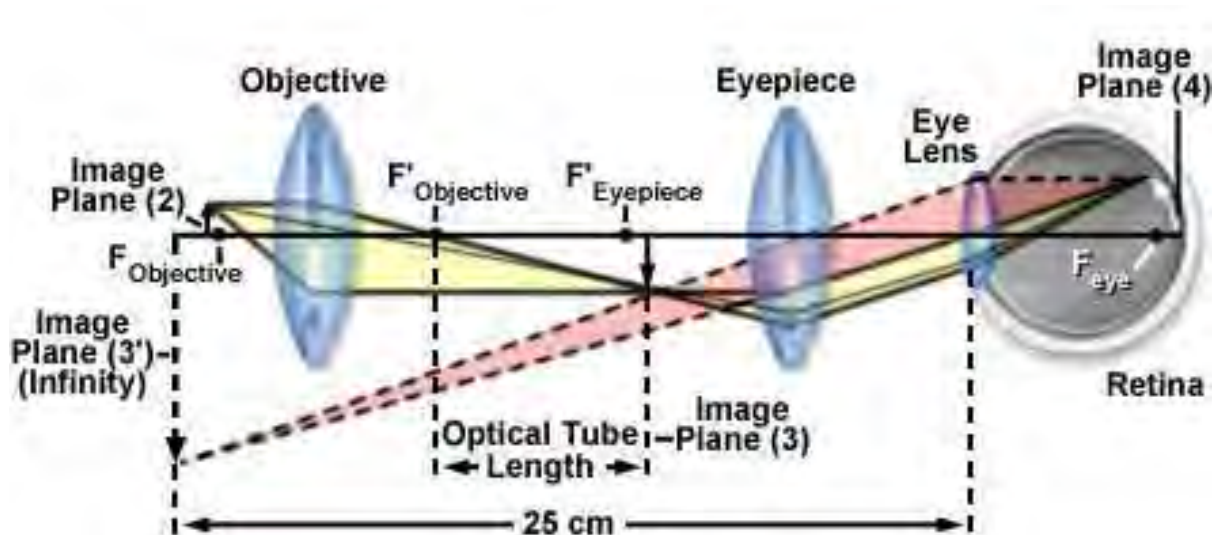


Figure 1-1: Conjugated field planes in a simple compound microscope

Basic light path in a compound microscope. The sample image (image plane 2) is magnified by the objective lens and projected onto image plane 3. The eyepiece then further magnifies this image and projects it onto the eye. At the retina, image plane 4 is projected which corresponds to the imaginary image plane 3 at infinity. Total magnification is the product of the objective and eyepiece magnification. (Figure adapted from <http://www.microscopyu.com/articles/optics/components.html>)

In contrast to historical compound microscopes, modern light microscopes consist of a plethora of lenses to achieve highest image quality. However, their basic principle did not change since the invention of compound microscopes more than 400 years ago.

As shown in Figure 1-1, the basic components are the objective that magnifies the specimen and projects the resulting image as an intermediate image. This is magnified again by the eyepiece to produce an image on the cornea of the eye. The magnification of a microscope is therefore the product of objective magnification (typically between 4 - 100x) and eyepiece magnification (typically 10x).

1.1.3 Optical resolution

The microscopic image of a point source is not a point but a spot called Airy disk due to diffraction of light (49). As illustrated in Figure 1-2, two points are just resolved when the center of one Airy disk falls on the first minimum of the other Airy disk (Rayleigh's criterion). The radius of the Airy disk therefore defines the lateral resolution of an objective (49). It can be calculated as $d = (0.61 \lambda / \text{NA})$ with λ being the used light wavelength and NA the numerical aperture. The numerical aperture (NA) was defined as the maximum cone width that can be collected with a given focus (5). This means that with high NA oil objectives and short wavelengths around 450 nm, a theoretical maximum resolution of approximately 200 nm can be achieved, however, in praxis resolutions range around 250-300 nm.

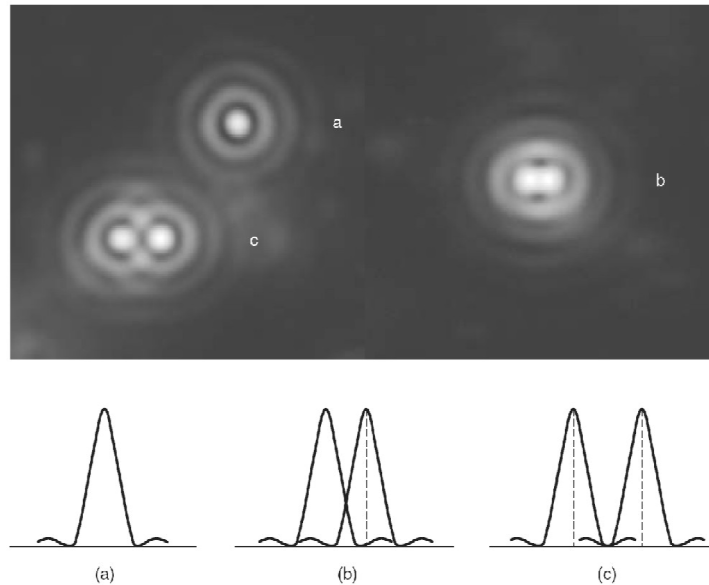


Figure 1-2: Rayleigh criterion for spatial resolution.

Profile of diffraction patterns (upper panel) and its intensity distributions as a function of separation distance (lower panel): (a) the bright Airy disk and 1st- and 2nd-order diffraction rings of a single spot are visible. (b) two disks separated by a distance r_{Airy} such that the maximum of a disk overlaps the first minimum of the other disk: the points are just barely resolved. (c) two disks at a separation distance of $2 \cdot r_{\text{Airy}}$: the points are clearly resolved. (Figure and legend adapted from (71) and (49))

1.1.4 The discovery of fluorescence

Over 150 years ago in 1852, George Gabriel Stokes described a phenomenon which was in essence already observed by Nicolás Monardes in 1565 and many others thereafter (106). He used a prism to refract sunlight and then held a tube containing a quinine solution into the rays. As long as he moved the tube through the visible parts of the spectrum, nothing happened. However, when he held it into the invisible part next to the violet portion, the solution lit up in blue (106). He later called this phenomenon *fluorescence* and noted that the emitted light was always of a longer wavelength than the exciting light (*Stokes shift*).

Later the physics of fluorescence was worked out. It is basically the re-emission of light by a molecule after absorption of light. A Jablonski diagram as depicted in Figure 1-3 illustrates what happens when a photon is absorbed by a fluorophore: The molecule is excited from its ground state S_0 to a higher electronic state in S_1 . In picoseconds, the molecule relaxes to the lowest vibrational level of S_1 , which means part of the absorbed energy is released. The molecule typically stays in the lowest vibrational level of S_1 for nanoseconds. Then, a transition to a higher excited level of S_0 occurs. During this transition, light is emitted. Afterwards, the molecule reaches its thermal equilibrium quickly (3, 6). The Stokes shift can therefore be explained by the “loss” of energy before the transition from S_1 to S_0 . Due to this

1 | Introduction

effect, the wavelength of the emitted light is longer and has less energy than the light used for excitation (Stokes shift).

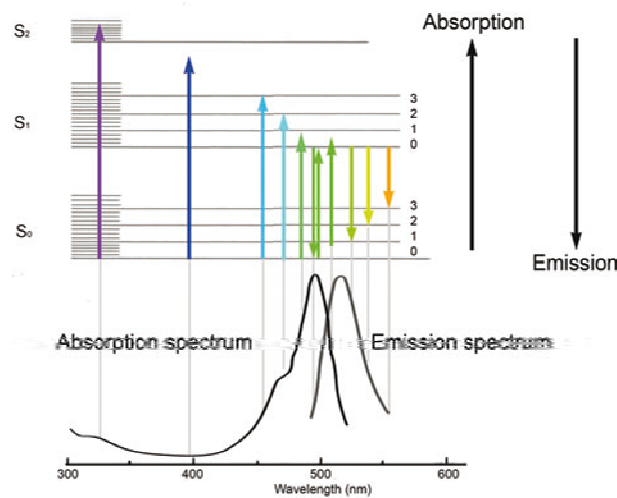


Figure 1-3: Physics of fluorescence

Jablonski diagram depicting the energy steps needed to bring a fluorescein isothiocyanate-molecule from one energy level to another (upper row). These steps are related to the absorption and emission characteristics (lower row). Up-pointing arrows depict the amount of energy (wavelength) a photon has to deliver to excite the molecule to a given vibrational state (horizontal lines) in S₁ or S₂. Down-pointing arrows indicate the amount of energy (wavelength) an emitted photon can have. As energy in the form of photons is only emitted from the lowest vibrational level of S₁, emitted photons have a longer wavelength (less energy) than the absorbed light (Stokes shift). (Figure and legend adapted from (57)).

1.1.5 The quest for contrast

Early microscopes used visible light to shine through the sample and illuminate it (brightfield microscopy). However, sample contrast was often poor and specific structures, especially at higher magnification, were hard to identify. Therefore, different methods were developed to increase the contrast. One way is the staining of structures with dyes. A prominent example is the Gram stain which was developed by the Danish scientist Hans Christian Gram, who published the method in 1884 (45). This method allows the characterization of bacteria into two large groups based on the properties of their cell walls. A lot of other stainings were developed, many of them still used today. Still, for some applications even higher contrast was needed.

1.1.6 The advent of fluorescence microscopy

It took almost another 50 years after the observation of fluorescence by Stokes in 1852, that it was realized that fluorescence could be used to increase contrast in microscopy. 1908, Köhler and Seidentopf built the first fluorescence microscope (87). The illumination source was a

1 | Introduction

cadmium spark, but it was much too dim to be of practical use. However, two years later Lehmann combined suitable filters with a carbon arc. Based on this work, the first fluorescence microscopes were sold by Reichert and Carl Zeiss only a year later (87).

However, suitable fluorescent probes that stained biological samples still had to be developed. This was achieved soon after. Especially acridine dyes played an important role after Bommer found in 1929 that a certain acridine stained the nuclei of tissue sections (87).

The breakthrough for fluorescence microscopy followed in 1941 when Albert H. Coons and his colleagues reported the specific staining of tissue with a fluorescein labeled antibody solution (17, 18, 87). Immunofluorescence was born and its ability to greatly enhance optical contrast while being very specific at the same time transformed fluorescence microscopy from a technique for specialists into a standard application.

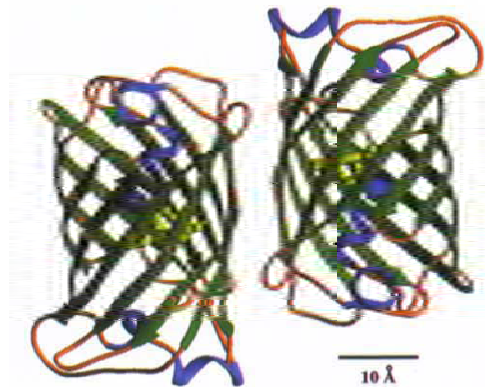


Figure 1-4: Molecular structure of wildtype GFP

Quaternary structure of wildtype GFP depicted as ribbon diagram. Green arrows indicate the typical beta-barrel structure consisting out of 11 strands of beta-sheets. Orange, less ordered sequence parts bridge the sheets and blue sequence parts fold as alpha-helix. The yellow residues depicted in the middle form the fluorophore. Two molecules of wildtype GFP form a dimer in the crystal structure as well as in solution. (Figure and legend adapted from (110))

1.1.7 The discovery of green fluorescent protein

The invention of immunofluorescence enabled the specific localization of almost any protein of interest in *fixed* cells. However, a simple, widely applicable method to specifically label subcellular structures of interest in *living* cells was still missing. This changed in 1994 when Martin Chalfie and his colleagues described the use of a green fluorescent protein (GFP) for the genetic labeling of proteins (13).

When this protein was first described by Shimomura et al. (98) in 1962, even the authors could not have imagined the impact this protein would eventually have on modern life sciences. This jellyfish protein that looked “greenish in sunlight” and exhibited “a very bright,

1 | Introduction

greenish fluorescence in the ultraviolet of a Mineralite” (98, 105) remained a curiosity for almost 30 years until it revolutionized the biological sciences as a genetic fluorescent tag that is suitable for live cell imaging (105). From there on, a wide panel of variants was developed and other related proteins were found in several invertebrates resulting in a multicolored, bright toolbox ready for every life scientist to use (96, 105).

Subsequently, 46 years after its original description, the Nobel Prize in chemistry was awarded in 2008 to Martin Chalfie, Osamu Shimomura, and Roger Y. Tsien for their discovery and development of the green fluorescent protein (GFP).

1.1.8 Basic structure of modern fluorescence microscopes

Modern fluorescent microscopes can be roughly divided into widefield- and confocal microscopes. They both have in common that the same objective is used to excite the sample and to collect the emitted light. For this reason, a beam splitter of some sort is needed to split the emitted light from the exciting light (Figure 1-5 left). Often so called filter cubes are used. These are typically assemblies of 3 filters (Figure 1-5 right). The excitation light is filtered by an excitation filter that only permits the desired wavelength(s). The selected light is then reflected onto the sample by a dichroic mirror, which transmits most wavelengths but the ones used for excitation. The emitted light from the sample is then transmitted through the dichroic mirror and subsequently filtered by an emission filter.

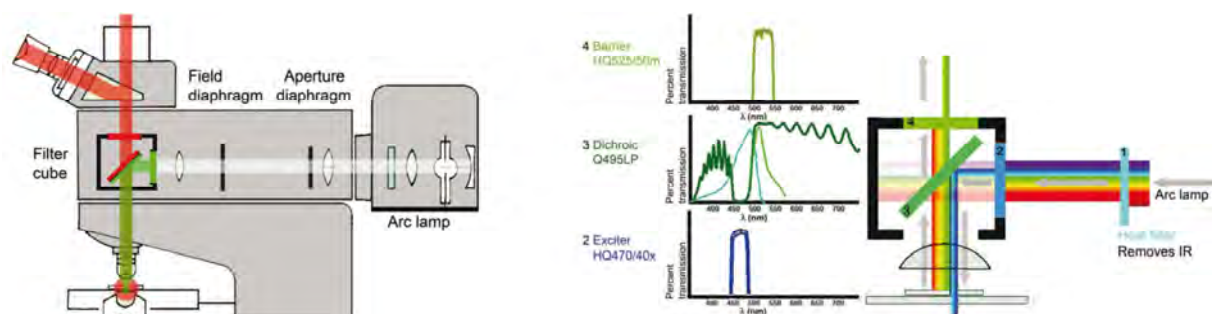


Figure 1-5: Basic beam path in a fluorescence microscope

The general beam path in an epi-fluorescence microscope is shown (left). The objective is both used to excite the specimen and to collect emitted fluorescence. A filter cube is used to separate both beam paths. (right) The principle of a filter cube specifically designed for the excitation and detection of GFP (emission and excitation characteristics of GFP are overlaid on the dichroic mirror properties in light blue (excitation) and light green (emission)) (3). Light from an arc lamp is filtered by an excitation filter (2). Resulting light in the range of 480 nm is reflected onto the specimen at the dichroic mirror which is non-permissive to this range of wavelengths. Emitted fluorescence light collected by the objective is focused onto the dichroic mirror and permitted through. Afterwards, it is filtered by an emission filter (4) to remove last traces of excitation light. (Figure and legend adapted from (57))

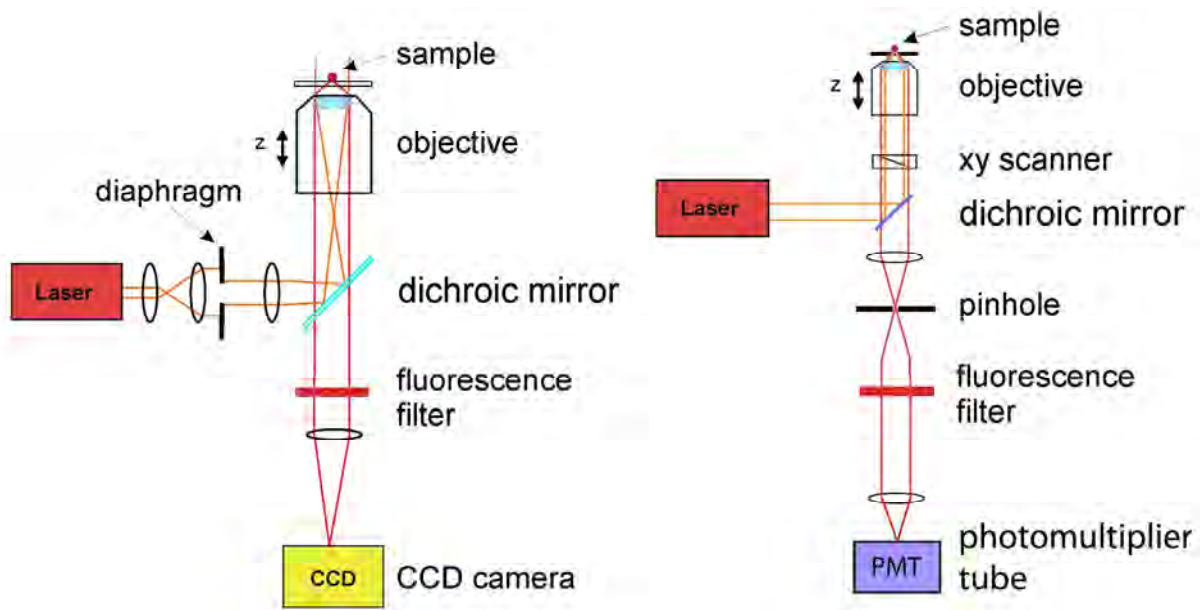


Figure 1-6: Basic features of widefield and confocal fluorescence microscopes

The basic constituents and optical pathways of a widefield (left) and a confocal laser scanning microscope are shown. In case of a widefield-setup, either an arc lamp or a laser can be used as a light source. In case of a laser, the beam is widened to illuminate the whole image and then projected by the objective onto the sample. A dichroic mirror separates exciting from emitted light which is further filtered by an additional emission filter. The signal is then recorded by a CCD camera. In a confocal setup, a very small diameter laser beam is focused onto the sample leading to the illumination of only the confocal volume. The confocal volume is scanned over the sample by an xy-scanner consisting of 2 mobile mirrors. The emitted light is focused through an aperture called pinhole that eliminates most of the out-of-focus signal. Because the picture is built up over time by scanning, the signal from each confocal volume is recorded by a photomultiplier tube or avalanche photo diode. (Figure modified from(49))

The basic features of widefield and confocal laser scanning microscopes (CLSM) are depicted in Figure 1-6. In a widefield microscope, the whole image is illuminated and recorded on a charge-coupled device (CCD) camera. Typical resolutions range around 300 nm laterally and 2.5 μm axially. In a CLSM however, only a diffraction limited volume, the so-called confocal volume, is illuminated. The dimension of this confocal volume is dependent on the used wavelength, the numerical aperture of the used objective and the refractive index of the used medium between objective and object (49). Additionally, a confocal pinhole (aperture) is placed in front of the detector. This pinhole greatly reduces the detection of out-of-focus light. Thereby, an about three times better axial resolution compared to widefield microscopes is achieved. Typical resolutions for CLSMs range around 300 nm laterally and around 1 μm axially (49). To build up a picture, the confocal volume has to be scanned over the sample. This is achieved by using two mirrors, which can be tilted very quickly (Figure 1-6 right). Still, scan time can be limiting if high image quality is needed and often widefield setups with attached CCD-cameras are superior in speed as well as in sensitivity if state-of-the-art CCD cameras are employed.

1.1.9 Fluorescence live cell imaging

To enable the fluorescence imaging of living cells, the microscopy setup has to be adapted to the environmental needs of the cells in question. Especially if cellular properties are quantified, incubation under stable physiological conditions is mandatory to measure meaningful data. Most mammalian cells have to be incubated at 37° C in a specific growth medium with defined amounts of nutrients, salts and a stable pH. To achieve this, special setups were developed over the last decade or so.



Figure 1-7: Schematic drawing of a live imaging setup

An inverted fluorescence microscope is depicted. Most of the body is enclosed in an incubation chamber that is heated and controlled by an environmental control unit (right). CO₂ is mixed into the air supply to keep the pH of the carbonate-buffered cell culture medium constant. A CCD camera to acquire digital images is mounted on the left port. (Figure adopted from <http://www.microscopyu.com/articles/livecellimaging/livecellmaintenance.html>)

As shown in Figure 1-7, heating is normally achieved by an enclosure of some sort that is used to insulate the sample. Heating is typically done by a combination of devices. Often the sample holder is heated. Additionally, the objective can be heated, and the whole enclosure is normally supplied with warmed air. To keep the pH of the sample medium stable, either a buffered cell culture medium is used, or a carbonate buffer system employed, which needs the supplementation of CO₂ into the air supply.

To prevent focus drift during acquisition, the imaging setups are often mounted onto vibration-isolated tables as shown in Figure 1-7. Moreover, systems are often set up in climatized rooms to prevent focus drifts due to thermal gradients.

1.2 Diffusion theory and single particle tracking

1.2.1 Cellular transport processes

Life in the form of a unicellular microbe or a huge multicellular organism heavily depends on the flux of substances, or in other words, transport processes. Depending on the distances and other factors like the size of the molecule or cargo as well as the viscosity of the surrounding medium that need to be bridged, two modes are possible. The first is molecular diffusion, which is self-propelled by thermal energy. Larger molecules diffuse by Brownian motion which is originated from collisions with solvent molecules. Diffusion can be along concentration gradients and these gradients might be maintained by the use of energy, as in the case of nuclear-cytoplasmic shuttling of import/export factors (77). The second mode is biochemical energy consuming, directed transport of cargo along cellular tracks.

Diffusion is very effective at short distances in dilute environments. As reviewed by Sodeik (100), a herpes simplex virus capsid particle of approximately 120 nm in diameter would need approximately 14.6 seconds to cross a diameter of 10 μm by diffusion. However, in the viscous and crowded intracellular environment, the same particle would need around 2 h. Therefore, it becomes clear that big molecules or cargo like a herpesvirus capsid cannot depend on diffusion alone to cross the cell. In these cases, the second described mode is employed which is the energy-dependent, directed transport along cellular tracks by the use of molecular motor proteins.

1.2.2 Methods to study particle mobility in a cellular environment

Several techniques were developed in the last decades to study the mobility of molecules and particles in cellular environments. Most of them are based on live cell fluorescence microscopy as its high contrast allows the localization of even very small entities. Some examples are fluorescence recovery after photobleaching (FRAP), fluorescence correlation microscopy (FCS) and single particle tracking (SPT) (as reviewed in (25)). While the two former methods mainly provide average information on molecule dynamics, SPT can provide information on the mobility of individual molecules or particles (25).

1 | Introduction

1.2.3 Determination of particle positions in SPT

As described before, the optical resolution of light microscopes is diffraction limited. Therefore, practically no better resolution than 250 to 300 nm can be achieved with typical commercially available systems. This means for example that the architecture of an assemblage of fluorescent molecules, such as a virus particle carrying hundreds of individual fluorophores, cannot be resolved. However, the *position* of the center of such a particle can be determined to much greater accuracy. The only caveat is that the particle concentration has to be sufficiently low to exclude the overlapping of individual particles due to the diffraction limit.

One way to determine the position of a fluorescent particle is to fit its diffraction limited spot with a two-dimensional Gaussian function:

$$I = A_0 e^{-\frac{(x-x_0)^2}{2\sigma^2}} e^{-\frac{(y-y_0)^2}{2\sigma^2}}$$

where A_0 and σ are the amplitude and the width at half-maximum of the two-dimensional Gaussian curve, and x_0 and y_0 the coordinates of the position of the individual particles (49). The positioning accuracy of this method is dependent on the signal to noise ratio but can be as high as +/- 2nm (49). Typically it ranges around +/- 10 to 30 nm and is therefore much better than the optical resolution as long as particle signals do not overlap.

1.2.4 The mean square displacement as a measure of particle behavior

Once the positional changes of a particle are recorded, the diffusion of a moving particle can be described by the behavior of the mean square displacement (MSD) over time. A particle diffusing freely describes a random walk. In this case, the MSD is directly proportional to time.

$$\langle r^2(\Delta t) \rangle = \text{MSD}(\Delta t) = 2kD\Delta t$$

where $r^2(\Delta t)$ is the displacement of the particle position within a time interval Δt , D the diffusion coefficient, and k the number of dimensions the particle diffuses in (49).

1 | Introduction

In cases where free particle diffusion is somehow influenced by the surrounding environment, different functions can be applied to describe particle movement.

Three major functions are:

Normal diffusion	$MSD = 4 D t$
Anomalous diffusion	$MSD = 4 D t^\alpha$
Directed motion with diffusion	$MSD = 4 D t + (vt)^2$

where α is the anomalous exponent and v the velocity of the directed transport (92).

By classifying particle tracks into these classes it is possible to deduce predictions about the particle surroundings. For example, a particle exhibiting directed motion is most likely associated to a molecular track of some sort like a microtubule. A particle exhibiting anomalous diffusion, on the other hand, has to be in some kind of viscous environment which inhibits its free diffusion. Thereby SPT can be used to not only describe particle behavior but also to probe the direct environment of an individual particle. Especially in virology, SPT can be of great use as viruses can be engineered to produce fluorescent virus particles. These particles are often smaller than the diffraction limit, but with the above mentioned toolkit it is possible to analyze the diffusive behavior of such labeled virus particles at high detail.

1.3 Herpesviruses

1.3.1 The Order Herpesvirales

Herpesviruses (HVs) are an order of doublestranded DNA viruses (*Herpesvirales*) which have coevolved with their respective hosts for millions of years (86). Currently, 91 different HVs are listed by the international committee on taxonomy of viruses (ICTV, <http://www.ictvonline.org/>). The order is divided into three families with the HVs of mammals, birds and reptiles in the family *Herpesviridae*. Fish and frog HVs are clustered into the family *Alloherpesviridae*, and the family *Malacoherpesviridae* contains the only known bivalve HV *Ostreid herpesvirus 1*. The family *Herpesviridae* can be further divided into three subfamilies named *alpha-*, *beta-* and *gamma-herpesvirinae* (21). This classification was originally based on their biological properties, but a profound body of sequence data accumulated in the last two decades supports this framework (76).

1 | Introduction

Currently, eight human HVs are known. Three can be grouped into the alpha-subfamily (herpes simplex virus 1, HSV-1; herpes simplex virus 2, HSV-2; varicella zoster virus, VZV), three into the beta-subfamily (human cytomegalovirus, HCMV; human herpes virus 6, HHV-6; human herpes virus 7, HHV-7) and two into the gamma-subfamily (Epstein-Barr virus, EBV; Karposi-sarcoma associated virus, KSHV).

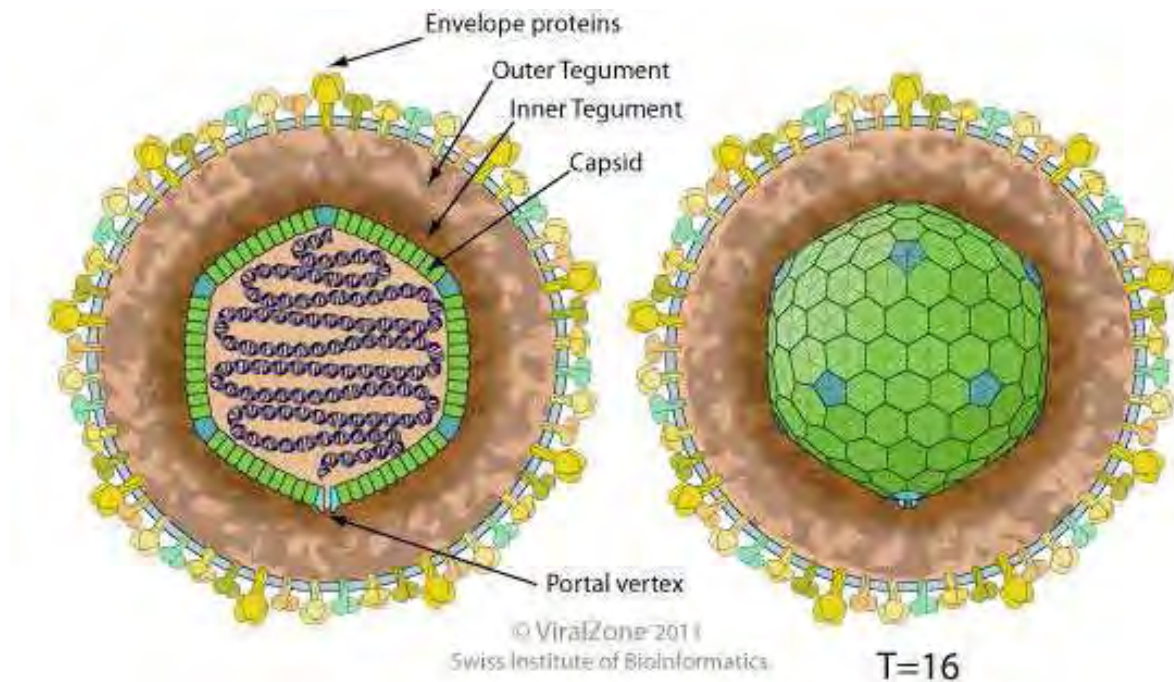


Figure 1-8: Herpesvirus Particle

The general structure of a herpesvirus particle is depicted with main constituents marked. The left part depicts a central cross-section through the virus particle while the right part shows the capsids surface in a particle cross-section. The linear dsDNA genome (dark blue) is depicted filling up the inner capsid space. Capsid hexons are drawn in green, while pentons are depicted in light blue. The number of MCP proteins needed to form hexons and pentons is indicated in the right part. The tegument is drawn as an amorphous layer (brown), the inner tegument is indicated in darker brown. The envelope is drawn in light blue with different viral glycoproteins incorporated (green, brown, yellow). Figure adopted from *ViralZone* (www.expasy.org/viralzone, Swiss Institute of Bioinformatics).

1.3.2 General structure of herpesvirus particles

HV particles consist of a DNA core (ranging from 120 to 230 kb) protected by a highly ordered protein shell called capsid. Capsids are ~120 nm in size and share a common $T = 16$ icosahedral geometry consisting of 162 subunits. Based on their position on the capsid, these capsomers can be subdivided in 150 hexons (the subunits forming the facets) and 12 pentons (the subunits at the vertices). Because of their strong conservation, the herpesvirus capsid was used historically to classify newly discovered viruses (76).

1 | Introduction

The capsid is surrounded by a more or less amorphous layer of proteins called tegument which, according to new data, seems to consist of different assemblies. One function of the tegument is the introduction of transcription factors or the subversion of innate host defenses right upon entry into the host cell (86). The tegument is surrounded by a host-derived membrane called envelope in which a variety of viral membrane proteins are embedded. The amount as well as type of embedded glycoproteins varies between herpesviruses. The glycoproteins are responsible for recognition of the host cell virus receptors and orchestration of the fusion events during virus entry.

1.3.3 The herpesvirus lifecycle

The general HV lifecycle can be divided into a lytic and a latent phase: During the lytic phase, a plethora of viral proteins are expressed. Lytic infection of a cell results in the production of progeny virus and typically leads to its destruction.

In certain cell types, HVs can establish latency. Latency is defined as a persistent state during which the viral genome is maintained in the host nucleus. Occasionally, viral genomes reactivate and a new lytic cycle is started. Typically, only very few viral proteins and some non-coding RNAs are expressed during latency, which facilitate genome maintenance and an immunological mode of stealth. Reactivation events happen at relatively low rates and are normally well controlled by the immune system. However, in immunodeficient hosts the reactivated virus can initiate new symptomatic infections. The mechanisms by which latency is initiated as well as how reactivation is induced are still not completely understood (86).

1.3.4 Entry of herpesviruses

The process of initial attachment of a herpesvirus particle followed by fusion of the envelope with cellular membranes is termed penetration and marks the beginning of a new round of HV replication. During this process virus particles initially bind reversibly to glycosaminoglycans at the cell surface. In a next step, the envelope fuses with cellular membranes. Fusion occurs directly either at the plasma membrane or after internalization of virus particles by endocytosis. The actual used pathway depends on the cell type being infected.

After penetration, the tegument separates and releases the capsid (63). The capsid then recruits molecular motors like kinesins and dyneins which enables the microtubule-mediated transport to the microtubule organizing center and subsequently to the nucleus (80). Here, capsids bind to nuclear pores and inject their genome through the portal into the nucleus (86).

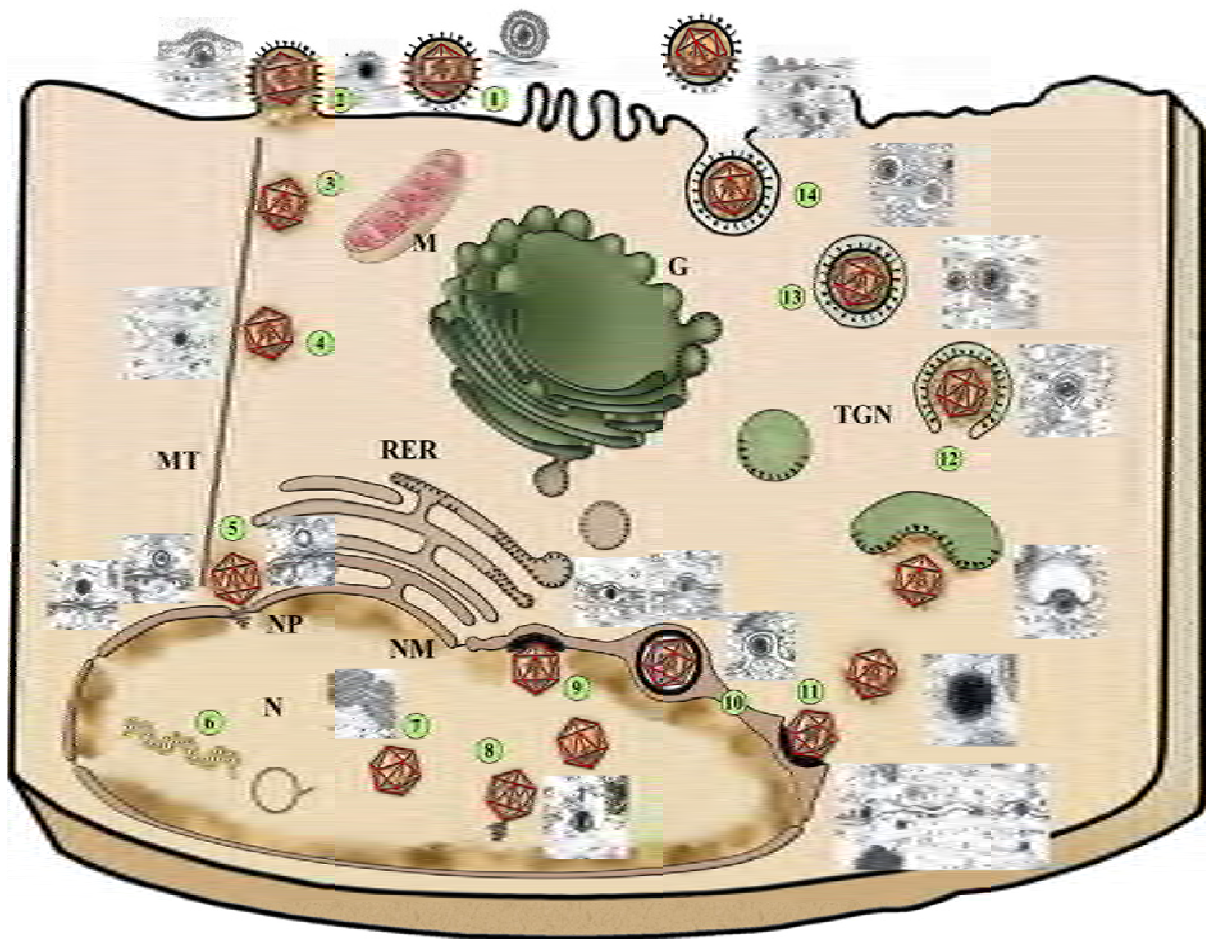


Figure 1-9: General herpesvirus lifecycle

Virus particles attach to the cell surface (1) and either fuse with the plasma membrane (2) or enter by endocytosis and subsequent membrane fusion (not shown). After fusion, capsids are recruited onto microtubules and transported to the nuclear membrane where they attach to nuclear pores (3-5). The viral DNA is subsequently injected into the nucleus and viral transcription and genome replication begins (6). Capsids are assembled in the nucleus from preformed subunits (7) and concatameric DNA is packaged into them. During this process, the concatamers are cleaved into unit-length genomes (8). Packaged capsids subsequently reach the inner nuclear membrane (8) and bud into the perinuclear space (9-10) (primary envelopment). Afterwards, primary enveloped particles fuse with the outer nuclear membrane and are released into the cytoplasm. Cytoplasmic capsids acquire several layers of tegument and subsequently bud into trans-Golgi-derived membranous structures enriched with viral glycoproteins (secondary envelopment). Resulting vesicles are transported to the plasma membrane where they fuse and release enveloped virions. (RER: rough endoplasmic reticulum; M: mitochondrion; G: Golgi apparatus). (Figure adopted from (67))

1.3.5 Viral gene expression cascade

After injection into the nucleus, the linear viral genome circularizes and the most important decision in the HV lifecycle takes place. In most cases the genomes will remain silent or silenced and latency is established. In some rare occasions however, the viral expression starts in a highly regulated cascade leading to genome replication and subsequently to the formation of new particles. Mechanistically, lytic genes can be grouped into three classes. The first class consists of transcription units that do not depend on other viral gene products for their

1 | Introduction

expression. They are called immediate early (IE) genes because they are the first to be expressed upon the start of the lytic replication cycle. Still, tegument proteins from the incoming particle act as viral transcription factors and can modulate IE gene expression (86). The production of IE proteins leads to modulation of the host cell to favor virus replication and the expression of early (E) genes are induced. This in turn leads viral DNA replication. After viral DNA replication has started, late (L) genes are expressed. Late proteins are mostly structural proteins which are needed to form new viral particles (for a review see (86)).

1.3.6 Nuclear steps of morphogenesis

Spatially, the replication machinery is assembled near nuclear domain 10 (ND10) sites. ND10 sites subsequently break down and prereplicative sites are formed (86). As viral genome replication processes, they enlarge with time and coalesce to form replication compartments. In this process, host chromatin is marginalized at the nuclear rim (69).

The genome is mainly replicated in a “rolling cycle” mechanism that leads to the formation of linear genome concatamers (86). One genome each is packaged into preformed capsids by the so-called terminase complex. The ATPase subunit of this complex is conserved in the order *Herpesvirales* but also in T4-like phages of the family *Myoviridae* (21), which might indicate a common ancestry of HVs and tailed DNA bacteriophages (4), and that the nuclear stages of HV morphogenesis are perhaps more ancient than the cytoplasmic stages (64, 67).

Capsids are believed to be assembled in replication compartments from preformed capsomer complexes which are imported into the nucleus after their assembly from individual components in the cytosol. This process is autocatalytic and results in the formation of procapsids. Procapsids undergo a structural shift after viral genomes are packaged into them.

After genome packaging, capsids reach the nuclear periphery. The process by which this is achieved is not clear yet. An F-actin mediated transport mode was proposed (36) which was underlined by the discovery that some alpha-herpesviruses can induce nuclear F-actin (33). It is, however, still not clear which molecular motors are employed and which viral proteins are involved in these processes.

As nuclear pores seem to be too small to allow the transport of capsids through them at most stages of infection, capsids undergo a complex envelopment-deenvelopment at nuclear

1 | Introduction

membranes to reach the cytoplasm (primary envelopment). This process termed nuclear egress is dependent on the conserved UL34/UL31 complex in most HVs (86) and either occurs directly at the inner membrane or at virus-induced membrane infoldings (12). This process seems to involve the phosphorylation and destabilization of the nuclear lamina by virus- as well as host-kinases (70).

1.3.7 Cytoplasmic steps of morphogenesis

After capsids reach the cytoplasm, further tegument proteins are acquired. Then, secondary envelopment occurs at modified, possibly trans-Golgi-derived cellular membranes (86). This results in the formation of vesicles with enveloped virus particles inside. These vesicles, possibly mimicking exocytotic cargo, are subsequently recruited onto microtubules and actively transported to the plasma. Transport to the plasma membrane again seems to be mediated by dyneins and kinesins. There, vesicles fuse and release the virus progeny. This last step might also use myosins (84), possibly to cross the actin cortex as reported for cellular exocytotic vesicles or to facilitate particle release.

1.3.8 Herpesvirus capsids

The assembly of capsids occurs in the host nucleus as described earlier. At least five conserved proteins are needed to assemble basic capsids: The major capsid protein (MCP), the triplex monomer (TRI1), the triplex dimer (TRI2), the maturational protease (PR) as well as the assembly protein (AP) which is released from the C-terminal part of the same poly-protein by the autocatalytic PR. Moreover the portal protein (PORT) is needed to assemble the portal which is needed for DNA packaging (68). An additional constituent, the small capsid protein (SCP) is widely conserved among herpesviruses and forms a complex with the MCP in hexons. However it is only essential in beta- and gamma-herpesviruses.

Capsids assemble auto-catalytically on the basis of the scaffold that is most likely determined by the AP. Its hexons consist of 6 copies of both MCP and SCP, while pentons are made out of 5 copies of MCP only. Together they form a shell with a closely packed inner surface and star like outer layer, which were termed floor and external protrusions, respectively (104). At trigonal positions, triplexes consisting of one copy of TRI1 and two copies of TRI2 overlay the floor (104). Pentons are found at the vertices. One penton-position of each capsid serves

1 | Introduction

as portal, which, at least in HSV-1, consists out of 12 copies of PORT (68). It serves as a site for the genome entry into the preformed procapsids during the final packaging step of capsid morphogenesis.

As illustrated by cryo-electron microscopy with concurrent image reconstruction, six small capsid proteins cover the tips of the crown-like hexon protrusions (68, 104), but not the pentons. The SCPs constitute therefore the outermost of the capsid structure. Interestingly, these outermost structures appear to be quite similar in beta- and gamma-herpesviruses, but have a different appearance in alpha-herpesviruses (104). This observation correlates with the fact that the SCP is essential in most beta- and gamma-herpesviruses (8, 78) but dispensable in most alpha-herpesviruses (14, 23, 52).

1.4 Murine models of human beta and gamma-herpesviruses

1.4.1 MCMV as an animal model for HCMV pathogenesis

HCMV is the prototypic beta-herpesvirus. This is mainly due to its importance as a human pathogen: As all HVs, HCMV establishes persistence after primary infection in immuno-competent individuals. It is estimated that the prevalence of CMV infection among adults over 40 years ranges from 50% to 80 % in the US (<http://www.cdc.gov/cmV/overview.html>) but might reach near 100% in developing countries. In the western world, it is the major viral cause of birth defects, causing deafness and mental retardation (46, 50).

The primary HCMV infection, occurring mainly during the early childhood, is asymptomatic or associated with mostly mild pathology but results in establishment of life-long latency.

Thereafter, persistent HCMV infection in immuno-competent individuals is typically not associated with disease. However, HCMV can cause severe disease in immuno-compromised individuals like transplant-recipients, AIDS and cancer patients. This includes pneumonitis, enteritis, retinitis hepatitis, esophagitis, colitis, encephalitis, polyradiculopathy, adrenalitis, and also graft loss (30).

Due to its restricted host range, HCMV infection cannot be studied in animals. This lead to the establishment of rodent CMVs as animal models, especially murine CMV (MCMV) for HCMV pathogenesis. These *in vivo* models were very fruitful in elucidating the basic mechanisms by which CMVs hijack the immune system.

1 | Introduction

Since the establishment of reverse genetics for MCMV (66), this model virus is also used to study beta-herpesvirus morphogenesis in cell culture. Cloning of the infectious MCMV genome as the first HV bacterial artificial chromosome (BAC) became a milestone in HV genetics in general. It provided the basic genetic tools to study essential genes, which was very cumbersome using traditional methodology (8, 9). Moreover, compared to HCMV, MCMV has several technical advantages too. Its replication cycle is much shorter (1 day compared to 3-5 days), the kinetics of its lytic infection is far more synchronous, it is permissive in widely accessible and well-characterized mouse cell lines (instead of hard to standardize human primary lines) and its security classification as safety level 1 (S1) organism allows its study in standard molecular biology labs. In addition, MCMV strains show outstanding genetic stability compared to HCMV isolates, which suffer major genome rearrangements due to their adaptation into tissue culture (28). Still, the basic characteristics of beta-herpesvirus biology are conserved between HCMV and MCMV (e.g. very similar dependence on the same set of essential genes). This makes MCMV an ideal tool to study principles of beta-herpesvirus morphogenesis in vitro.

1.4.2 Murine gamma-herpesvirus 68 as model for EBV and KSHV pathogenesis

The gamma-herpesviruses currently include two known human herpesviruses. EBV is an oncogenic virus. After primary infection, which is mostly asymptomatic in childhood while often associated with the clinical syndrome of infectious mononucleosis during or after adolescence, the virus establishes persistence in B-lymphocytes. This state of the virus is associated with a variety of oncogenic diseases like Burkitt's lymphoma in sub-Saharan Africa, Nasopharynx Carcinoma or Posttransplant Associated Lymphoid Disease (PTLD).

The Human Herpesvirus 8 or Kaposi's Sarcoma associated Herpesvirus (KSHV) was discovered as a cause of the Kaposi's Sarcoma, a vascular tumor, which is mainly found in HIV infected individuals. KS meanwhile became one of the most frequent forms of cancer in Africa. Other KSHV-associated diseases are the Multicentric Castleman's Disease as well as the Primary Effusion Lymphoma.

Analogous to HCMV, the human gamma-herpesviruses EBV and KSHV are highly species-

1 | Introduction

specific. Therefore, as in the case of HCMV, the discovery of a small rodent model virus had a major impact on the understanding of the *in vivo* biology of gamma-herpesviruses (73).

The MHV-68 isolate of Murid herpesvirus 4 was originally isolated from bank voles (*Myodes glareolus*) in Slovakia (6), but closely related viruses were also found in shrews and wood mice (39). In stark contrast to EBV and KSHV which are often hard to culture due to their strong propensity to latently infect most cell types, MHV-68 is strongly lytic in cell culture and grows to high titers. In comparison to EBV, it also does not immortalize B-cells in cell culture. However, it is a robust model of gamma-herpesvirus latency and reactivation *in vivo*. Two closely related MHV-68 lab strains were cloned as bacterial artificial chromosomes (BACs) (2, 109) and reverse genetics systems are available for this virus. It is therefore a convenient model to study the otherwise hardly accessible basic mechanisms of lytic gamma-herpesvirus biology in cell culture.

1.4.3 Fluorescent herpesvirus particles uncover the dynamics of herpesvirus morphogenesis

Besides the the many open questions of HV morphogenesis, the most elusive ones are the principles of viral particle transport. These dynamic events are studied best by fluorescently labeled virus particles in combination with live cell fluorescence microscopy. In recent years, recombinant viruses expressing fusions of structural proteins to fluorescent proteins widely extended our understanding of the dynamic processes involved in the morphogenesis of a large number of different viruses (19, 24, 32, 34, 41, 44, 55, 59, 83, 91, 108).

The reported labeling approaches concerning herpesviruses can be roughly divided into three groups. The first approach is the labeling of a glycoprotein. This allows the tracking of the first steps of infection from attachment to fusion with host membranes, or after envelopment to release (42, 79). The second approach is the utilization of a tegument protein as fusion partner (29, 31, 91). Depending on the protein used, this approach allows the tracing of events after fusion until the separation of the tagged tegument component from the capsids and before envelopment after the attachment of the fusion product to the capsid. The last approach utilizes a capsid protein such as SCP and pUL25 (14-16, 24, 99). Only this approach allows the tracing of all steps of viral entry until the release of viral genomes and morphogenesis after capsid assembly. However, a combination of these approaches (3, 22, 72, 103) can be useful to discern morphogenesis steps, e.g. enveloped from non-enveloped capsids. A capsid-

1 | Introduction

tagged recombinant virus is therefore most desirable as it allows the tracing of almost all morphogenesis steps. Until now, however, only alpha-herpesviruses like HSV-1, pseudorabies virus (PRV) and equine herpes virus type 1 (EHV-1) (15, 16, 24, 38, 99) could be engineered to express fluorescent capsids. In contrast, all attempts to fuse fluorescent proteins to beta- or gamma-herpesviruses capsid proteins failed so far (8, 48, 88).

1.5 Aims of this thesis

Despite the different principles of pathogenesis of the eight human herpesviruses, most pioneering basic research was so far done on alpha-herpesviruses. It is, however, not clear to what extent results obtained in one subfamily fit the situation in other herpesviruses. This is especially important considering that most currently approved HV reactive drugs target viral genome replication which is conserved among HVs. However these drugs also affect the host DNA metabolism and have considerable side-effects. In addition cross-resistant strains can appear. Thus comparative studies on the herpesvirus lytic life cycle are needed to discover new virus specific drug targets. Therefore, there is an urgent need for targeted comparative studies of key functions of HV morphogenesis. These are only possible since the introduction of reverse genetics into all subfamilies (2, 7, 66, 72).

As described above, the dynamics of viral capsid transport during herpesvirus morphogenesis by live cell imaging were studied mostly in the alpha-herpesvirus models using capsid tagged recombinants. This was due to the lack of fluorescent, capsid-tagged beta- and gamma-herpesviruses.

We therefore aimed to establish new recombinant beta- and gamma-herpesviruses expressing labeled capsids by fusing a fluorescent protein (FP) to a capsid protein. Unfortunately, the SCPs of beta- as well as gamma-herpesviruses are essential. All reported attempts to fuse a fluorescent protein to SCPs of these subfamilies resulted in non-viable or even dominant negative mutants

Herpesvirus capsid proteins undergo numerous and highly ordered interactions with themselves or other proteins to build the capsid (48). The pure bulk of several copies of fluorescent proteins (FPs) that are needed to deliver a bright fluorescent signal induce sterical problems and might render the recombinant viruses non-viable. As first described by Desai et al. (24), the SCP of some alpha-herpesviruses like HSV-1, PRV (99) VZV (14) and EHV (38)

1 | Introduction

seem to tolerate an aminoterminal fusion to FPs. This capsid protein is exceptionally suitable as a fusion partner as it is located at the outermost of the core-capsid structure, which apparently gives sufficient steric freedom to accept a fusion to bulky fluorescent proteins. Moreover, it is a very abundant protein with 900 copies per capsid (6 copies per hexon), which results in a sufficiently bright fluorescent signal if fused to a fluorescent protein. Yet, later studies showed that the aminoterminal fusion with GFP nonetheless renders the product biologically non-functional in PRV (52). It emerges therefore, that the tagging of alpha-herpesvirus-SCPs is apparently only possible because they are not essential for virus replication.

This thesis reports on the successful construction of fluorescent capsid-tagged MCMV as well as MHV-68 recombinants. Successful construction of FP labeled viruses involved a multi-step-approach: First, potentially conserved protein domains were defined by multiple sequence alignments on the amino acid level. Then, fluorescent proteins were inserted into potential linker sequences between conserved domains. Subsequently, the resulting fusion proteins were inserted ectopically into the viral genome leaving the respective WT SCP locus untouched. This way any inhibitory or dominant negative feature of the fusion proteins could be easily assessed. The resulting recombinant viruses were viable and exhibited bright fluorescence signals.

They were then used to study capsid transport both during virus entry and egress by single particle tracking. It could be shown that fluorescently labeled virus particles were transported actively along extracellular protrusions prior entry, and that intracellular transport of particles is mostly directed and dependent of microtubules.

2 Materials and Methods

2.1 Cells and viruses

BALB/c murine embryonic fibroblasts (MEFs), M2-10B4 bone marrow stromal cells (ATCC CRL-1972), and NIH-3T3 fibroblasts (ATCC CRL-1658) were prepared and treated as described previously (65). Rat embryonic fibroblasts stably transfected to express Cre-recombinase (REF-Cre) as well as baby hamster kidney cells (BHK, ATCC CCL-10) were cultured as described in (2).

All MCMV recombinants used in this work are based on the pSM3fr- Δ m1-16-FRT BAC (62). The corresponding virus MCMV- Δ m1-16-FRT lacks 16 genes from the left end of the genome that are not required for virus replication in tissue culture. The morphogenesis of MCMV- Δ m1-16-FRT was analyzed extensively in previous studies and found to be indistinguishable from the wildtype (WT) BAC derived MCMV. Therefore, MCMV- Δ m1-16-FRT is designated as WT throughout this work (62). All recombinant viruses were reconstituted from their respective BACs by nucleofection of NIH/3T3 cells. Nucleofection was done using an Amaxa 96-Well Shuttle system (Lonza) according to the manufacturer's instructions for NIH-3T3 cells. In brief, 5×10^5 cells were nucleofected with 400 ng purified BAC-DNA and seeded together with 1.5×10^5 non-transfected cells into one well of a 24 well plate. Three days after nucleofection, the cell layer was checked for plaques and split 1:4. Usually, six days after nucleofection, full cytopathic effect (CPE) could be observed. Cultures were harvested and samples were frozen as passage zero. Afterwards, virus inoculi were scaled up on M2-10B4 cells as described previously (65).

All MHV-68 mutants used in this work are based on the pHA3 BAC (2). To generate an acceptor BAC for ectopic insertions of transgenes, the M1 gene was deleted by ET-mediated homologous recombination (Vidy et al. manuscript in preparation) and called it pHA3-D2. The M1 gene deletion has been shown to have no influence on virus replication, neither in tissue culture nor *in vivo*, except for a stronger tendency to reactivate from latency. The construction of pHA3-D2 is briefly described in chapter 1.4. Reconstitution of all MHV-68 BACs was done by lipofecting REF-Cre cells (2) in 6-well plates with BAC DNA mediated by Lipofectamine 2000 (Invitrogen) according to the manufacturer's instructions.

The infectivity of MCMV as well as MHV-68 preparations was quantified on MEFs by

2 | Materials and Methods

standard plaque assay (81).

To biologically clone MHV-68 mutants, limiting dilutions of reconstituted viruses were done by infecting REF-Cre cells in 96-well plates with 0.1, 1 and 10 particle forming units (PFU) per well. After 4 days, wells were checked for single fluorescent plaques. The supernatant of these wells was saved and cells fixed and checked for revertant, non-fluorescent plaques by staining against MHV-68 proteins with a polyclonal serum (101). Supernatant from single wells with single fluorescent plaques, lacking any sign of non-fluorescent infectivity, was used to inoculate virus stocks.

2.2 Analysis of viral growth in vitro

MEFs were infected with the viruses to be analyzed in duplicate at a multiplicity of infection (MOI) of 0.1 for MCMV or 0.01 for MHV-68 at 37° C. The inoculi were removed after 1 h, then the cultures were washed three times with Dulbecco's phosphate-buffered saline (DPBS), normal medium was added and the incubation was continued. Supernatants of infected cells were harvested daily on days 1 to 6 for MCMV or days 1 to 4 for MHV-68 after infection, and the amounts of the released infectious particles were determined by plaque assay (81) on MEFs.

2.3 Measurement of plaque sizes

To determine mean plaques sizes, standard plaque assays were performed (81). Four (MHV-68) or five (MCMV) days after infection, the overlay was removed and cells were fixed with 4% paraformaldehyde (PFA) for 10 min. Afterwards standard immuno-staining was performed against IE-1 (MCMV) or SCP (MHV-68) with specific mouse monoclonal antibody solutions and Alexa-coupled mouse specific secondary antibodies (Invitrogen). Digital images of individual plaques were obtained using LSM 510 or LSM 710 confocal laser scanning microscopes (Zeiss). Plaque diameters in pixels were measured on the digital images using ImageJ software (1) and converted into micrometers.

2.4 Plasmid construction

To generate the plasmid pOTO-S-GFP-SCP we amplified a sequence with primers SCPPfor and SCPPrev (Table 1) binding to positions 74153-74173 and 73766-73786 of the MCMV

2 | Materials and Methods

Smith strain (NCBI Reference Sequence: NC_004065.1), respectively. The amplicon coded for a proposed m48.2 promoter sequence as well as the first 34 amino acids (aa) of m48.2. The primer SCPPfor added an *EcoRV* site to the 5' end, while SCPPrev fused *AflIII* and *SpeI* sites as well as a hemagglutinin (HA)-tag coding sequence to the 3' end. The PCR fragment was cut with *EcoRV* and *AflIII* and inserted into the previously described plasmid pO6-IET-gfpSCP (82) replacing its *AflIII*-*SspI* fragment.

Further variants of pOTO-S-GFP-SCP coding for SCP fusions to mCitrine and mCherry were generated by amplifying the respective fluorescent proteins with primers SP-*AflIII*-FP-*BsrGI* and ASP-*AflIII*-FP-*BsrGI* (Table 1) from YFP-Rac2 (Joel A. Swanson/Addgene) or pmCherry-C1 (Clontech) which added *AflIII* and *BsrGI* sites to the respective ends. The PCR-products were cut with *BsrGI* and *AflIII* and inserted into the plasmid pOTO-S-GFP-SCP, replacing its *BsrGI*-*AflIII* fragment resulting in pOTO-S-mCitrine-SCP and pOTO-S-mCherry-SCP, respectively. pOTO-S-GFP-SCP and above described variants are coined rescue vectors through this thesis as they are used to generate recombinant viruses by a single step ectopic rescue (10).

To generate the S-GFP-SCP* mutant, lacking the last 14 C-terminal codons of the SCP open reading frame (ORF), the parental vector pOTO-S-GFP-SCP was cut with *PvuII* and *ApaI* thereby removing the coding sequence for the last 17 aa of the C-terminal region of m48.2. To subsequently restore the missing nine codons as well as the stop codon, the corresponding region pOTO-S-GFP-SCP was amplified with primers SP-MCP and ASP-MCP (Table 1) and inserted by *PvuII* and *ApaI* resulting in pOTO-S-GFP-SCP*.

To generate pOTO-ORF65-EGFP we amplified a sequence corresponding to position 102895-103759 in the MHV-68 BAC genome (2) with primers ORF65for and ORF65rev (Table 1). The amplicon coded for a proposed ORF65 promoter sequence as well as the whole ORF65. The primers added an *SspI* and *BclII* site to the amplicon. The PCR fragment was then cut with *SspI* and *BclII* and inserted into the above described plasmid pOTO-gfpSCP (88) which resulted in pOTO-ORF65.

pOTO-ORF65-GFP was generated by amplifying the GFP coding sequence from pEGFP-C1 (Clontech) with primers EGFP65for and EGFP65rev (Table 1) which added *StuI* and *ApaI* sites to its ends and inserting this fragment into pOTO-ORF65.

pOTO-ORF65-mCherry was generated by digesting pOTO-ORF65-EGFP with *StuI* and *ApaI* and inserting a PCR product generated by using primers mCherry65for and mCherry65rev (Table 1) using pmCherry-C1 (Clontech) as template which was digested with *AfeI* and *ApaI*. (20) pOTO-ORF65-EGFP and above described variants are coined rescue vectors through this thesis as they are used to generate recombinant MHV-68 by a single step ectopic rescue (see chapter 1.4).

Recombinational cloning to generate yeast bait and prey vectors for yeast two hybrid (Y2H) tests was essentially done as described in Fossum et al. (37). The plasmids pOTO-S-GFP-SCP or pOTO-S-GFP-SCP* were used as PCR templates for insert amplification with primers attB1-S-GFP-SCP-attB2-SP, attB1-S-GFP-SCP-binding-negative-No-Stop-attB2-ASP and attB1-SCP-S-GFP-SCP-no-stop-attB2-ASP (supp. Table 1). Resulting PCR products were subjected to BP-recombination by Gateway-mediated recombination into pDONR-221 according to the manufacturer's instructions (Invitrogen). Subsequently, the coding regions were transferred to the prey plasmid pGADCg (102), generating the plasmids pGADCg-S-GFP-SCP and pGADCg-S-GFP-SCP* which code for a C-terminal fusion to the activation domain (AD).

The integrity of all constructs mentioned above was confirmed by restriction pattern analysis and DNA sequencing of modified elements.

2.5 Construction of recombinant MCMV and MHV-68 BACs

To generate an acceptor vector for the ectopic insertion of MHV-68 SCP-fusions, we replaced the M1 gene with an FRT site. To this end, a PCR product was generated with the primers Del M1 for and Del M1 rev (Table 1) on the pcp15 plasmid as a template. This linear fragment was then used to delete the region from bp 10662 to bp 12579 of the MHV-68 pHA BAC (2) representing M1 gene by homologous recombination mediated by recombinases expressed from the plasmid pKD46. The inserted Kanamycin-resistance cassette was subsequently deleted by an Flp-mediated recombination as described earlier (10). The resulting BAC was called pHA3-D2.

To insert the expression cassettes encoded by the above described rescue plasmids into the MCMV or MHV-68 BACs, we used the single step FRT/Flp system described originally for

2 | Materials and Methods

MCMV (10). *Escherichia coli* strain DH10B (Invitrogen) containing the MCMV pSM3fr- Δ m1-16-FRT BAC (62) or the MHV-68 pHA3-D2 BAC and the temperature-sensitive Flp recombinase expression plasmid pCP20 (85) were transformed with the various R6K gamma driven pOTO-constructs (88) carrying the different SCP fusions and treated as described previously (82). Correct recombination was verified by analysis of the restriction patterns of the respective BACs and sequencing of the inserted ORF.

2.6 Yeast two hybrid analysis

Y2H analysis of interactions between SCP constructs and MCP was performed as described in the manufacturer's protocol (BD Biosciences/Clontech). Briefly, the bait plasmid pGBKT7-MCP (37) was transformed into the yeast strain Y187 while the prey plasmids pGADCg-S-GFP-SCP and pGADCg-S-GFP-SCP* were transformed into the AH109 strain. Diploid yeast cells carrying both vectors were generated by mating the strains and subsequent selection on SDC-Leu-Trp medium. Growth of diploid cells on SDC-Leu-Trp-His medium was used to assess bait-prey interaction via the HIS3 reporter. Bait and prey vectors without inserts were used as a control.

2.7 Density gradient purification of virus particles

Nycodenz-gradient purification was essentially done as described in Doehner et al. (27). In brief, supernatants from virus-infected cells were centrifuged at low speed (5500 g/15 min) to remove cell debris. Afterwards, virus particles were concentrated by high-speed centrifugation (23000 g/210 min) and the resulting virus pellet was carefully resuspended in VS-buffer (0.05 M Tris, 0.012 M KCL, 0.005 M EDTA, pH 7.8). Free DNA/RNA was removed by overnight treatment with 625 U/ml *Benzonase* (Novagen) at 4° C. Afterwards, the resulting suspension was loaded onto a continuous 10-40 % Nycodenz (Axis-Shield) density gradient prepared on a *GradientStation ip* (Biocomp) and separated at 20000 g for 105 min in a Beckman SW28 rotor at 4° C. The resulting bands were visualized and collected on a *GradientStation ip*. Each fraction was analyzed by standard negative-stain electron microscopy (EM) (47), verifying their integrity and purity.

2.8 Analytical polymerase chain reactions (PCRs)

Viral DNA was extracted from cell culture supernatant of infected cells and gradient purified virions using the DNeasy blood and tissue kit (Qiagen) according to the manufacturer's instructions. For qualitative analysis, PCR amplification was done using High-Fidelity PCR system (Roche) according to the manufacturer's instructions. PCR products encoding potential SCP fusions were gel-purified and sequenced.

In the case of MCMV, the viral DNA from purified virions was quantified by real-time PCR using an ABI Prism 7700 sequence detector (Applied Biosystems). Prior to amplification, the DNA which was extracted from gradient-purified, Benzonase (Novagen) treated virions and digested with *PaeI* for 1h, 37 °C followed by heat inactivation. To determine the ratio of viral DNA copy number to PFU, a quantitative PCR was performed for each sample in triplicate using MCMV M54 specific primers and probes as described by Scrivano et al. (95). Viral DNA copy numbers were calculated by relating the determined crossing point to a standard curve. The standard curve was generated by using serially diluted pSM3fr-BAC DNA as templates with known copy numbers and determining their crossing points based on the inherent M54 sequence. To normalize for loss of DNA during purification, we determined the ratio of a defined quantity of pSM3fr-BAC DNA before and after purification.

In the case of MHV-68, the viral DNA was purified and quantified by real-time PCR as described in (35).

2.9 Immunoblotting

In the case of MCMV, viral protein expression was analyzed 48 h after infection of a confluent layer of M2-10B4 cells in 6 cm dishes at a MOI of 1. Subsequently, cells were washed with DPBS and lysed in total lysis buffer (62.5 mM Tris, pH 6.8, 2% (v/v) sodium dodecyl sulfate (SDS), 10% (v/v) glycerol, 6 M urea, 5% (v/v) β -mercaptoethanol, 0.01% (w/v) bromophenol blue, 0.01% (w/vol) phenol red) plus 125 U of *Benzonase* (Novagen) for 90 min at 4° C. After denaturation at 95° C for 10 min, samples were loaded onto 15% SDS-polyacrylamide gels and separated by electrophoresis (SDS-PAGE).

To analyze proteins from purified virions, a sample corresponding to approximately 1.1×10^5 PFU of gradient-purified virus preparation per lane was mixed with trichloroacetic acid to a final concentration of 13% and incubated over night at 4° C. Precipitated protein was pelleted by

2 | Materials and Methods

centrifugation at 15.000 g for 15 min. The supernatant was discarded, the pellet was air-dried, and resuspended in total lysis buffer, neutralized with 1M NaOH, loaded onto a 15% SDS-polyacrylamide gels and separated by SDS-PAGE.

After SDS-PAGE, separated proteins of MCMV were transferred onto *Hybond-P* membranes (Amersham Biosciences) in the presence of blotting buffer (25 mM Tris, 192 mM glycine, 20% (v/v) methanol, pH 8.3). Membranes were blocked in TBS-T (Tris- buffered saline, 0.05% (v/v) Tween 20) containing 5% BSA for 1 h at room temperature (RT). To detect the SCP of MCMV, a polyclonal antiserum directed against SCP was generated by immunizing rabbits with Ovalbumin (OVA) -coupled peptides corresponding to aa 36-50 and 59-86 m48.2 ORF (Metabion). To detect MCP, a rat polyclonal antiserum was used (88). GFP was detected by a polyclonal rabbit antiserum (Invitrogen). The blocked membranes were incubated with the respective antisera overnight at 4° C and subsequently washed with TBS-T and incubated with the appropriate horseradish peroxidase-conjugated (POX) secondary antibody (Dianova). The HA-tag was detected with a HA-specific, POX-conjugated monoclonal rat antibody (Roche) according to the manufacturer's instructions.

In the case of MHV-68, one million NIH-3T3 cells were infected at a MOI of 1 in 6-well plates and incubated for 24 h. Subsequently, cells were washed with DPBS and lysed in total lysis buffer, and blotted as described in (82). To detect MHV-68 SCP, a hybridoma supernatant was used (43). A polyclonal anti-MHV-68 rabbit serum was used as to detect further virus proteins as a loading control (101). GFP was detected by a polyclonal rabbit antiserum (Invitrogen) and mCherry by a polyclonal rabbit antiserum (kindly provided by T. Mertens, Ulm). The membranes were incubated with the appropriate horseradish peroxidase-conjugated secondary antibody (Dianova).

All Western blot reactions were visualized with SuperSignal West Dura Extended Duration Substrate (Pierce) using a Fusion luminiscence reader (Vilber).

2.10 Immobilization of virions on glass coverslips

Immobilization of MCMV virus particles was performed by loading approximately 1×10^5 PFU of density gradient-purified virus preparations diluted in 200 μ l DBPS onto fibronectin-coated glass coverslips and incubated for 1 h at 37°C. In the case of MHV-68, supernatant from infected cells was cleared by low-speed centrifugation (1200 g/ 5 min) and loaded

2 | Materials and Methods

directly onto fibronectin-coated glass coverslips and further processed as described above. After binding, virions were subjected to immunostaining as described below.

2.11 Immunostaining for microscopy

Indirect immunofluorescence (IF) analysis was carried out on glass slides, channel- or 8 well μ -slides (Ibidi) by fixing cells or virions with 4 % PFA in DPBS (w/v) for 10 min at 37° C. The fixative solution was replenished twice with DPBS and the cells were permeabilized for 10 minutes with a solution of 0.1% Triton X-100 in DPBS. After extensive washing with DPBS, the cells were blocked using 3 % (w/v) bovine serum albumin (BSA) in DPBS (blocking solution) for 1 h at RT. Primary antibodies (see chapter 1. 8 for detailed description) were applied in blocking solution and incubated with the cells or virions at room temperature (RT) for 1 h followed by three DPBS washing steps and 1 h incubation at RT with 1:1000 dilutions of Alexa Fluor-conjugated, specific secondary antibodies (Invitrogen) in blocking solution. After a final extensive washing step with DPBS, the preparations were imaged directly or mounted on glass slides with Prolong Gold resin (Invitrogen).

2.12 Fluorescence microscopy

Confocal laser scanning microscopy was performed with either a Zeiss LSM510 Meta system, a LSM710 system or an Olympus FV1000 system equipped with high numerical aperture oil immersion objectives. GFP and mCitrine proteins were excited with a 488 nm laser line. mCherry was excited with a 543 nm or 561 nm laser line. Protein fluorescence emission was detected using corresponding filter sets of the microscopes. Alexa Fluor-Dyes were detected corresponding to the manufacturers' instructions. Pinhole diameters were adjusted to a width corresponding to an optical slice thickness of 1 μ m for all channels. Pixel sizes were chosen based on the Nyquist criteria and varied around 110 nm/Pixel in case of a 63x, NA 1.4 objective. In general, imaging conditions were chosen which resulted in an optimal compromise between light exposure and detector noise and were kept constant in between acquisitions of the same experiment.

Live cell imaging was performed with cells growing in μ -slides (Ibidi) or glass-bottom dishes (MatTek). During acquisition, the cells were incubated in an environmentally controlled chamber at 37°C with either 5% CO₂ or in CO₂-independent medium (Invitrogen). All images were processed according to the guidelines of the Journal of Virology

2 | Materials and Methods

(<http://jvi.asm.org/cgi/reprint/85/1/1>) using ImageJ (1) as well as Photoshop CS4 (Adobe) software. Specially, noise in time-lapse stacks was reduced by Kalman filtering in ImageJ. Gradiual bleaching was corrected by using the ImageJ Bleach Correction plugin (written by J. Riedorf). All images were contrast-enhanced to optimize for printing.

2.13 Single Particle Tracking

The single virus particle fluorescence patterns obtained were fitted by a two-dimensional Gaussian function:

$$I = A_0 e^{-\frac{(x-x_0)^2}{2\sigma^2}} e^{-\frac{(y-y_0)^2}{2\sigma^2}} \quad (\text{Equation 1})$$

where A_0 and σ are the amplitude and the width at half-maximum of the two-dimensional Gaussian curve, and x_0 and y_0 the coordinates of the position of the individual virus particles. The single particle tracking procedure was automated using a custom-written Labview software (National Instruments) (51).

For each trajectory, a set of values for the square displacement, $r^2(t)$, between two observations separated by the time lag $t_{\text{lag}} = n \cdot \Delta t$ (where Δt is the time interval between successive frames of the movies, $n = 0, 1, 2, \dots, N-1$ with N being the total number of points in a trajectory) was computed according to:

$$r^2(t) = (\vec{r}(t + t_{\text{lag}}) - \vec{r}(t))^2 \quad (\text{Equation 2})$$

The Mean Square Displacements $\text{MSD} = \langle r^2(t) \rangle$ were then plotted for every time lag t_{lag} and the MSD plots were fitted for the 10% first time lags (10 points) assuming three different modes of possible motion (92):

$$\text{Normal diffusion} \quad \text{MSD} = 4 D t \quad (\text{Equation 3})$$

$$\text{Anomalous diffusion} \quad \text{MSD} = 4 D t^\alpha \quad (\text{Equation 4})$$

$$\text{Directed motion with diffusion} \quad \text{MSD} = 4 D t + (vt)^2 \quad (\text{Equation 5})$$

where D is the diffusion coefficient, α the anomalous exponent and v the velocity of the

directed transport.

To determine for each single trajectory which mode of motion described the data best, each MSD plot was fitted by Equations 3, 4 and 5 and the reduced chi-squared of the fits were compared. The normal diffusion model (Equation 3) was used as long as the more complex model functions of for anomalous diffusion (Equation 4) and directed motion with diffusion (Equation 5) did not resulted in a at least two-fold decrease of the reduced chi-squared of the fit. In cases in which this condition was fulfilled, the mode of motion with the minimum reduced chi-squared was chosen. Hence, this procedure leads to the clustering of diffusing particles into three distinct classes representing different modes of diffusion.

Track separation of entry data was done manually by choosing sub-trajectories in which the particles clearly exhibit long-distance movements. Each obtained sub-trajectory was then analyzed individually by computing their MSDs and fitting the resulting MSDs plots according to Equation 5.

2.14 Transmission electron microscopy

NIH 3T3 or M2-10B4 cells were grown on carbon-coated sapphire discs and infected at a MOI of 0.5 with centrifugal enhancement at 1600 g/RT for 30 min. After an additional hour, the inoculum was replaced by normal medium and cells were incubated for 48 h. Then, cells were fixed by high-pressure freezing with an *HPF 01* instrument (M. Wohlwend GmbH), freeze-substituted, and plastic embedded as described previously (107). Embedded samples were thin-sectioned and viewed on a Zeiss EM 10 at 80 kV in transmission mode. The phenotype of infected NIH 3T3 or M2-10B4 cells did not differ. Pictures were recorded on EM film (MACO), digitalized at 1200 dots per inch, contrast-enhanced and sharpened with an unsharp mask according to the guidelines of the Journal of Virology (<http://jvi.asm.org/cgi/reprint/85/1/1>) in Photoshop CS4 (Adobe).

3 Results

3.1 Construction of capsid-tagged fluorescent beta- and gamma-herpesviruses

Our aim was to study beta- and gamma-herpesvirus capsid dynamics in living cells. While viable capsid-tagged alpha-herpesviruses were reported some time ago (14, 24, 38, 99) no viable, fluorescent, capsid tagged beta- or gamma-herpesviruses could be achieved. Therefore, we first dissected the published approaches to succeed in generating capsid-tagged fluorescent herpesviruses. Most previous attempts have in common that they tried to label the SCP. Due to the location of this protein at the outer shell of the capsid, it should allow bulky protein-tags to be added without sterically disturbing important protein-protein interactions. However, the SCP is essential in beta- and gamma-herpesviruses (8, 48, 78), but not essential in HSV, PRV and VZV (14, 23, 52).

Therefore, we set out to develop mutagenesis approaches that would allow us to fuse a fluorescent protein to the essential SCP, while at the same time keep the recombinant viruses viable.

3.1.1 Construction of capsid-tagged MCMV recombinant

All published trials to tag beta-herpesvirus capsids were based on the direct fusion of the FP at the very N-terminus of the SCPs, which resembled the strategy originally published by Desai et al. (24). The resulting fusion proteins were non-functional and in some cases even dominant-negative, thereby preventing virus reconstitution (8, 48, 88).

Therefore, we reasoned that a free N-terminus or a sequence motif at the very N-terminus of the beta-herpesvirus SCP is essential for its function. This was further supported by an alignment of aa sequences of all annotated beta-herpesvirus SCPs, which showed some conservation in this region (Figure 3-1).

Of most importance in this context was the observation that MCMV encodes for a GS-linker like sequence in its SCP N-terminus (aa 10 to 34). This linker seems to separate the N-terminus into two distinct regions (Figure 3-1). We proposed that this linker gives the N-terminus the flexibility that may be required for its interaction with other capsid proteins. A bulky fusion partner like GFP would either hinder these interactions by sterical means, or the given flexibility of this linker sequence may not tolerate the unusual enlargement in size.

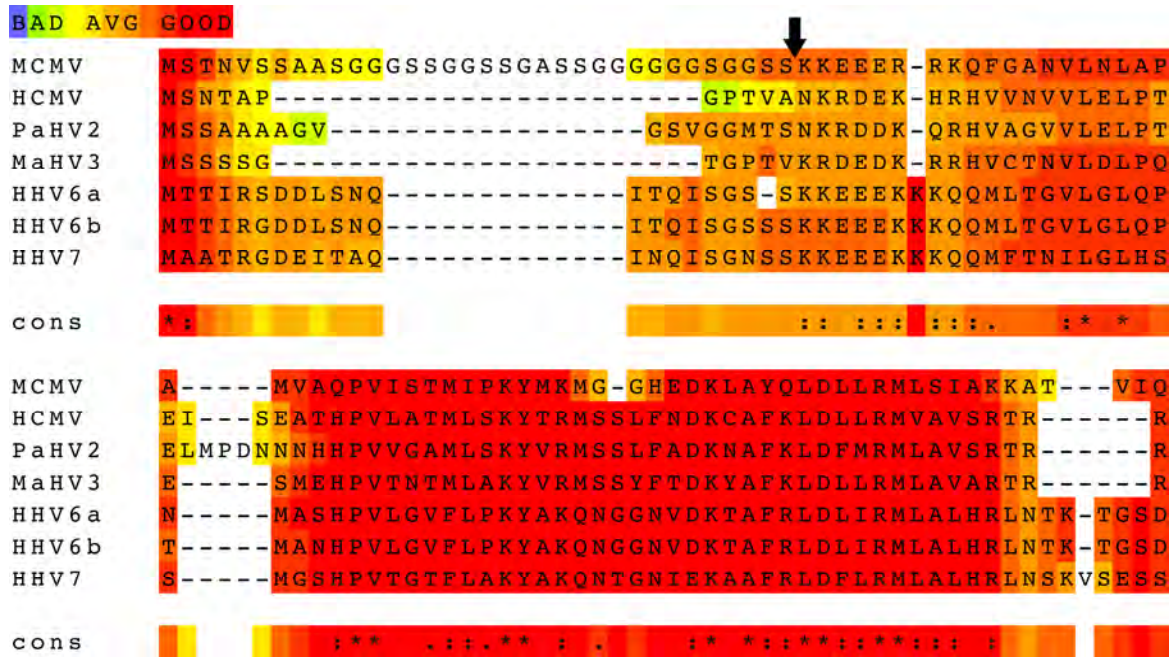


Figure 3-1: Alignment of beta-herpesvirus SCPs sequences

The shown alignment of all annotated beta-herpesvirus aa sequences was done with T-Coffee (<http://www.igs.cnrs-mrs.fr/Tcoffee/tcoffee.cgi/index.cgi>). Colors indicate the alignment quality ranging from blue (“bad”) to red (“good”). A naturally occurring glycin-serin-linker like sequence separates the N-terminus in MCMV. The very N-terminal region until the black arrow was duplicated and fused to various tags followed by the full length SCP.

Therefore, we decided to duplicate the very N-terminal region consisting of the first 34 aa and fused it, separated by an additional linker and a HA-tag, to the N-terminus of GFP. This construct was then fused to the full length SCP sequence, which includes a second, WT-copy of the N-terminal domain (Figure 3 2). As this construct is composed of the first third of SCP (S), the GFP and the full length SCP, we named this construct S-GFP-SCP. To allow BAC technology-based insertion into the viral genome by an Flp mediated reaction, we constructed these fusion genes using the previously published pO6-IET-gfpSCP plasmid (88). The plasmid pOTO-S-GFP-SCP was inserted ectopically into the pSM3fr-Δm1-16-FRT BAC. As the coding sequence of the fluorescent protein (FP) in the pOTO-S-GFP-SCP vector was flanked by SpeI-sites, it allowed the SpeI-mediated removal of the FP resulting in a fusion construct that was just tagged with an HA-tag. This construct was used to control for size dependent effects of the insertion. To enable the detection of the construct also in different imaging setups, we replaced the GFP coding sequence with the open reading frames of mCitrine or mCherry, keeping the same SCP context. **Figure 3-2** generally depicts the resulting constructs.

3 | Results

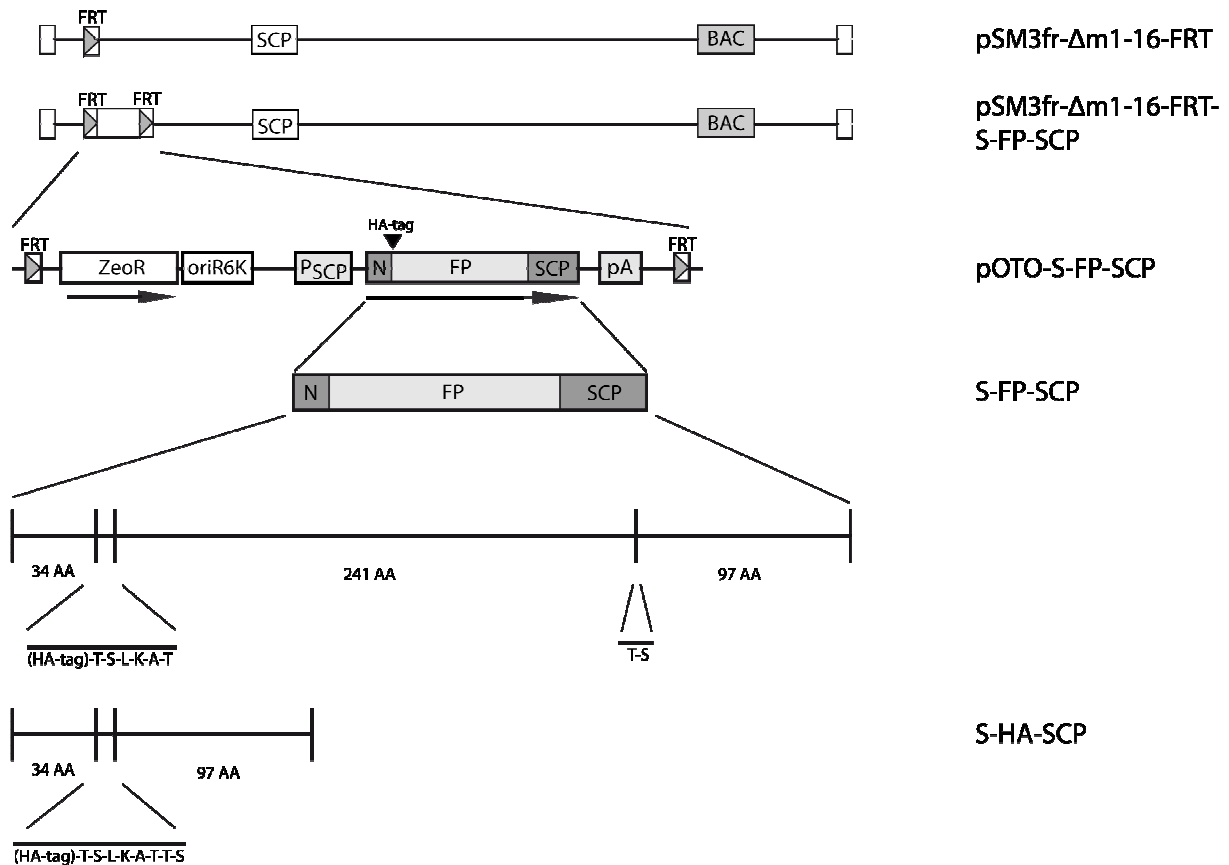


Figure 3-2: Construction of MCMV S-FP-SCP fusion proteins.

Detailed representation of the S-GFP-SCP fusion protein as well as the basic genetic layout of the used mutant viruses carrying a fluorescent protein (FP) and a hemagglutinin tag (HA). GFP or mCherry were used as FPs. The FP could be removed by a simple SpeI-mediated digest resulting in a construct encoding for just a HA-tagged SCP (S-HA-SCP). N marks the duplicated N-terminal region of SCP. The plasmids carrying the fusion constructs were inserted into the MCMV BAC by F1p-mediated recombination.

3.1.2 Reconstitution and basic characterization of recombinant MCMVs

Transfection of the pSM3fr- Δ m1-16-FRT-pOTO-S-FP-SCP constructs in NIH-3T3 cells resulted in fluorescent plaques with a distinct fluorescence pattern, which mainly localized to the nuclei of infected cells (see Figure 3-1 for a representative example of the S-GFP-SCP expressing recombinant). Plaque morphologies as well as size were comparable to WT virus plaques (Figure 3-3 and Figure 3-4 B). Comparable results were obtained for the other S-FP-SCP and the S-HA-SCP expressing recombinants (Figure 3-4 B). To elucidate the growth kinetics of the recombinant virus, we performed multi-step growth curves on MEF cells. The S-GFP-SCP as well as the S-HA-SCP mutant showed WT-like growth kinetics (Figure 3-4 A).

3 | Results

To compare the infectivity of the S-GFP-SCP virions to that of WT virions, we determined the genome to PFU ratio. To this end, we prepared gradient purified virus stocks of both viruses that were routinely checked for virion integrity and purity by negative-stain electron-microscopy. Subsequently, we determined the infectivity of the preparations by standard plaque assay as well as genome copies by quantitative PCR. The measured genome copies should equal the amount of DNA packaged into virus particles, as the virus stocks were treated with the DNA-degrading enzyme Benzonase during the purification process.

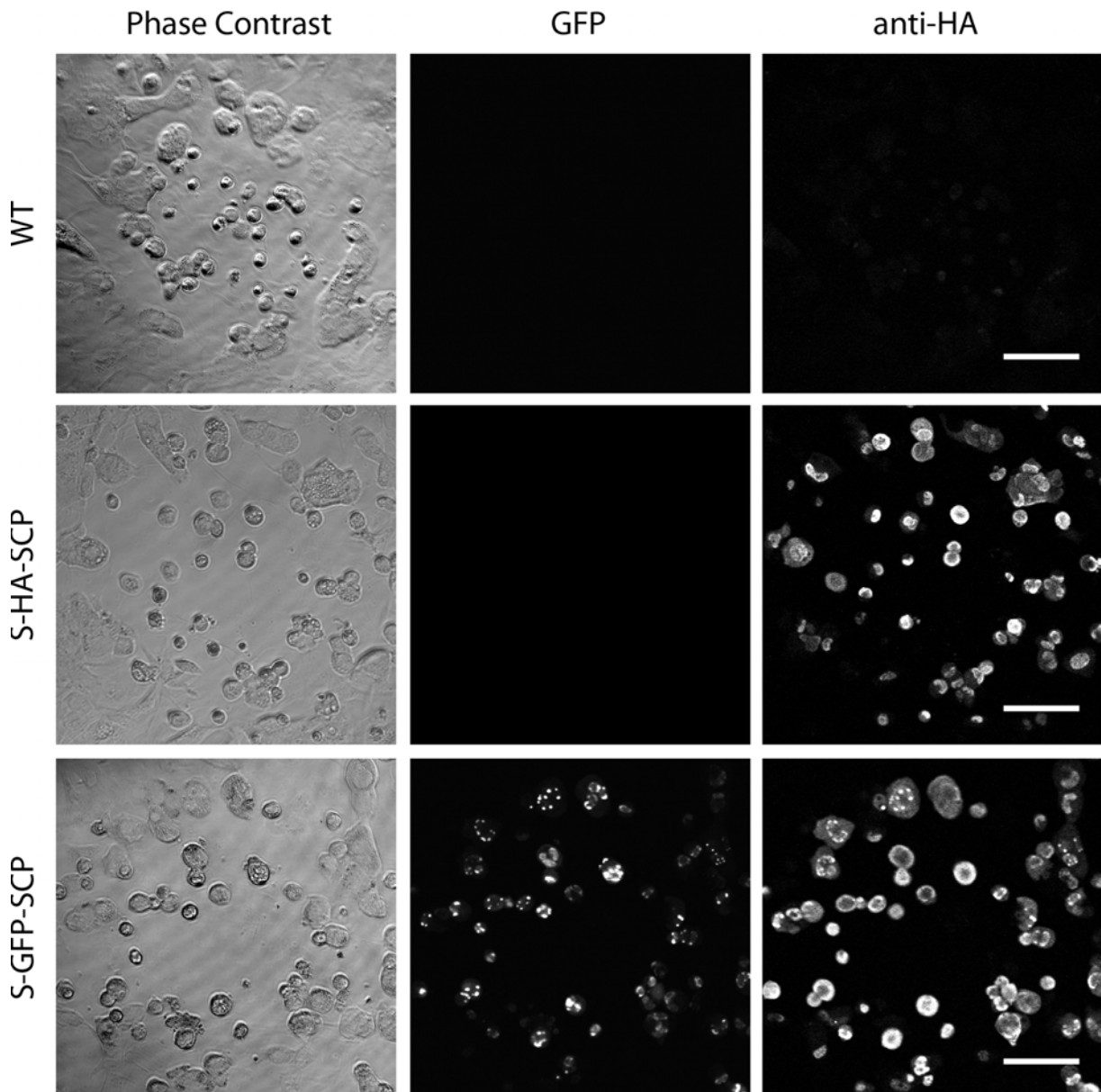


Figure 3-3: Plaque-phenotype of tagged MCMV mutants.

WT (WT) as well as mutant viruses coding for either HA- (S-HA-SCP) or HA-GFP-tagged SCP (S-GFP-SCP) were titrated on MEF cells. 4 days post infection (dpi) cells were fixed with PFA and processed for immunofluorescence against the HA-epitope. The scale bars represent 100 μm .

3 | Results

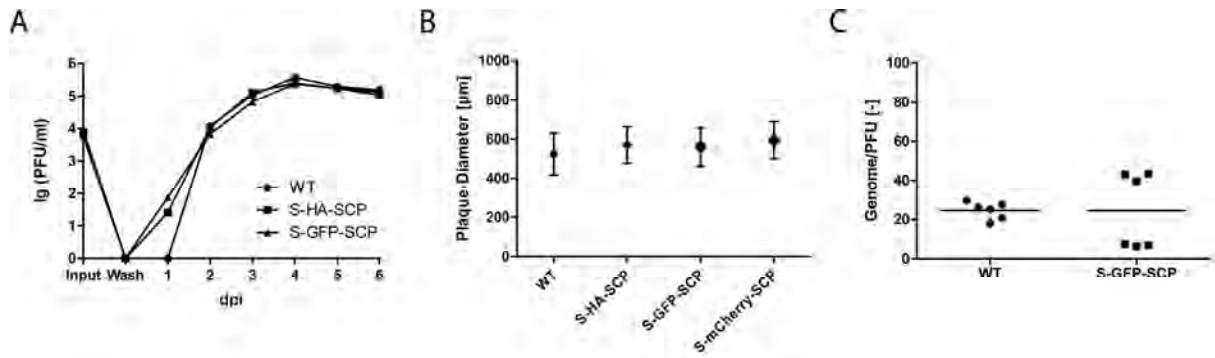


Figure 3-4: Tagged MCMV mutants are viable.

(A) Multistep growth curve of mutant viruses in comparison to WT virus. (B) Comparison of plaque diameters of simultaneously titrated WT, HA-, GFP-, and mCherry-tagged virus 4 days post infection (dpi) on MEF cells. (C) Genome to PFU ratio of GFP-tagged and WT virus. The ratio between genome content and titer for two independently prepared and purified virus stocks per virus was determined by titration and quantitative PCR in triplicates.

Average values from two independent gradient purifications with concurrent quantification of genome copies in triplicate, as well as titration to determine the amount of PFU, suggested that the S-GFP-SCP recombinant virus produces a genome to PFU ratio similar to that of WT virus (23 vs. 25 genomes/PFU, respectively) (Figure 3-4 C). From these data we concluded that our new SCP labeling approach did not detectably affect viability and infectivity of the recombinant MCMV.

3.1.3 Construction of fluorescent, capsid-tagged MHV-68 recombinants

As we were successful in the construction of a viable, capsid-tagged MCMV, we next asked if we could transfer this capsid-labeling strategy to gamma-herpesviruses. Because both the previously reported HSV-1 recombinant (22, 24, 72) and the MCMV-S-FP-SCP can productively infect MEF cells, we decided to modify MHV-68, which is the only known gamma-herpesvirus that infects mouse cells productively in vitro. We reasoned that by generating a capsid-tagged MHV-68, we would have a panel of labeled model viruses in hands that represented all three herpes subfamilies. With such a system, one cell type could serve to compare general principles of herpesvirus morphogenesis.

3 | Results



Figure 3-5 Alignment of gamma-herpesvirus SCP sequences with ClustalW (REF).

A naturally occurring glycine-serine-linker like sequence separates the N-terminus and C-terminus of the Alcelaphine herpesvirus 1 (AIHV1) SCP and also in the Ovine herpesvirus 1 (OvHV1) SCP sequences. MHV-68 SCP is referred as MuHV4.

Sequence alignments greatly facilitated the determination of potential insertion sites in the case of beta-herpesviruses, therefore we applied the same strategy to gamma-herpesvirus SCPs. Figure 3-5 shows a ClustalW alignment of all gamma-SCP sequences currently available in Uniprot (www.uniprot.org). Corresponding to this alignment, the N-terminal region until approximately position 140 to 150 as well as the very C-terminus seemed to be conserved. Surprisingly and similarly to MCMV SCP, a glycine-serine rich sequence stretch could be found in the Alcelaphine herpesvirus 1 (AIHV1) SCP and to a limited extent also in the Ovine herpesvirus 1 (OvHV1) SCP sequence as well as just before the less conserved C-terminal domain in the other sequences, indicating a hinge region between the two conserved parts of the gamma-HV SCPs, can be found. This stretch apparently separated the longer conserved N-terminal region from the shorter C-terminal region, indicating structural domains interspaced by a flexible linker sequence. We therefore reasoned that the insertion of an FP between these two potential protein domains should be tolerated in the MHV-68 ORF65, as it was the case in MCMV.

3 | Results

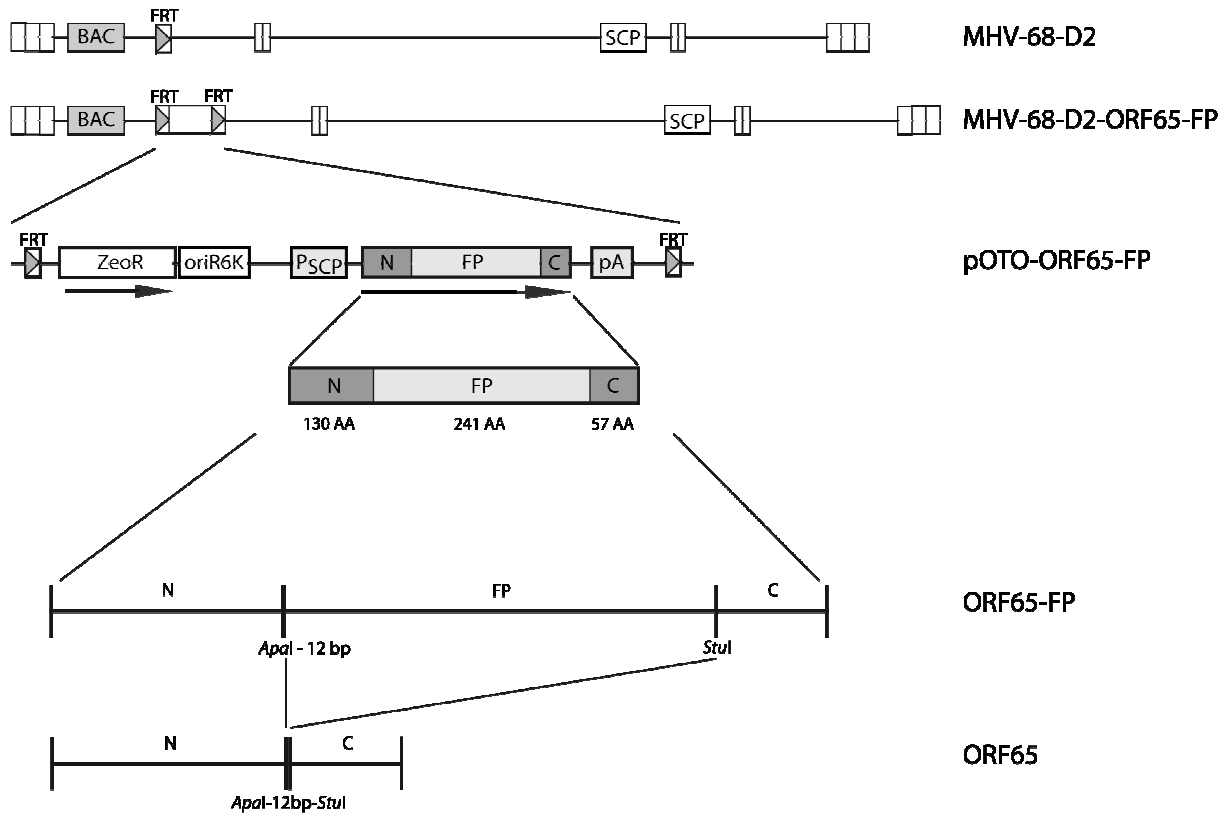


Figure 3-6: Construction of MHV-68 ORF65-FP fusion proteins.

Detailed representation of the ORF65-FP fusion protein as well as the basic genetic layout of the used mutant viruses carrying a fluorescent protein (FP)). GFP or mCherry were used as FPs. N marks the N-terminal and C the C-terminal region of SCP. The plasmids carrying the fusion constructs were inserted into the MHV-68 BAC by Flp-mediated recombination.

We therefore cloned the ORF65 coding sequence as well as the 300 bp upstream sequence as a probable promoter sequence into the R6K gamma driven pOTO-backbone generated for the MCMV tagging (Figure 3-6). The EGFP or mCherry coding sequence was inserted directly into the MHV-68 SCP between aa 132 and 133 without further addition of linker sequences.

The resulting plasmids pOTO-ORF65-GFP and pOTO-ORF65-mCherry were then transferred by Flp-mediated recombination into a modified MHV-68 BAC (pHA3-D2) harboring an FRT site replacing the M1 gene, resulting in a recombinant virus coding for both a WT- and a second tagged SCP copy.

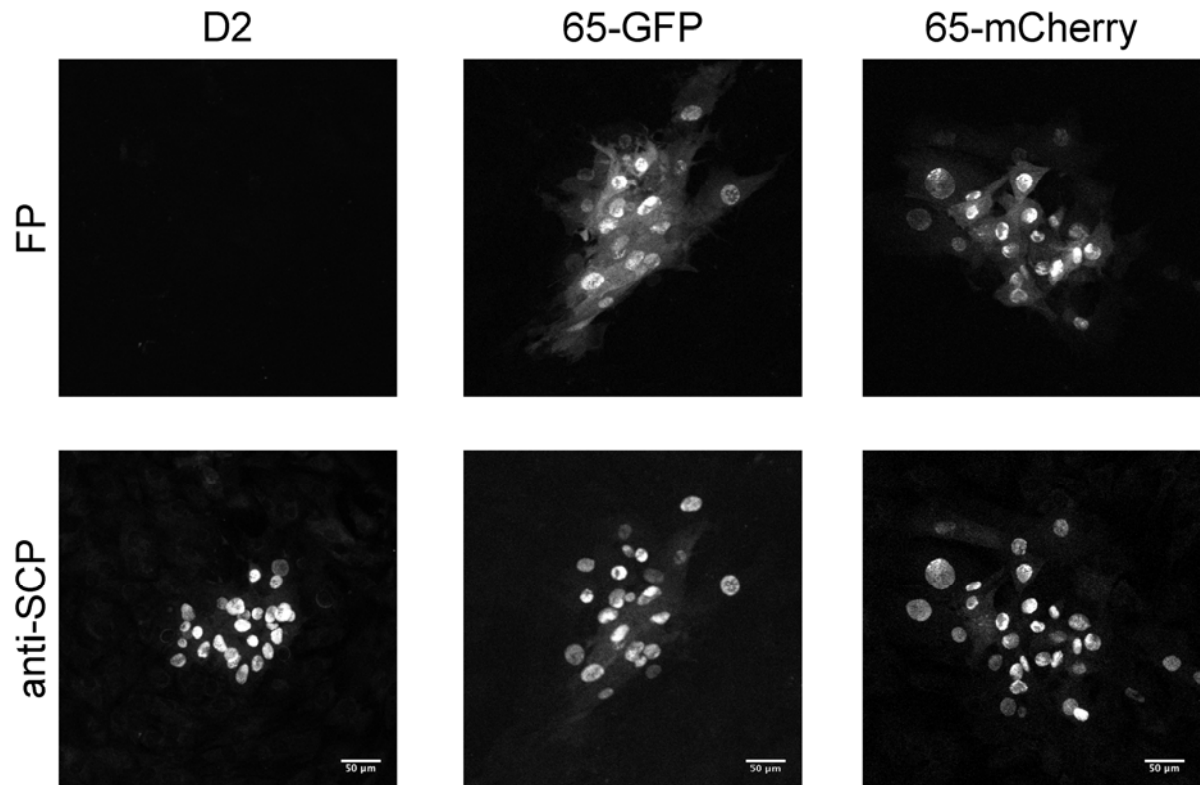


Figure 3-7: Plaque phenotype of GFP-tagged MHV-68 mutant.

WT (WT) as well as mutant viruses coding for either HA- (S-HA-SCP) or HA-GFP-tagged SCP (S-GFP-SCP) were titrated on MEF cells. 4 days post infection (dpi) cells were fixed with PFA and processed for immunofluorescence against the HA-epitope. The scale bars represent 50 μm .

3.1.4 Reconstitution and basic characterization of recombinant MHV-68s

Similar to the reconstitution of capsid-tagged MCMV recombinants, transfection of REF-Cre cells with recombinant MHV-68 BACs resulted in fluorescent plaques with a distinct fluorescence pattern, which mainly localized to the nuclei of infected cells (Figure 3-7). Plaque-morphology as well as -size were again comparable to WT plaques (Figure 3-7 and Figure 3-8 B). The same results were obtained for the ORF65-mCherry expressing recombinants (Figure 3-8 B). To elucidate the growth kinetics of the recombinant virus, we first studied the influence of the M1 deletion and FRT-site insertion. We therefore performed multi-step growth curves on MEF cells. The ORF65-GFP encoding recombinant was comparable to WT-virus. Interestingly, the MHV-68-D2 parental mutant grew slightly better compared to WT-BAC derived virus (Figure 3-8 A).

3 Results

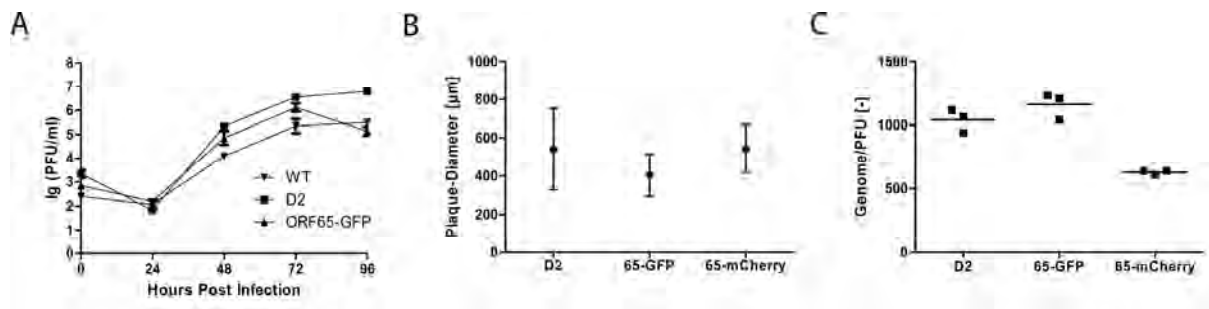


Figure 3-8: Tagged MHV-68 mutants are viable.

(A) Multistep growth curve of MHV-68-D2 (D2) and MHV-68-D2-ORF65-GFP (65-GFP) in comparison to WT virus (WT). (B) Comparison of plaque diameters of simultaneously titrated WT, GFP and mCherry-tagged (65-mCherry) virus 4 dpi on MEF cells. (C) Genome to PFU ratio of GFP- and mCherry-tagged virus in comparison to WT virus. The ratio between genome content and titer for two independently prepared and purified virus stocks per virus was determined by titration and quantitative PCR in triplicates.

The infectivity of the ORF65-GFP tagged virions was compared to that of the WT by determining the particle to PFU ratio. We observed in pretests that supernatants of MHV-68 infected cells seemed to contain only small amounts of cell debris compared to MCMV. Therefore, it sufficed to use precleared (1200 g/ 5 min) supernatants of MHV-68 infected cells, which were harvested before cytopathic effect occurred. As described for MCMV, we determined the infectivity of the preparations by standard plaque assay as well as the genome content by quantitative PCR in triplicates. Average values of particle to PFU ratios suggested that the ORF65-EGFP virus produced very similar infectivity compared to WT virus (Figure 3-8 B C). Altogether, we concluded that our new tagging approach was associated with only minor effects on viability and infectivity of the recombinant MHV-68.

3.2 Characterization of Labeled Particles

Having shown that the MCMV S-FP-SCP as well as the MHV-68 ORF65-FP mutants had growth properties comparable to their respective WT-parents, we wanted to analyze if these viruses produced fluorescent virus particles and not only fluorescent proteins. To this end, MCMV or MHV-68 virions were immobilized on fibronectin-coated cover-slips and IF analysis was performed. An antiserum against the MCP (88) was used for MCMV, while a monoclonal antibody directed against MHV-68 SCP was used for MHV-68 to stain virus capsids. Additionally, an antiserum directed against the SCP fusion partner GFP was used in both cases to amplify possible weak endogenous GFP signals (Figure 3-9).

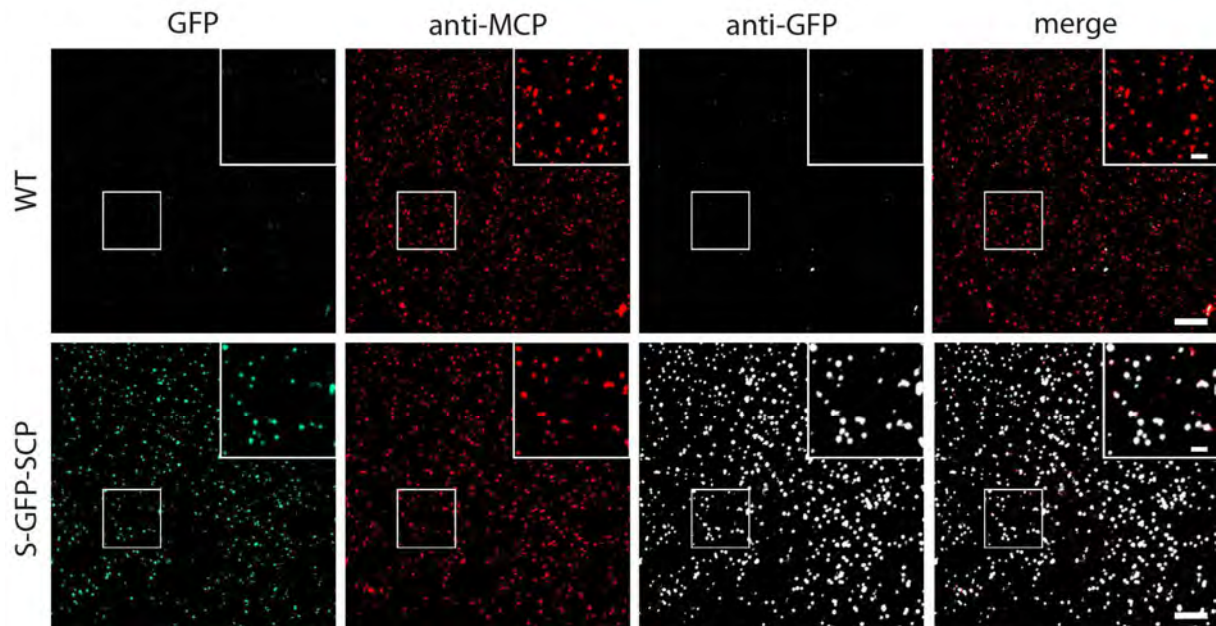


Figure 3-9: S-GFP-SCP produces a high percentage of labeled virus particles.

Gradient purified virus particles were immobilized on fibronectin-coated cover-slips, fixed and processed for immunofluorescence. A MCP specific polyclonal serum was used as indicator of virus capsids and a GFP specific polyclonal antiserum was used to compare MCP and GFP specific signals. Direct GFP fluorescence was detected by excitation with 488 nm laser light and appropriate emission filters. Inserts depict 2x magnifications. Scale bars represent 10 μm and 2.5 μm in inserts.

We then recorded the corresponding fluorescence signals and counted particle numbers in representative areas with the ImageJ plugin “Analyze Particles”. Colocalization was determined with the “Colocalization” command and subsequent counting of colocalized particles. In the case of MCMV we counted altogether 2653 MCP-positive particles. 91.46% \pm 3.88% of them colocalized with an antiserum directed against GFP, indicating that a high amount of particles incorporated detectable amounts of S-GFP-SCP. 83.42 % \pm 3.64% of all MCP-positive particles could also be detected by their endogenous GFP fluorescence.

In the case of MHV-68, 4807 particles out of 4972 (96.88 %) positive for SCP colocalized with the anti-GFP stain, while 4500 particles or 90.57 % detected by their GFP fluorescence colocalized with the SCP stain (Figure 3-10), indicating a slightly higher percentage of particles that could be visualized by their GFP labeling compared to MCMV S-GFP-SCP.

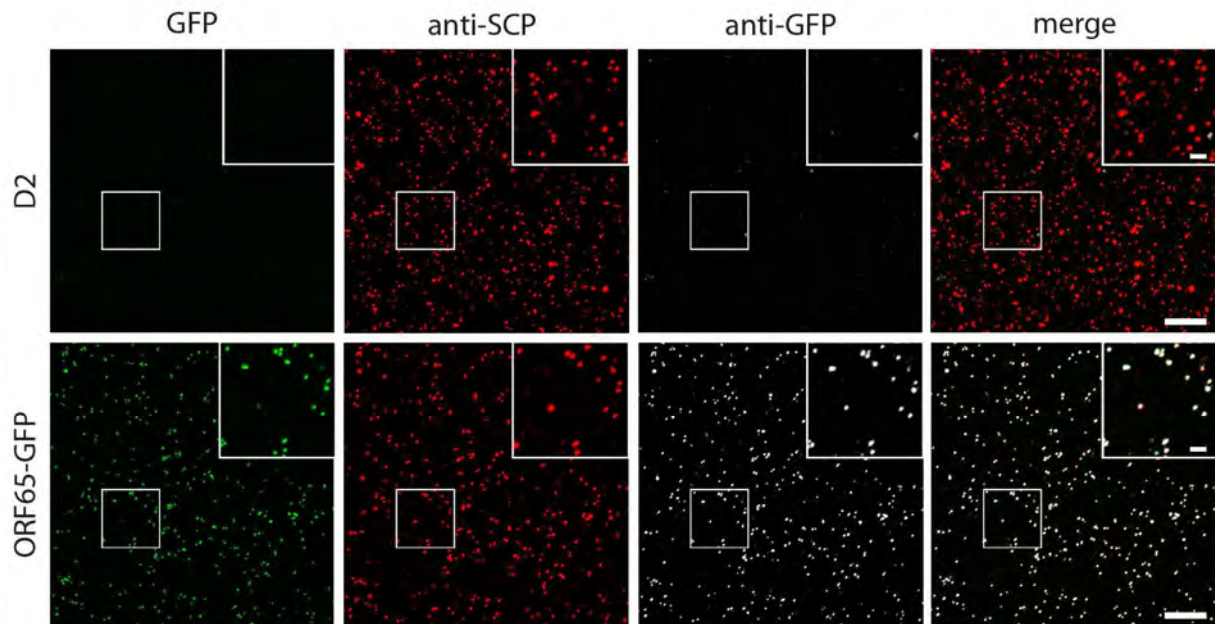


Figure 3-10: ORF-65-GFP labeled MHV-68 produces a high percentage of GFP labeled virus particles. MHV-68 virus particles were immobilized on fibronectin-coated cover-slips, fixed and processed for immunofluorescence. An SCP specific polyclonal serum was used as indicator of virus capsids and a GFP specific polyclonal antiserum was used to compare SCP and GFP specific signals. Direct GFP fluorescence was detected by excitation with 488 nm laser light and appropriate emission filters. Inserts depict 2x magnifications. Scale bars represent 10 μm and 2 μm in inserts.

Knowing the approximate proportion of GFP labeled particles produced by the respective viruses, we next wanted to determine the approximate ratio between GFP-labeled and non-labeled SCP molecules on virus capsids. Thus, we used WT and GFP virus preparations and visualized the mean ratio of tagged to WT SCP by Western blotting and concurrent immunostaining specific to SCP and GFP. Gradient-purified virus stocks were used in the case of MCMV as well as MHV-68 to reduce contamination by free proteins originating from cell lysis to a minimum. We used two antisera per virus, one reacting with GFP and the other with either MCMV or MHV-68 SCP.

In the case of MCMV, we could detect WT SCP in the parental as well as GFP tagged virus at approximately 15 kD, which is a little more than its calculated size of about 10 kD (Figure 3-11). By using the GFP reactive serum, we found several S-GFP-SCP specific bands. The upper two bands running at approximately 50 kD could also be detected by an antiserum reactive to SCP, indicating that at least these two bands correspond to S-GFP-SCP derivatives. These data indicated that the fusion protein is incorporated into virus particles. However, the detected specific bands were again running higher than the calculated molecular weight of the S-GFP-SCP, which is 42 kD. This might be in general due to the low complexity region at the N-terminus of the MCMV SCP, which contains a high amount of

3 | Results

glycins and serins.

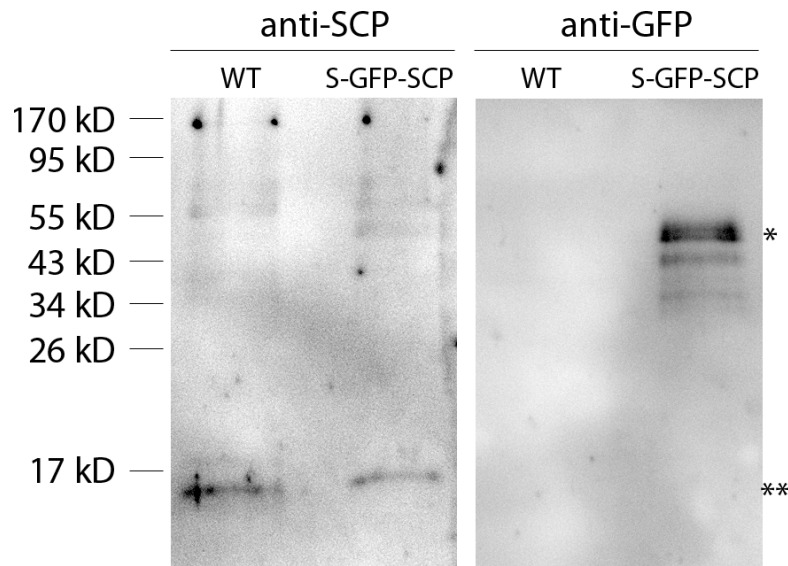


Figure 3-11: GFP-labeled SCP is incorporated into MCMV S-GFP-SCP virus particles.

Immunoblot of gradient-purified virus particles. Approximately $1.1 \cdot 10^5$ particles per lane were TCA-precipitated and lysed in total lysis buffer. Proteins were separated by SDS-PAGE, blotted and immunodetected with polyclonal sera for MCMV, SCP and GFP.

On the MHV-68 virion WB, we could detect the WT SCP protein at its calculated molecular weight of approximately 22 kD. The SCP-GFP fusion could be also detected at its calculated size of 49 kD. In comparison to MCMV S-GFP-SCP, no additional bands could be found (Figure 3-12).

To establish the approximate ratio between labeled and non-labeled SCP for both viruses, we quantified the SCP reactive signals and compared them with the signal found for WT SCP in the same lane by ImageJ.

For MCMV, the upper two S-GFP-SCP bands were used for quantification. An approximate signal ratio of GFP-fused SCP to unlabeled SCP of one third to two thirds was found. According to the current model of CMV virions, 900 WT SCP are incorporated into CMV particles (111). Therefore, our findings would translate to an average of 600 copies WT SCP and about 300 copies of S-GFP-SCP molecules per virus particle.

For MHV-68 we found a ratio of approximately two fifth of labeled to three fifth of non-labeled SCP. This would translate into about 540 copies of WT SCP and 360 SCP-GFP copies per virus particle (Figure 3-12).

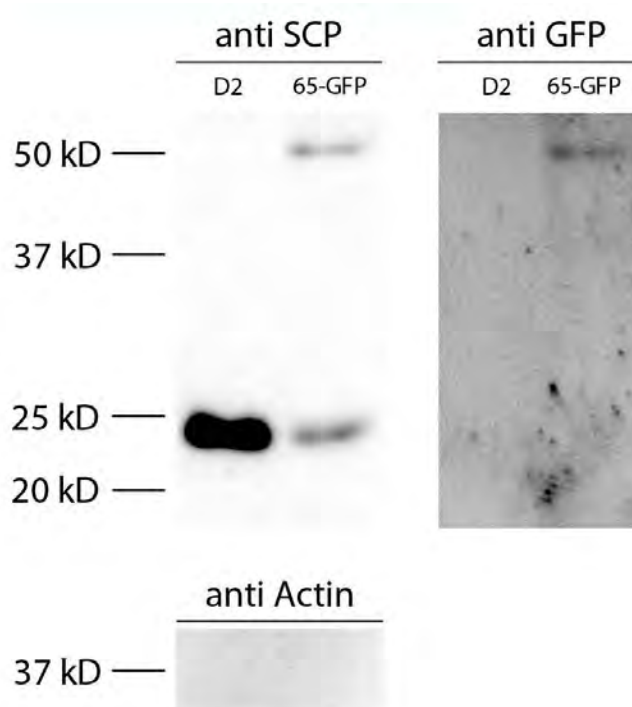


Figure 3-12: GFP-labeled SCP is incorporated into MHV-68 virus particles

MHV-68-D2 (D2) or MHV-68-D2-ORF65-EGFP (65-GFP) virus particles were gradient purified from supernatants and pelleted. Pellets were subsequently lysed in total lysis buffer. Proteins were separated by SDS-PAGE, blotted and immunodetected with a monoclonal antibody directed against MHV-68 SCP (anti SCP) or a polyclonal serum against GFP (anti-GFP). An antiserum against actin was used to control for cytoplasmic impurities.

3.3 MCMV S-GFP-SCP interacts with MCP

We could show that purified virus particles are fluorescent and that this fluorescence colocalizes with an anti-MCP staining. However, this assay is not sufficient to distinguish between a specific incorporation of the S-GFP-SCP into the capsid and the unspecific incorporation of the fusion protein into virions via the tegument due to its high abundance late in infection (see Figure 3-17). Therefore, we asked whether the S-GFP-SCP fusion protein could specifically engage with the capsid or a capsid constituent. It has been shown that HCMV SCP and MCP interact via a short C-terminal peptide of the SCP (54). We therefore checked first whether this was also true for the MCMV homologues used in our study. To this end, we deleted the corresponding peptide in the S-GFP-SCP fusion protein and tested this mutant (S-GFP-SCP*) as well as the parental S-GFP-SCP in an Y2H setup against MCP. The S-GFP-SCP fusion protein interacted with MCP while the S-GFP-SCP* mutant lacking the proposed MCP-binding region did not.

Knowing that S-GFP-SCP interacts with MCMV MCP via its MCP-binding motif, we were able to control the interaction between the S-GFP-SCP and the MCP in the virus context. It is

reported that the nuclear concentration of the HCMV SCP is dependent on its binding to MCP in the cytoplasm because it lacks a functional nuclear localization signal (NLS) (54). The observation of strong nuclear GFP signals in S-GFP-SCP infected cells (Figure 3-13) might therefore already argue for a MCP-dependent localization of S-GFP-SCP fusion proteins. To test this hypothesis directly, we constructed a recombinant MCMV expressing the S-GFP-SCP* mutant protein lacking its MCP interaction peptide. Cells infected with this recombinant virus did not show a specific nuclear S-GFP-SCP* accumulation, but instead a homogenous distribution of GFP fluorescence throughout the whole cell (Figure 3-13). We concluded that the S-GFP-SCP mutant interacts with MCP specifically and is therefore most likely correctly incorporated into the viral capsid during viral morphogenesis.

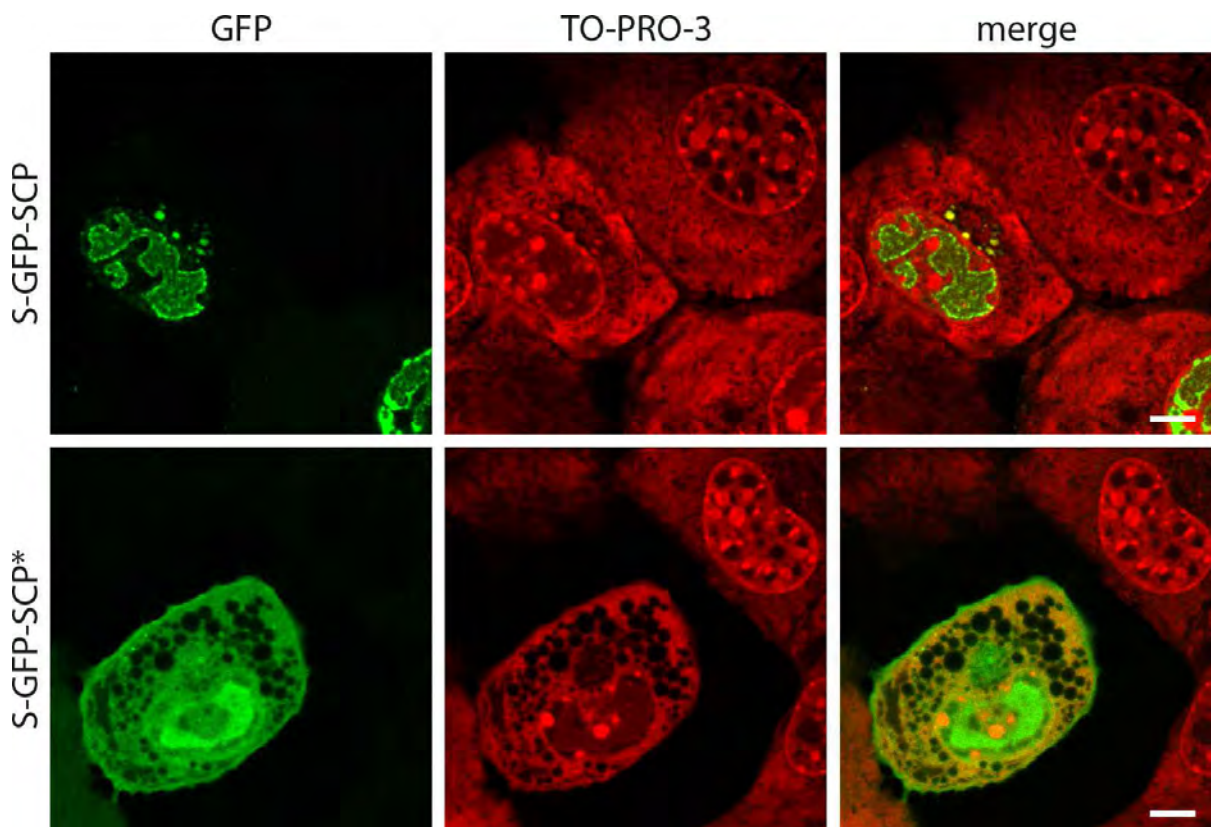


Figure 3-13: S-GFP-SCP nuclear transport is MCP dependent.

MEFs were infected at very low MOI with viruses expressing ectopically either S-GFP-SCP (top) or a S-GFP-SCP fusion protein lacking its proposed MCP-interaction peptide (S-GFP-SCP*, bottom). Cells were overlaid with methyl-cellulose after infection and fixed and processed for immunofluorescence 4 dpi. GFP fluorescence was visualized directly while the cytoplasm and cell nuclei were counterstained with a high concentration of TO-PRO-3, thereby staining whole cells but still indicating the cell nuclei. The mutant lacking the MCP interacting peptide is localized throughout the cyto- and nucleoplasm. Scale bars indicate 10 μ m.

3.4 Assessment of the genetic stability of capsid-tagged recombinant viruses

Viral genomes carrying unfavorable mutations are facing negative evolutionary pressure. The occurrence of adaptive genetic changes in a mutant locus is consequently a sign of reduced fitness associated with a mutation. This is important as beta- and gammaherpesvirus SCPs are essential for virus replication and thus even small growth defects combined with the strong recombinogenic potential of herpesviruses might lead to accumulation of non-fluorescent revertants. We therefore assessed the genetic stability of the capsid-tagged MCMV and MHV-68 mutants

3.4.1 MCMV S-GFP-SCP and S-HA-SCP labeled virus mutants are genetically stable

To address the genetic stability and to assess the fitness of our constructs, we passaged the S-GFP-SCP carrying virus 10 times on M2-10B4 cells. The number of 10 passages was chosen, as this is the maximum amount of passages used in our laboratory procedures. As controls we used WT virus and S-HA-SCP tagged virus. We reasoned that the latter serves as a good control for insertion-size dependent effects, given the very small size of the HA-tag compared to GFP.

First, we wanted to know how our fusion product was expressed and which changes in protein expression occurred after extended passages. We therefore infected M2-10B4 cells with passages 0, 5, and 10 of the above mentioned viruses. 48 hours post infection (hpi) cells were lysed and immunoblots specific for GFP, SCP and HA were performed. As shown in Figure 3-14, we could detect a SCP specific signal in all MCMV infected samples, however, the corresponding band (g in Figure 3-14) migrated again higher as predicted. Corresponding to this finding, we detected an S-HA-SCP specific band (band f) at approximately 22 kD instead of its predicted 12 kD with both the SCP and the HA tag specific antisera. In lanes corresponding to S-GFP-SCP infected cells, we could define three bands (bands a,b,c) that stained specific for SCP, GFP and the HA-tag. The two smaller ones (bands b and c), running near the 46 kD marker band were reminiscent of the ones found in purified virions (Figure 3-11) while a slower migrating band running beneath 58 kD (band a) marker was not detected in virions. Moreover, we could detect two more bands (bands d and e) beneath 46 kD which were stained positive only by the anti-GFP antiserum and seemed to be also found in blotted virus particles (Figure 3-11). More important, no major changes in protein expression levels nor in the banding pattern of SCP isoforms could be detected throughout 10 passages of any

3 | Results

of the recombinant viruses tested. These data indicated that the expression of the SCP fusion proteins by the recombinant viruses was stable for extended periods.

To test the genetic stability of the ectopic SCP locus at the sequence level, we amplified the region including the insertion locus by PCR from DNA purified from supernatants of cells infected with either passage 0, 5 or 10 of S-HA-SCP or S-GFP-SCP expressing viruses. The resulting PCR products were gel-purified, sequenced and checked for sequence alterations. Again, no alteration could be detected in either of the samples, arguing for extended genetic stability of both the S-HA-SCP and the S-GFP-SCP loci.

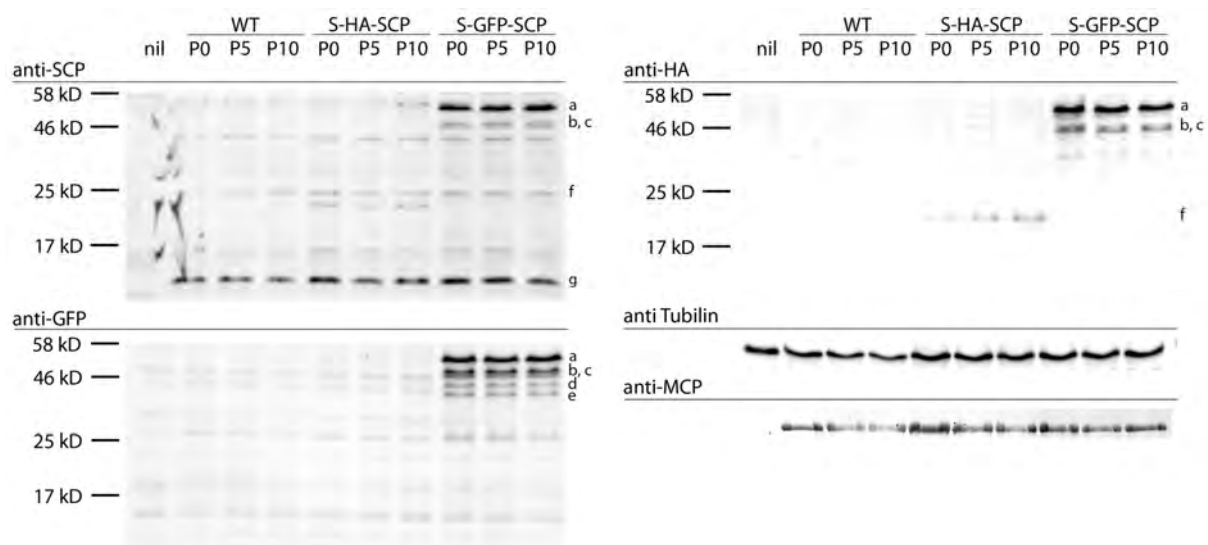


Figure 3-14: Viruses carrying labeled SCP mutants are genetically stable.

Immunoblot of M2-10B4 cells infected with either WT, S-HA-SCP, or S-GFP-SCP virus derived from passages 0, 5 or 10 after reconstitution. Cells were infected at a MOI of 1, and harvested 48 hpi by lysis in total lysis buffer. Proteins were separated by SDS-PAGE, blotted and immunoprobed for GFP, SCP, HA and MCP as well as beta-tubulin as loading controls. Lower case letters indicate specific protein bands.

3.4.2 MHV-68-D2-ORF65-FP viruses express less SCP-FP isoforms

As more SCP- and GFP-reactive bands could be detected on Western blots from MCMV-S-GFP-SCP infected cells, we next wanted to know if this was also the case for the ORF65-GFP tagged MHV-68 mutant. Here we had also the opportunity to compare SCPs tagged with different FPs after different number of passages. We therefore infected NIH-3T3 cells with low passage MHV-68-D2-ORF65-GFP, higher passage MHV-68-D2-ORF65-mCherry or MHV-68-D2 as a control for 24 h and blotted the lysates. As depicted in Figure 3-15, a polyclonal MHV-68 specific serum was used as a virus-expression control.

An antiserum against GFP revealed one band running shortly under 50 kDa. The same was

3 | Results

found with an antiserum reactive against mCherry (bands labeled with “a” in Figure 3-15). The monoclonal antibody 12B8 (43), reactive against MHV-68 SCP, detected bands running at the same height in lanes corresponding to GFP- or mCherry-tagged virus. As the ORF65-GFP and ORF65-mCherry fusion proteins had a theoretical molecular weight of 49 kDa, we assumed that these bands are the fusion proteins. Additionally, a band running between 25 and 20 kDa could be detected in all lanes corresponding to virus infected cell lysates (bands labeled “b” in Figure 3-15 with the anti-SCP antibody). As WT MHV-68 SCP has a theoretical molecular weight of 22 kDa, this fitted nicely. Notably, the amount of WT MHV-68 SCP expressed by the tagged viruses seemed to be decreased in comparison to non-tagged MHV-68. Moreover, the proportion of mCherry-tagged SCP to WT SCP seemed to be lower than in the case of GFP-tagged MHV-68, which might be because higher-passage virus stock was used to infect cells in the case of mCherry-labeled virus.

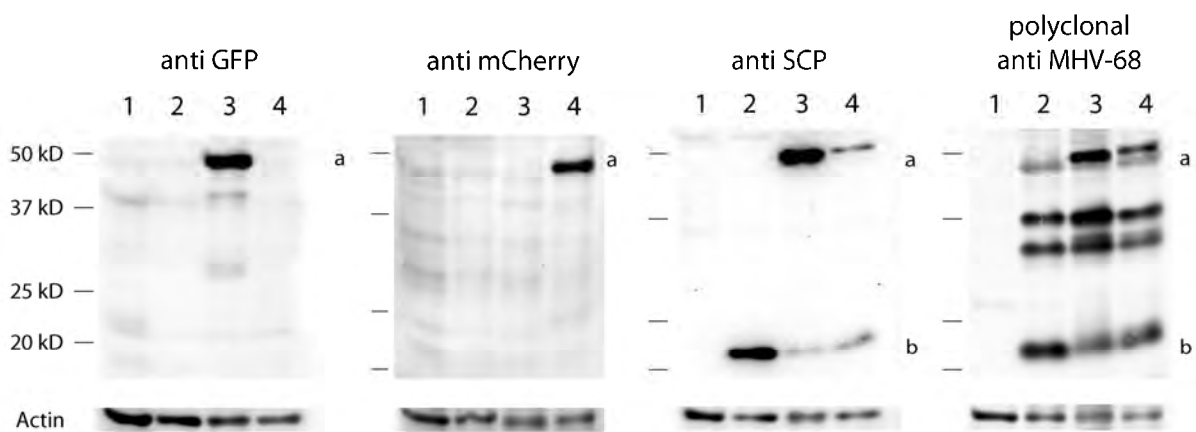


Figure 3-15: Capsid-tagged MHV-68 mutants express only one ORF-65-FP isoform.

Immunoblot of NIH-3T3 cells either mock-infected (1) or with a MOI of 1 of MHV-68-D2 (2), MHV-68-D2-ORF65-GFP (3) or MHV-68-D2-ORF65-mCherry (4). Cells were infected at a MOI of 1 and harvested 24 hpi by lysis in total lysis buffer. Proteins were separated by SDS-PAGE, blotted and immunoprobed for GFP, mCherry, MHV-68 SCP. A polyclonal anti MHV-68 antiserum (101) as well as an antiserum against beta-actin served as loading controls. Lower case letters indicate specific protein bands. The detected banding pattern with the anti SCP antibody matches the pattern detected in immunoblots from purified virus particles.

3.4.3 MHV-68 capsid-tagged viruses are not stable over extended passages

As we observed a decrease in the ORF65-mCherry-specific signal when we used a higher-passage MHV-68-D-ORF65-mCherry inoculum compared to a low-passage MHV-68-D-ORF65-GFP inoculum MCMV (Figure 3-15), we reasoned that the MHV-68-D-ORF65-FP genomes might not be stable over extended passages. We therefore assessed the genetic stability of ORF65-GFP labeled virus compared to its parental MHV-68-D2 virus by reconstituting these viruses from their respective BACs and passaged them on NIH-3T3 cells

for up to 10 passages. We could follow the loss of fluorescence over extended passages. Moreover, we sequenced four PCR-products spanning the whole insertion site as well as adjacent genome areas after passages 0, 5 and 10. Interestingly, we could not detect any sequence alteration, but a decrease in PCR products which indicated a loss of the GFP fusion sequence most likely due to recombination with the WT locus (data not shown). This notion was further supported by the fact that a virus deleted in WT SCP but ectopically tagged with the SCP-GFP fusion regained its WT SCP cassette after extended passages (data not shown). Therefore, we purified MHV-68-D2-ORF65-GFP by limiting dilution. Virus stocks were prepared from these limiting dilutions by restricting passages to an absolute minimum. In general, no more than 3 passages after limiting dilution were allowed. All used virus preparations used, were checked for non-fluorescent revertants by plaque-assay and staining against MHV-68 with an antiserum (101).

3.5 Normal morphogenesis of S-FP-SCP tagged recombinant MCMV

To analyze whether virus morphogenesis is affected due to the expression of the S-GFP-SCP fusion protein, cells were infected with S-GFP-SCP virus and processed for transmission EM 48 h post infection. As depicted in Figure 3-16, all major steps of virus morphogenesis e.g. capsid assembly, capsid packaging, primary envelopment in the nucleus as well as secondary envelopment appeared to be indistinguishable from WT virus with respect to phenotypic appearance and overall frequency. However, in some nuclei of S-GFP-SCP infected cells, semi-crystalline structures could be detected (data not shown). These structures mostly consisted of non-filled capsids similar to what was observed previously for a HSV VP26-mRFP virus (22), but also during WT HSV infection (74). These data demonstrated that the major intracellular steps of the viral life cycle appeared to be normal in the fluorescent tagged MCMV recombinant virus.

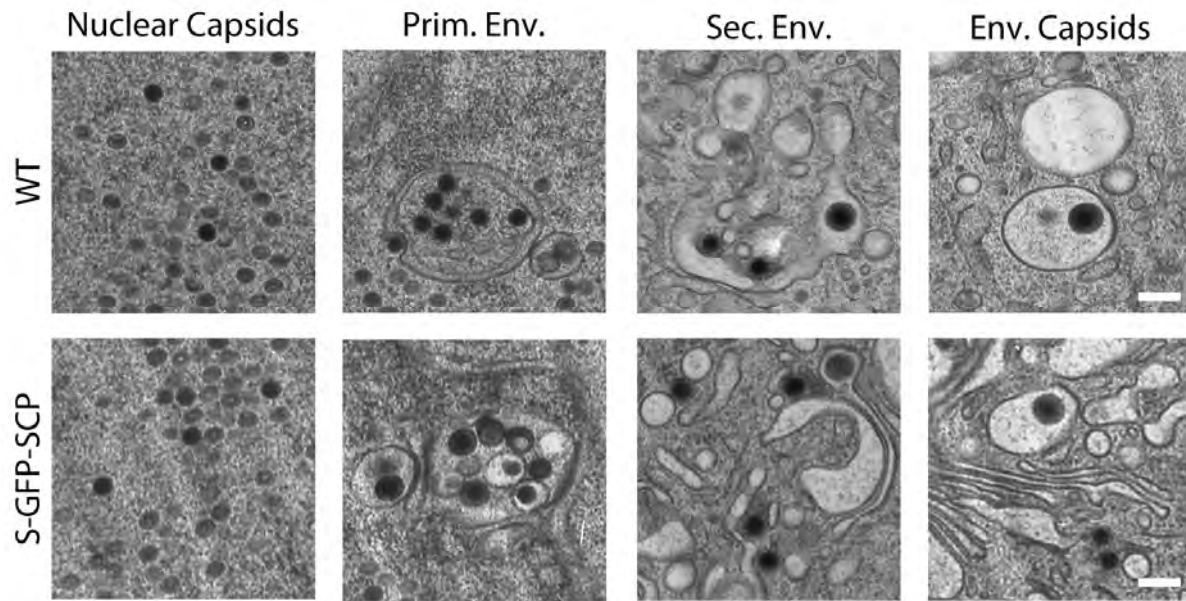


Figure 3-16: Ultrastructural assessment of S-GFP-SCP infected cells.

NIH-3T3 (upper row) or M2-10B4 cells (lower row) were infected at a MOI of 0.5 and centrifugal enhancement with WT (upper row) or S-GFP-SCP labeled virus (lower row) and incubated for 48 h. Afterwards, cells were high-pressure frozen, freeze-substituted, plastic-embedded and thin-sectioned. Depicted are representative details of two independent experiments showing non-enveloped B- and C-capsids in the nucleus (first column), primary envelopment in the nucleus (2nd column), non-enveloped C-capsids near cellular membranes possibly during secondary envelopment (third column), as well as enveloped capsids in the cytoplasm (right column). Scale bars indicate 200 nm.

3.6 MCMV and MHV-68 fluorescent capsids are transmitted between cells

Next, we analyzed whether fluorescent virus particles spread from cell to cell in tissue culture. To this end NIH-3T3 cells were seeded on cover slips in 24 well plates and infected with a low MOI of either MCMV S-GFP-SCP or MHV-68 ORF65-GFP (100 PFU per 50000 cells). To prevent virus spread via the supernatant, we overlaid the infected cells with carboxymethyl-cellulose as described for standard plaque assay (81). Four days after infection, the overlay medium was removed, plaques were fixed and IF was performed. MCMV MCP was detected by a specific polyclonal antiserum and compared to S-GFP-SCP fluorescence. MHV-68 SCP was detected by a monoclonal antibody and compared to ORF65-GFP fluorescence. In addition, TO-PRO-3 (MCMV) or Hoechst33258 (MHV-68) was used to stain cell nuclei.

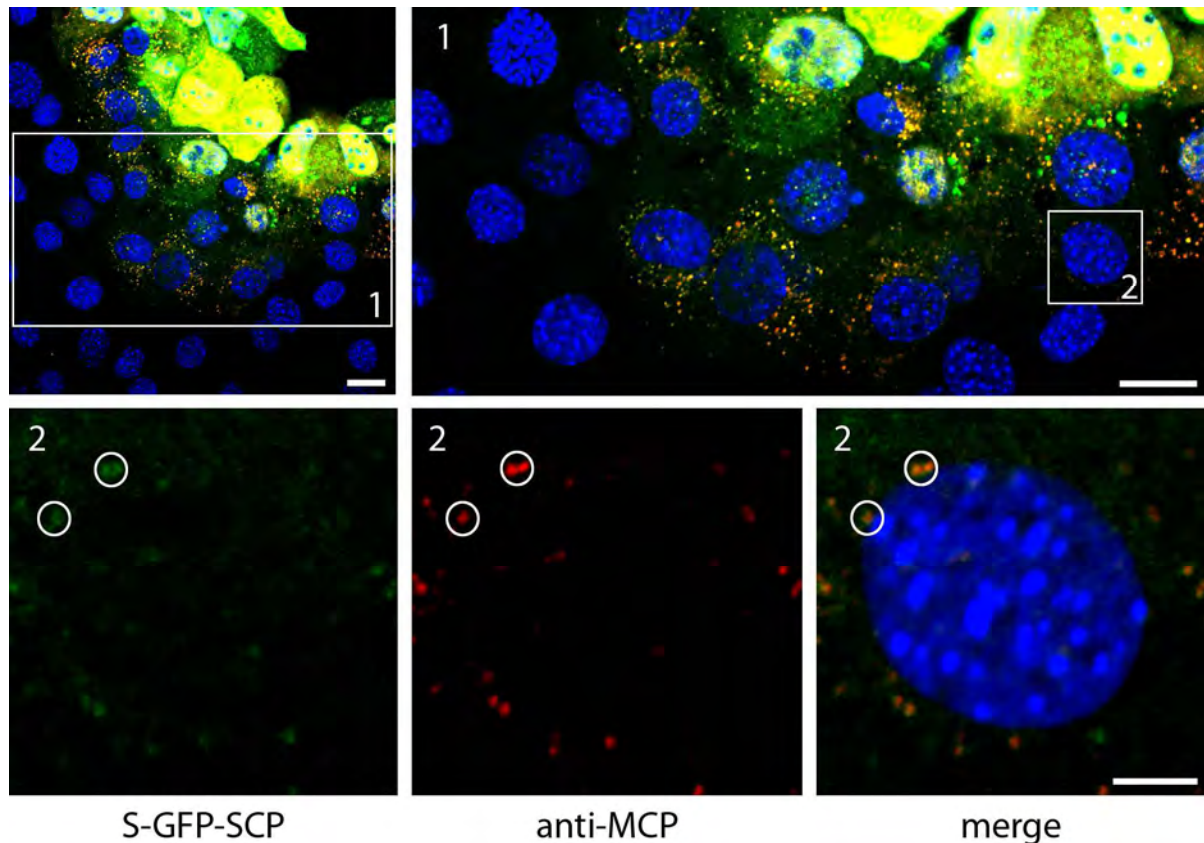


Figure 3-17: MCMV fluorescent virus particles are spread-competent.

Confluent M2-10B4 cells were infected with S-GFP-SCP labeled virus on cover-slips in 24-wells with 100 PFU per well and overlaid with methyl-cellulose. 4 dpi cells were fixed and processed for immunofluorescence. MCP-specific antiserum was used to detect virus producing cells as well as single virus particles while GFP fluorescence was visualized directly. Cell nuclei were counterstained with TO-PRO-3. Inserts depict single virus particles surrounding a cell nucleus (circles) not showing any evidence for being on the late stage of infection and producing infectious particles. Scale bars indicate 20 μm in the upper row and 5 μm in the lower row.

As shown in Figure 3-17 and Figure 3-18, cells at the center of a plaque exhibited abundant MCP stain and GFP fluorescence (yellow) inside nuclei, indicating a late infection stage. Cells at the edge of the plaque (Figure 3-17, insert 1 and Figure 3-18, insert 1), however, lacked any MCP or GFP signal in their nuclei, indicating that these cells did not started de novo synthesis of MCP, SCP or the GFP-SCP fusion proteins.

Yet, in some of these cells, we could detect fluorescent spots next to the nucleus, adjacent to the nuclear rim (Figure 3-17 insert 2 and Figure 3-18, insert 2 as well as lower rows each). These spots were positive for both GFP fluorescence and MCP or SCP stains. Therefore, we concluded that these particles were virus particles that were transported to the nucleus of freshly infected cells. This finding suggested that labeled MCMV as well as MHV-68 virions were correctly transmitted from infected to non-infected cells.

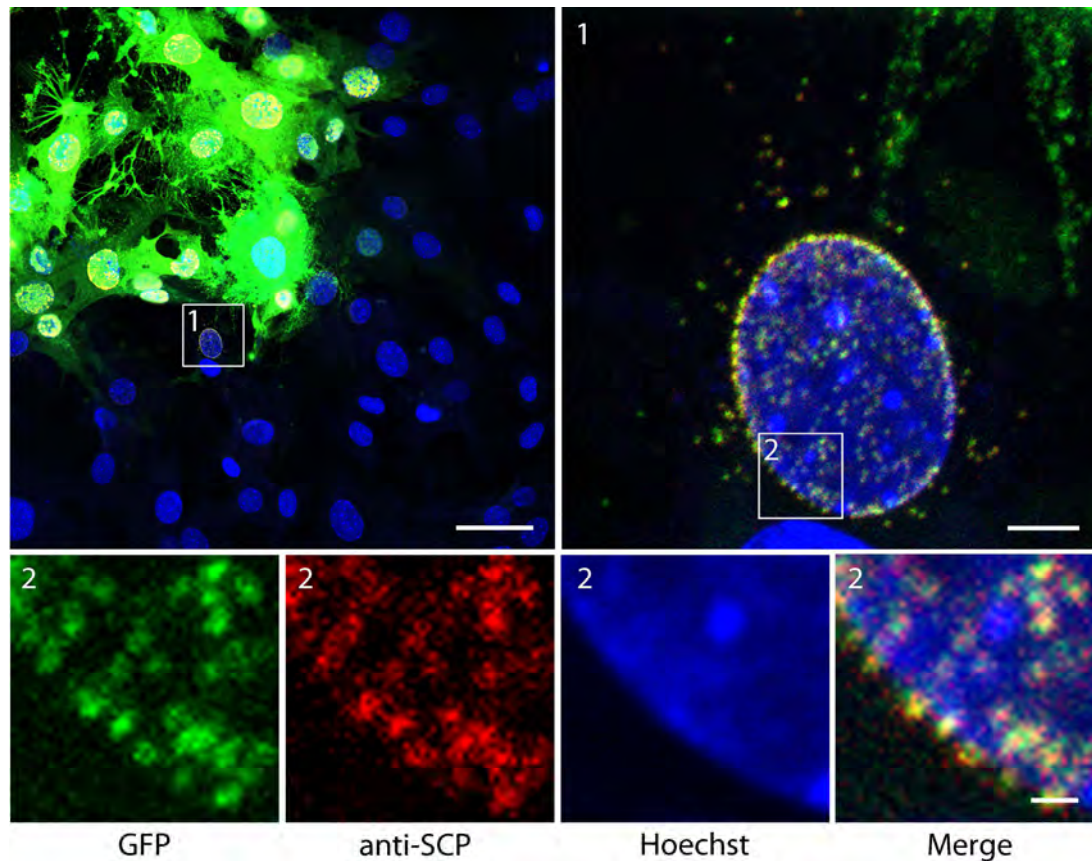


Figure 3-18: MHV-68 fluorescent particles are spread-competent

Confluent NIH-3T3 cells were infected with ORF65-GFP labeled virus in 8-well slides with 100 PFU per well and overlaid with methyl-cellulose. 4 dpi cells were fixed and processed for immunofluorescence. An SCP-specific monoclonal antibody (43) was used to detect virus producing cells as well as single virus particles while GFP fluorescence was visualized directly. Cell nuclei were counterstained with Hoechst 33258. Insert1 depicts a single nucleus surrounded by various virus particles not showing any evidence for being on the late stage of infection and producing infectious particles. Insert 2 shows a magnification with virus particles surrounding and on top of the nucleus. Scale bars indicate 50 μm in overview, 5 μm in the first magnified insert and 1 μm in the lower row.

3.7 Labeled MHV-68 particles can be visualized throughout the infection cycle

To follow the general morphogenesis of ORF-65-GFP tagged MHV-68 over time and control if the GFP fluorescence matches the capsid-incorporated SCP-distribution, we infected NIH-3T3 cells in channels with MHV-68-D2-ORF65-GFP at a MOI of 10 and incubated the cells at 4° C. Afterwards we shifted the cells to 37° C and allowed entry. Thereby, we achieved a simultaneous infection.

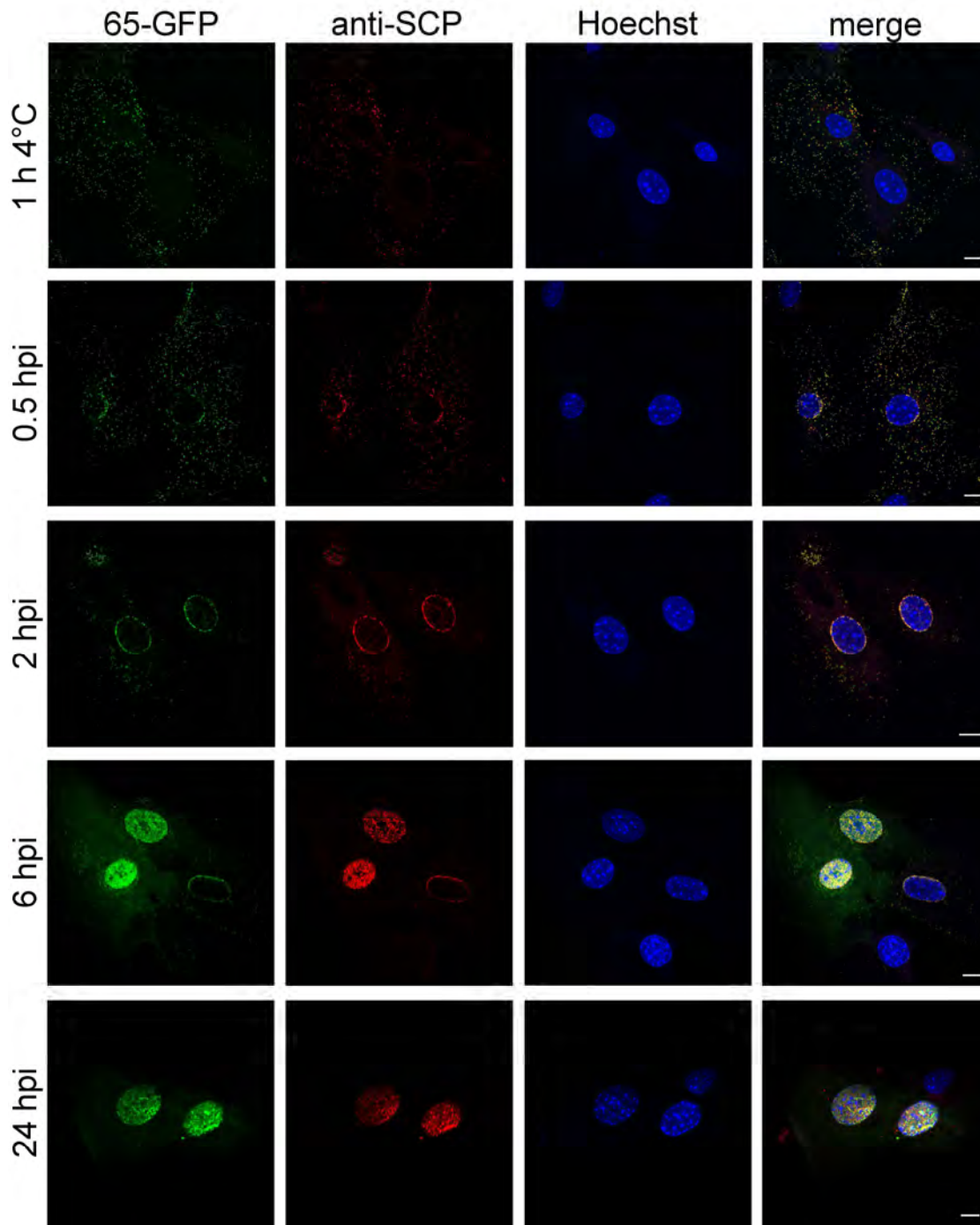


Figure 3-19: ORF65-GFP can be detected throughout the infection cycle by its fluorescence

NIH-3T3 in channels were infected at a MOI of 1 for one hour one ice, afterwards washed and shifted to 37° C. Cells were fixed 0, 0.5, 2, 6 and 24 hpi and stained with a monoclonal antibody specific for MHV-68 ORF65 and counterstained with Hoechst 33258. 0.5 hpi virus particles are translocated to the nucleus of cells. 6 hpi first signals of newly expressed ORF65 appear. Except for the cytoplasmic staining, the ORF65-GFP signal matches the anti -SCP signal. Scale bars indicate 5 μ m.

infection of the cells. Directly after shifting to 37°C or after 30 min, 2 h, 6 h or 24 h, we fixed the cells. As a control, we stained all samples with a monoclonal antibody directed against MHV-68 MCP and Hoechst 33258 to indicate nuclei. As depicted in Figure 3-19, 30 min after permitting entry, GFP-tagged virions could be visualized around the nuclei of cells. 6 hpi,

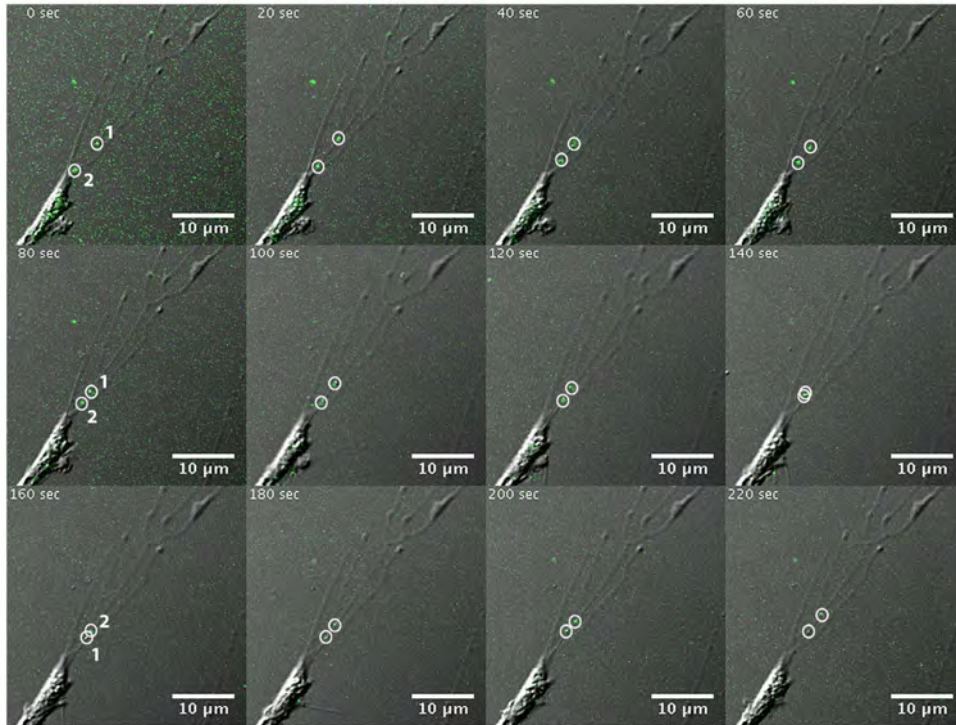
strong ORF65-GFP fluorescence could be detected, which even intensified 24 hpi. The ORF65-GFP pattern matched the anti-SCP staining except the diffuse cytoplasmic staining, 6 and 24 hpi.

3.8 Labeled MCMV capsids allow insights into beta-herpesvirus entry

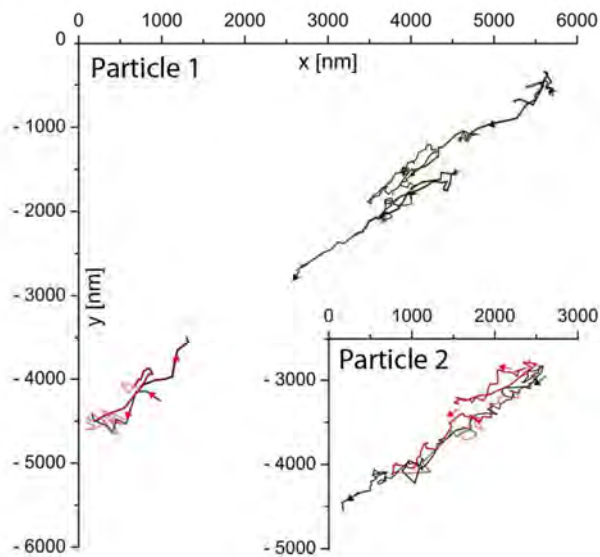
After verifying that the S-GFP-SCP recombinant had WT-like properties, we used this new virus to track MCMV-infection. To establish a particle tracking workflow, we aimed for a system with low background fluorescence and optimal imaging conditions. We therefore chose virus entry on cell protrusions, as virus particle movement is most easily observed in almost plane areas. To this end, M2-10B4 cells were seeded at low density and infected at high MOI (approx. 100 PFU/cell) with MCMV-S-GFP-SCP virus. For these experiments, all used virus stocks were gradient-purified and controlled by EM to verify the purity of viral particles. We then excited with 488 nm laser light and recorded simultaneously GFP emission as well as differential interference contrast (DIC) by confocal microscopy. By combining these two methods we could identify single virus particles with high confidence, as DIC allows, due to its high contrast, the visualization of very small objects floating in suspension while GFP fluorescence identified them as viral particles.

We observed various attachment events at cell protrusions (data not shown) and could monitor movements of several virus particles. Figure 3-20 A shows 2 particles moving on such cell protrusion. To establish a quantification workflow, we used this phenomenon and tracked selected fluorescent signals that seemed to be attached to cell protrusions. For this task we used a custom written software package(51). It determines the position of a spot by fitting a two-dimensional Gaussian curve resulting in a very high, subpixel positional accuracy (45 ± 19 nm in this experiment).

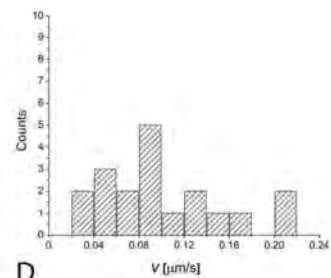
A



B



C



D

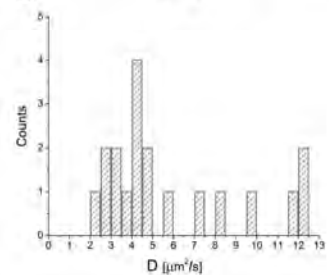


Figure 3-20: Tracing of extracellular particle trafficking.

M2-10B4 cells were seeded at low density on glass-bottomed culture dishes and infected at a MOI of 100 with gradient purified and EM-controlled S-GFP-SCP virus stock. Directly after infection, live imaging with 488 nm laser excitation as well as differential interference contrast (DIC) was started in an environmentally controlled chamber. Virus particles attached to cell protrusions were identified by their fluorescence and recorded with 1.8 frames per second. (A) The changing positions of two fluorescent particles on a cell protrusion are depicted over time (circles). Numbers indicate individual particles. (B) Tracks of particle 1 and particle 2 (insert). No positions for the particles 1 and 2 could be obtained at time points when particle tracks overlapped, therefore each particle track is divided into two parts (both black for particle 1, red and black for particle 2). The 19 manually chosen subtracks in which particles clearly showed long distance movements are indicated by color overlays. The direction of movement is indicated by arrows. (C) Histogram displaying the distribution of measured mean track velocities for all used subtracks in which particles showed long-distance movements. (D) Histogram depicting the distribution of measured diffusion coefficients for the same subtracks as in (C).

Tracking of particle dynamics was done for the whole image sequence with the exception of the area in which particle tracks overlapped at some time points and particle identity was hard to define. Therefore, each particle track was divided into two parts (Figure 3-20 B). The resulting tracks were plotted and manually split into subtracks by choosing parts in which the particles clearly exhibited long distance movement (depicted as color-overlays in Figure 3-20 B). Next, we determined the mode of motion for these subtracks. This was done by clustering them corresponding to their mode of diffusion. The mode of diffusion was determined by calculating the MSD and plotting them against the lag time. The resulting curves were then fitted according to three different diffusion models. These models were anomalous diffusion ($\text{MSD} = 4Dt^\alpha$), free diffusion ($\text{MSD} = 4Dt$) and directed motion with diffusion ($\text{MSD} = 4Dt + (vt)^2$).

We divided the tracks of the two particles into 23 subtracks. Three of these subtracks showed free diffusion, one anomalous diffusion and 19 directed motion. From the latter we could determine the overall mean track velocity v . For the two selected particles the mean track velocity of all subtracks was $0.10 \pm 0.05 \mu\text{m}/\text{sec}$ (Figure 3-20 C). Moreover, we determined the diffusion coefficient D from all subtracks. The mean of D was $5.87 \pm 3.3 \mu\text{m}^2/\text{sec}$ which indicated a high mobility (Figure 3-20 D).

3.9 Quantification of cytoplasmic movement paths in herpesvirus egress

Next, we wanted to know whether the quantification of intracellular particle movements during the late stages of infection is possible. For the following experiments, we used the mCherry-labeled MCMV variant named S-mCherry-SCP. Around 20 hpi, the first fluorescent signals emerged in nuclei of MEFs with detection parameters suitable for live-imaging (data not shown). Around 24 hpi, fluorescent spots of varying intensity could be followed in the cytoplasm. These spots most likely represented both, non-enveloped as well as enveloped viral particles, inside of vesicles. For alpha-herpesviruses, directed cytoplasmic transport of viral capsids is microtubule-dependent (61). We therefore asked if this is also true for the beta-herpesvirus MCMV. We infected MEF cells at a MOI of 0.5 with MCMV encoding the S-mCherry-SCP fusion protein and dissolved the microtubule network in control cells 23 hpi by the addition of $5 \mu\text{g}/\text{ml}$ Nocodazole for 1 h and subsequently imaged cytoplasmic fluorescent signals. An antibody stain against beta-Tubulin was used to control the effect of Nocodazole on infected cells (Figure 3-21).

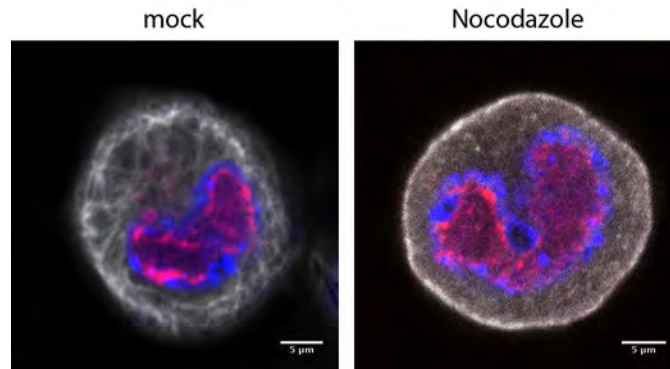


Figure 3-21: Nocodazole treatment leaves no detectable Microtubule filaments after 1 h

MEF cells were infected with MCMV-S-mCherry-SCP (red) at a MOI of 1. 23 hpi 5 µg/ml Nocodazole was added (Nocodazole) or not (mock) and cells were incubated further for 1 h. Afterwards, cells were fixed and stained for beta-Tubulin (white). Hoechst 33258 was used as nuclear counterstain. No intact Microtubule filaments are detectable after Nocodazole treatment.

The disruption of the microtubule network had a dramatic effect on the motility of cytoplasmic fluorescent spots. As shown in Figure 3-22, cytoplasmic movements of fluorescent spots basically stopped, arguing for a microtubule dependent transport of the bulk of viral particles in the cytoplasm of MCMV infected cells.

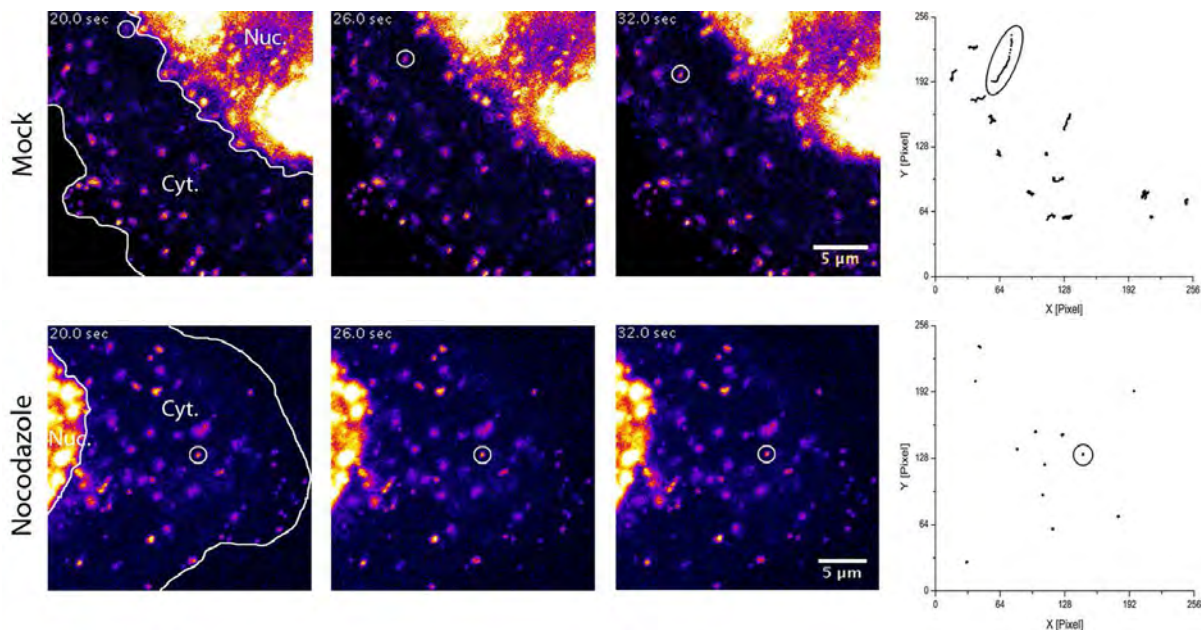


Figure 3-22: Nocodazole blocks MCMV fluorescent particle mobility.

MEF cells were infected with S-mCherry-SCP for 23 h and treated with 5 µg/ml Nocodazole for 1 h or not. S-mCherry-SCP-emission in live cells recorded under environmentally controlled conditions with 5 frames per second. Fluorescence intensity is coded in false-colors from dark blue to yellow. Three frames from a time-lapse stack each recorded 6 seconds (30 frames) apart are shown for a non-treated (upper row) and Nocodazole treated cell (lower row). Lines indicate the nucleus (Nuc.) as well as the cytoplasm (Cyt.). Circles indicate the position of a fluorescent particle. The right picture depicts all quantified tracks with ellipses marking the tracks from the particles highlighted on the left.

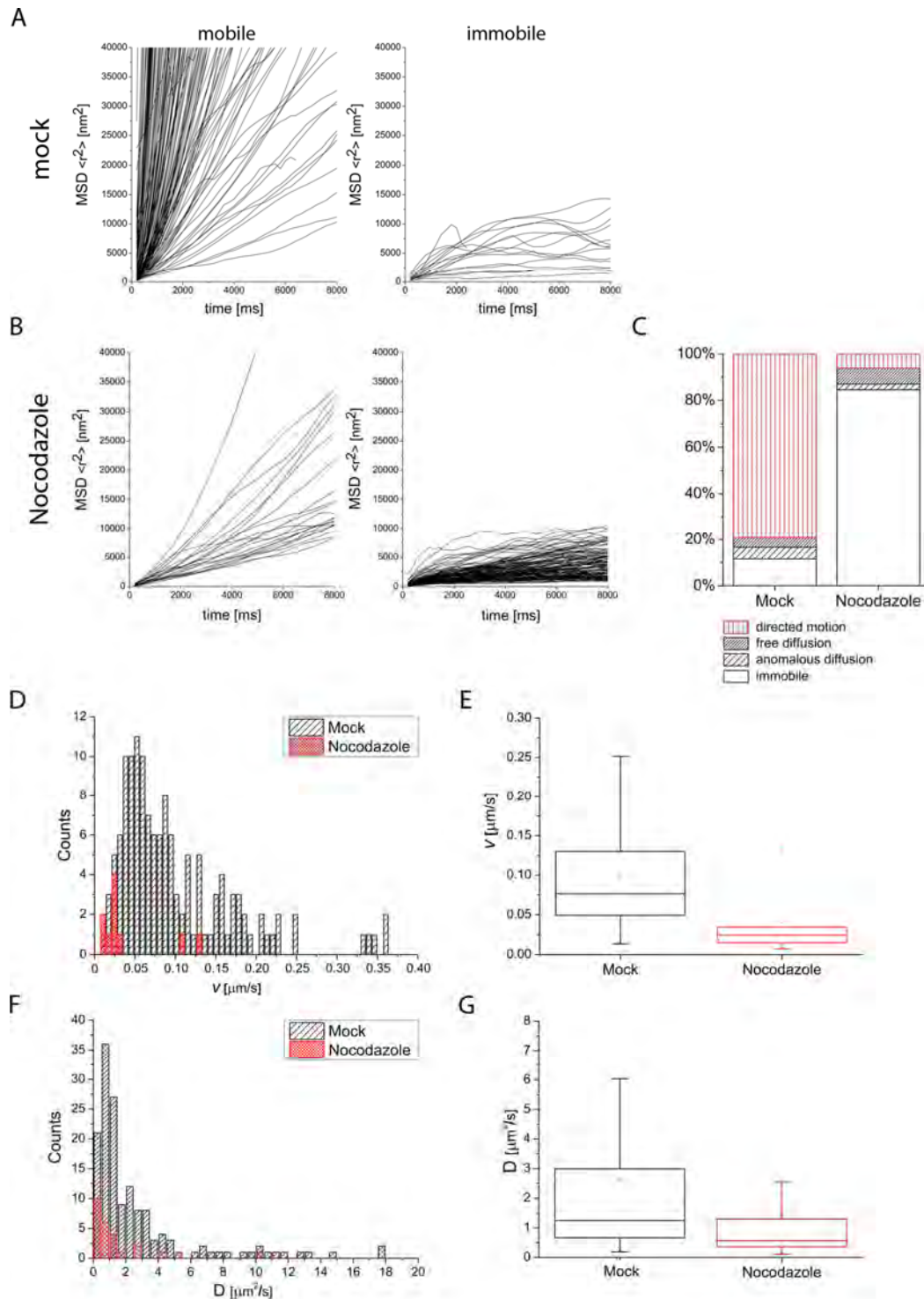


Figure 3-23: Quantification of particle tracks.

(A) 180 particles from mock treated cells were tracked and their MSDs plotted against the lag time. Particle tracks were clustered into two classes representing mobile (left diagram) and immobile particles (right diagram) depending on the MSD trend. (B) 163 tracks from Nocodazole treated cells were clustered the same way as in (A). Mobile particles were further clustered depending on which mode of diffusion they exhibited according to their fit to three different diffusion models. (C) Distribution of particle mobility classes for mock- as well as Nocodazole-treated cells depicted in percent. The data is categorized into four classes (immobile, anomalous diffusion, free diffusion, directed motion). (D) Histogram displaying the distribution of mean track velocities of all particles exhibiting directed motion. (E) The same data as in (D) summarized in a box plot with median (line) mean (square), 25th to 75th percentile (box) and whiskers (5th to 95th percentile). (F) Histogram showing the distribution of all measured diffusion coefficients. (G) Box plot of the same data shown in (F).

To quantify these cytoplasmic effects, we recorded the periphery of seven infected mock and

3 | Results

seven Nocodazole treated cells at five frames per second and subsequently tracked randomly most identifiable fluorescent particles (altogether 180 particles in mock-treated cells / 163 particles in Nocodazole-treated cells). We then calculated their MSD curves and clustered them into two classes. The first class included all mobile particles and the second all immobile particles. We discerned between these two classes by analyzing their MSD curves and taking the experimental positioning accuracy of the used tracking algorithm into account. We determined an experimental positioning error of around 30 nm per axis which translates into approximately 14.500 nm^2 in our MSD plots. All curves that did not exceed this value were classified as immobile, because their change in position during acquisition was less than the experimental localization accuracy of 30 nm per axis. In contrast, all particles that exceeded this value were classified as mobile (Figure 3-23 A, B). According to this quantification, 88.4 % of particles in mock treated cells were mobile. In contrast, 84.6 % of particles in Nocodazole treated cells were immobile. Yet, 15.4 % of the particles in Nocodazole treated cells were still mobile after 1 h incubation with 5 $\mu\text{g/ml}$ Nocodazole (Figure 3-23 C).

To analyze the properties of the mobile populations further, we fitted the corresponding MSD curves in a two-step process according to the three diffusion models described above (for details see materials and methods).

79.2 % of mobile particle tracks in mock treated cells could be fitted with the function $\text{MSD} = 4Dt + (vt)^2$ compared to 6.2 % in Nocodazole-treated cells, indicating that a small fraction of particles in Nocodazole-treated cells exhibited directed motion, hinting to a possibly Nocodazole-resistant transport mode.

Interestingly, Nocodazole treatment did not strongly influence the amount of particles diffusing freely (fit with $\text{MSD} = 4Dt$) or in an anomalous fashion (fit with $\text{MSD} = 4Dt^\alpha$) (Figure 3-23 C). Together with the strong increase of immobile particles under Nocodazole treatment, these findings might suggest that viral particles were either trapped in a very small molecular cage or fixed to some molecular anchor after Nocodazole treatment.

As we fitted the mobile fraction of particles that exhibited directed movement with $\text{MSD} = 4Dt + (vt)^2$, we could directly determine the overall mean velocity of a given particle track without its diffusion component. As shown in Figure 3-23 D, mean track velocities (over the complete acquisition time of approximately 20 sec) in mock treated cells had a mean

3 | Results

of $0.101 \pm 0.073 \mu\text{m}/\text{sec}$. In Nocodazole treated cells, however, particles that exhibited directed movement had a mean track velocity of only $0.041 \pm 0.042 \mu\text{m}/\text{sec}$. This finding indicated that high mean track velocities are based on a Nocodazole-sensitive (microtubule-associated) transport mode.

The second parameter we could determine was the diffusion coefficient D . It was calculated for all mobile particles and the median in mock-treated cells was $1.24 \cdot 10^{-8} \text{ cm}^2/\text{s}$ while $0.56 \cdot 10^{-8} \text{ cm}^2/\text{s}$ in Nocodazole-treated cells (Figure 3-23 E). Interestingly, the distribution width of D in mock treated cells was higher than expected for a monodispersed particle suspension (Figure 3-23 E). D is inversely proportional to the hydrodynamic radius of a particle, as long as all other variables like temperature and the viscosity of the medium are not changed ($D = kT/6\pi\eta r$). Therefore, the observed distribution of D could be an indicator for a wider range of tracked particle diameters and different particle types e.g. non-enveloped capsids and enveloped capsids or enveloped multi-capsid assemblies.

4 Discussion

This thesis describes the construction, characterization and first application of beta- and gamma-herpesviruses that are genetically tagged at their capsid by FPs for live cell imaging. Only the fluorescent tagging of the viral capsid allows the tracking of all steps of HV morphogenesis by fluorescence microscopy, as it is the first specific viral morphological structure made out of proteins. In contrast, approaches that utilize a tegument protein (91) or an auxiliary capsid protein added later after initial capsid assembly (15, 16) might not be able to study all steps of HV morphogenesis. That is why we decided to fluorescently tag a core capsid protein like the SCP. But in contrast to alpha-herpesvirus, all capsid proteins, including the SCP, are essential in the beta- and gamma-herpesvirus subfamilies. Therefore, a labeling strategy had to be found that either did not affect the biological properties of the target proteins at all or inevitable labeling effects had to be compensated to allow the generation of viable mutants.

The general herpesvirus capsid structure is a highly ordered and evolutionary optimized assembly with numerous protein-protein-interactions. Thus, almost every mutagenesis approach will almost certainly interfere with its function to some extent. Therefore, as applied in the case of HSV-1 (24) we also chose the SCP as a fusion partner. This small protein is positioned at the outermost of the capsid structure (Figure 4-1.) This should give maximal sterical freedom to insert a bulky fluorescent protein. Nevertheless, previous studies reported no success with exchanging the WT SCP with a simple FP-SCP fusion in beta-herpesviruses (8, 88). Moreover, even the widely used HSV-1 and PRV SCP-FP mutants were reported to be biologically impaired (52, 72) and only viable because the SCP is not essential for viral growth in these viruses. This non-essentiality of the alpha-HV SCP might be due to a different structure of the capsid hexon (Figure 4-1) (104). We therefore concluded that it might be very difficult to generate an FP-capsid fusion protein that is close to indistinguishable from the WT parent in all its multiple functions. Yet, herpesvirus capsids consist of multiples of each capsid protein with 900 copies in the case of the SCP. The phenomenon that a wt allele can compensate for a non-functional mutation present on a separate allele is well known in herpesvirus genetics. It was utilized to map temperature-sensitive mutants in the past (93) Therefore, we speculated that placing the tagged allele in addition to the WT allele into the virus genome, can result in a functional capsid.

We therefore split our approach into two steps: The first step was to engineer a FP-SCP fusion

that was not inhibitory and was as comparable to WT as possible. The second step was then to express this recombinant fusion protein from a second locus *in addition* to the WT SCP. In the resulting virus, the WT SCP fraction should complement for possible deficiencies of the FP-SCP fusion protein (cross-complementation).

To find a concept for engineering optimal FP-SCP fusions, we employed multiple sequence alignments of a wide array of related herpesviruses. We could define conserved protein regions and linker sequences in between. Such linker sequences were subsequently used to insert the FPs. In the case of MCMV, the FP was inserted by duplicating the conserved N-terminus and adding additional linker sequences. In the case of MHV-68, the FP was inserted directly into the C-terminus.

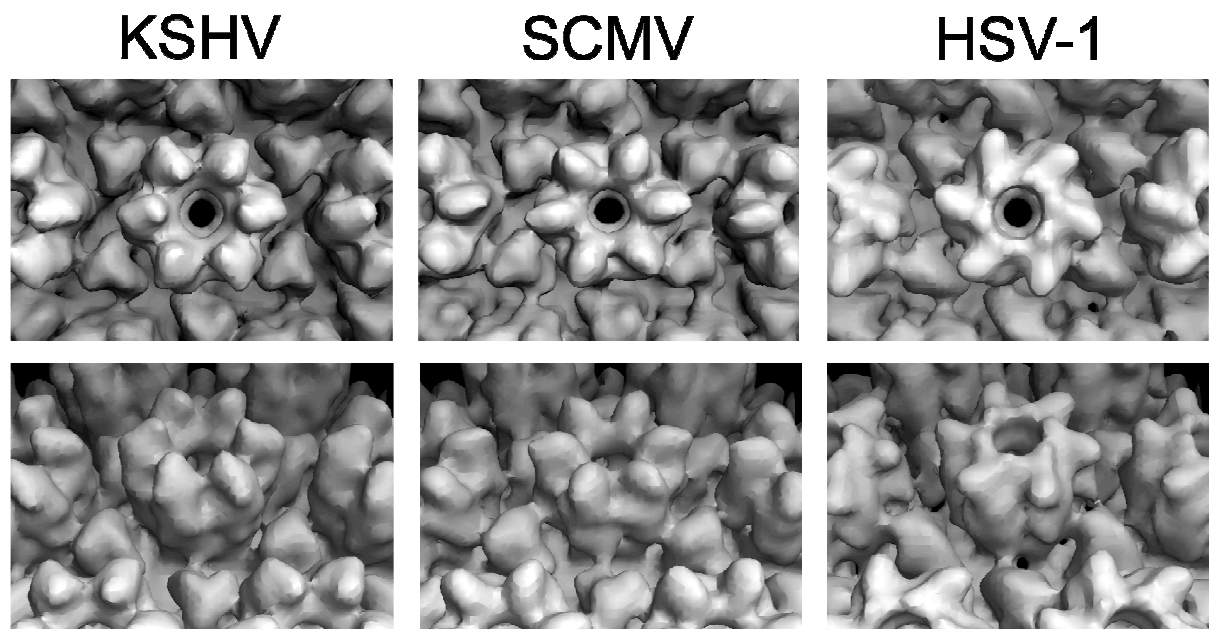


Figure 4-1: Comparison of hexon morphologies for KSHV, SCMV and HSV-1

Structures of the E-hexon (hexon on the icosahedral twofold axis) determined by cryoelectron microscopy viewed from the top and from the side. The hexon structure in KSHV and SCMV (gamma- and beta-HV) are similar, while the HSV-1 structure (alpha-HV) is different with respect to the outer chimney-like protrusions at the top of the hexons which most likely are SCP densities. (Figure adapted from (104)).

To express the FP-SCP fusion proteins *in addition* to the WT SCP, the coding sequences were inserted ectopically into the viral genomes. To this end we used the pO6-vector system (10) that allowed us to insert the expression cassettes in a quick and versatile way by Flp-mediated recombination. The FP-SCP fusion sequences were first inserted into these plasmids and put under the control of their own promoters to maintain physiological levels of expression. As all elements needed were encoded on the plasmid, simple restriction enzyme-based cloning could be used to modify the cassette. This allowed us to change FPs and whole expression cassettes

very quickly and adopt them to technical needs.

In a second step, the resulting plasmids could be transferred into the virus BACs by Flp-mediated recombination. Under these conditions, the WT locus was not touched and the mutant SCP was expressed ectopically in cis. This system has a big advantage compared to classical homologous recombination (89) typically used to modify large herpesvirus genomes. First, a high percentage of resulting clones was positive for the inserted vector. Moreover, the danger of recombinase-based reshuffling of the repetitive sequences present especially in the MHV-68 genome was strongly reduced by the use of the Flp-recombinase which catalyzes selectively the recombination between specific FRT sites.

However, this approach has also disadvantages. An ectopic insertion site is needed with a different genomic context that might lead to differences in the expression levels. Moreover, the tolerance for genome oversize varies from virus to virus. Thus compensating deletions elsewhere in the virus genome might be necessary. Also, as discussed in details later, recombination between the WT and ectopic loci can be a problem.

Altogether, this strategy resulted in the assembly of capsids that carried a mixture of approximately one third of labeled and two thirds of unlabeled SCP in the case of the MCMV-S-GFP-SCP mutant, and approximately two fifth of labeled and three fifth of non-labeled SCP in the case of the MHV-68-D2-ORF65-GFP mutant.

Proving our premise, the remaining non-labeled SCPs were important, as recombinant MCMV and MHV-68 BACs in which the endogenous SCP locus was deleted could not be reconstituted (data not shown). Interestingly the recombinant MCMV carrying S-HA-SCP was viable after a functional deletion of the native SCP locus (data not shown) arguing for tag-size dependent inhibitory effects. One explanation are sterical constraints as the bulky fluorescent protein might be perhaps too large to fit six times into a volume which can be occupied by one hexon, while a mixture of unlabeled and labeled SCPs does. Another explanation is that the labeled variant cannot engage in essential interactions with neighboring proteins. As not all molecules are needed to engage in this interaction, the unlabeled proportion of SCP molecules is needed to compensate this deficit.

The S-GFP-SCP fusion protein was incorporated into virus particles. This is most likely due

to its interaction with MCP. However, we cannot exclude that the S-FP-SCP as well as the MHV-68 SCP-GFP fusion proteins lack binding functions other than to MCP that have to be substituted by endogenous SCP. Therefore, although our mutant fusion proteins are not a substitute for WT SCP, they are not inhibitory as shown either by virus growth kinetics, plaque diameter and genome to PFU ratios. The WT-virus like properties of the new recombinant FP tagged viruses represented an important success. As in the case of MCMV the N-terminal GFP-SCP fusion constructed earlier in our laboratory showed a very strong dominant negative effect on virus growth (88). The difference between the MCMV GFP-SCP and S-GFP-SCP fusions is essentially the duplication of the first 34 aa that are added to the N-terminus of the fluorescent protein. These 34 aa might apparently engage in important interactions or provide additional flexibility that discerns the S-GFP-SCP fusion from its dominant negative ancestor gfp-SCP.

Further examination of the S-GFP-SCP recombinant virus showed that this virus was genetically stable for at least ten passages, supporting the notion that the S-GFP-SCP fusion did not inhibit virus growth as attenuating features often favor compensatory sequence alterations.

In the case of MHV-68 expressing SCP-GFP we noticed slightly reduced growth kinetics compared to the MHV-68-D2 parent but not compared to WT MHV-68. During passaging we found the occurrence of non-fluorescent plaques which reoccurred after purifying fluorescent virus by the limiting dilution. Sequencing of the ectopic locus gave evidence for the loss of GFP tagged SCP over time. Most likely this is due to recombination of the large homologues ORF65 promoter and coding sequences flanking the inserted FP with the WT-locus of another MHV-68 genome during replication. This would lead to one genome having two copies of tagged SCP while the other would have two WT SCP copies. As WT SCP is needed for replication, the double-labeled genome would not grow, while the other would. This hypothesis was underlined by a MHV-68 SCP-knockout mutant with an additional SCP-GFP in the ectopic locus. Here, the WT ORF65 locus as well as the promoter region could not be removed completely due to overlapping ORFs. This mutant almost did not grow at the beginning but then reverted to normal growth. As it showed fluorescence it was not a WT contamination. Sequencing as well as immunoblotting confirmed the reestablishment of the WT locus in this passaged mutant (data not shown). Therefore, recombination between the remaining ORF65 sequences and the ectopic locus must have occurred. Hence it seems as if recombination between the ectopic locus and the WT locus regularly occurred in MHV-68 but

not in MCMV. Herpesviruses are known for their strong recombinogenic potential, a fact that was used for decades to generate mutants before the advent of BAC technology. Therefore, in future studies the ectopic MHV-68 SCP-FP site should contain a synthetic, codon altered, SCP coding sequence. This way, recombination and loss of the fluorescent virus should become less frequent.

Moreover, it is possible, that MHV-68 has a lower tolerance for genome oversize than MCMV. As only the M1 gene (1598 bp) is deleted in the parental MHV-68-D2 genome, insertion of the pOTO-ORF65-FP vectors lead to an approximate genome oversize of 1653 bp. This might reduce the viability of genomes carrying the ORF65-FP cassettes and favor the replication of genomes carrying adoptive mutations.

When we checked for phenotypic changes in the ultrastructure of MCMV S-GFP-SCP infected cells, we could not find obvious morphological differences except for some cells that showed parachrySTALLINE arrays in a late stage of infection which seemed to be B-capsids. Notably, this phenomenon is also described for HSV-1 carrying an mRFP-tagged SCP as well as for WT HSV-1 infection (22, 74).

The quantification MCMV and MHV-68 capsid labeling intensity as well as the proportion of labeled particles revealed that most particles are labeled to an extent that permitted particle tracking. Interestingly, labeled MHV-68 particles appeared to be much brighter than MCMV S-GFP-SCP particles. Moreover, immunoblotting indicated a possible decrease in the expression of WT-SCP compared to FP-labeled SCP. Also, only one major form of FP-labeled MHV-68 could be found while labeled MCMV expressed different isoforms that were incorporated into virions. Taken together, these factors argue for a superiority of the MHV-68 mutant in some applications, where brightness is an issue. However, genetic stability of the MHV-68 mutants remains an issue.

Altogether the results of the characterization of our MCMV as well as MHV-68 mutants stressed the importance of a thorough quantification of the generated mutants. In the case of HSV- and PRV capsid labeled mutants this was initially not carried out (24, 99). Later studies (52, 72) revealed that labeling of the SCP in these viruses had the same effect on the growth kinetics as the deletion of the respective gene. As it is not completely known which additional functions the SCP has in alpha-herpesviruses, an ectopic labeling strategy might be preferable also in these viruses to compensate possible functional artifacts due to the lack of the WT

protein. Moreover, other capsid proteins like the MCP might be considered as alternative fusion partners. However, due to its size and different conformational structures in pentons or hexons, an appropriate insertion site is hard to predict. A random insertion approach could be a solution. The random mutagenesis approach published earlier by this group might be a basis (10, 58).

To test if our new recombinant viruses could be used for SPT, we tested purified virus preparations of MCMV S-GFP-SCP in an assay for cell entry and detected particle attachment to cell protrusions and trafficking along those. We were able to establish a tracking workflow with few particles that resulted in a very accurate localization of single virus particles (45 ± 19 nm) with high temporal resolution over extended time frames. Compared to recently published data for retroviruses (56) and also HSV-1 (26, 75) where also FP-labeled viruses were used, our data was acquired with 1.8 frames/sec., which is 17 to 53 times faster than in the studies mentioned above. These two factors together gave us the possibility to track particle movements with much higher accuracy. Moreover, by fitting the resulting MSD curves we could determine the overall mean track velocity separately from the diffusion coefficient D . Thereby, we found that the tracked particles showed iterations of directed movement, likely due to an active transport mechanism as recently described for retroviruses (56) and also HSV-1 (26, 75). In contrast to data described there, we were able to resolve the iteration of periods of directed motion and obstructed diffusion by manual track segmentation as well as its associated fluctuations in velocities with much higher spatial precision and temporal resolution. We found a mean track velocity of 0.10 ± 0.06 $\mu\text{m}/\text{sec}$ for the measured tracks which is three to four fold higher than reported in other other studies (0.025 $\mu\text{m}/\text{sec}$ - 0.033 $\mu\text{m}/\text{sec}$ (56, 75). Yet, the small number of experiments only shows the feasibility of the approach. To pin down the exact transport mechanism in the future, more extensive studies are needed with a considerably larger sampling to thoroughly quantify extracellular transport of MCMV as it was recently done for chemically labeled papillomavirus (94).

Tracking extracellular viral particles provides a favorable environment with low background and low particle densities. Particle movement in the cytoplasm during virus egress, however, happens in an environment characterized by high background noise, high particle counts and a reduced cell cross section due to virus induced cell rounding. We tracked particles shortly after they first appeared in the cytoplasm and tracked their motility. As negative-control we used infected cells treated with the microtubule depolymerizing drug Nocodazole. By using a

fitting approach we could cluster the obtained particle tracks into four classes representing immobile particles and mobile particles exhibiting either anomalous diffusion, free diffusion or directed motion. We found that almost 80 % of particles showed a diffusive behavior indicative of directed transport. Nocodazole treatment reduced the fraction of mobile particles drastically. This effect was mainly due to the reduction of particles exhibiting directed motion (79 % to 6 %), while the proportion of particles exhibiting free or anomalous diffusion did not change strongly. This was anticipated as it was shown before that viral cytoplasmic transport is mainly microtubule-mediated. However, it was surprising that the dissociation of microtubules by Nocodazole did not increase the proportion of free or anomalous diffusing particles (4.4% to 6.8% and 5.2 % to 2.5 % respectively). This finding might indicate that particles are still bound to microtubule fragments after Nocodazole treatment as the tracking data indicated a very large proportion of particles that did not move more than the localization precision of 30 nm (classified as immobile). Yet, other mechanisms for immobilization of capsids, such as entrapment in a molecular cage or fixation to a molecular anchor, are also possible.

The second surprising finding was that still around 6 % of particle tracks from Nocodazole-treated cells could be fitted according to a directed motion model. Two explanations seem plausible. First, the remaining movement upon treatment with Nocodazole may be caused by the presence of stabilized Nocodazole resistant microtubules, similar to those which have been described for HSV-1 infections (31). Alternatively, the observed Nocodazole-resistant movement is based on actin filaments, a hypothesis that is underlined by the recent report describing the dependence of HSV-1 virion secretion on Myosin V (84) as well as by a comparable study using a tagged tegument protein (60). However, to specifically address these questions, future experiments are needed.

Notably, instead of a focused distribution of the diffusion coefficient as anticipated for a monodisperse solution of particles we found a wider distribution of D . Assuming a uniform cytoplasmic viscosity this finding would translate into a non-uniform distribution of vesicle sizes used by the virus to transport particles. As we could observe a great difference in vesicle sizes containing virus particles in transmission EM (Fig. 3-16 and data not shown) this interpretation fits to the observed phenotype. Moreover, it demonstrates the power of single-particle tracking to probe the environmental conditions of the measured particles without the need of co-labeling.

We calculated mean track velocities from particle tracks which could be fitted according to a model for directed movement. Notably, these mean track velocities were much smaller than what is reported for HCMV (91). This might have several reasons apart from intrinsic differences between HCMV and MCMV: First, we randomly accepted all particles that were technically possible to track. We did not select for mobile particles. Therefore, our mean step velocities must be smaller as more slowly moving particles were included. In addition, we used a different tracking and calculation approach. The mean track velocities used here display the mean velocity a given particle exhibits over the whole measured track. As we did neither select for fast transport processes during tracking nor used track segmentation as in Figure 3-20, again our mean track velocities had to be smaller than velocities from selected (sub-) tracks. The approach taken here should therefore be closer to approximate a realistic mean transport velocity with which cytoplasmic herpes particles are transported over longer time spans.

Up to now, we did not quantify the cytoplasmic motility of MHV-68 capsids. Future studies are aimed at it. Moreover, the combination of the herein described capsids-tagged mutants with additional glycoprotein-FP fusions will enable the discrimination between enveloped and non-enveloped particles and thus will add more accuracy to the quantification. By including a membrane-tag it will also be possible to correlate the obtained diffusion coefficients to different particles from e.g. capsids and enveloped capsids. Also, future studies might include the direction of transport to produce a more detailed picture of cytoplasmic transport processes during herpes egress.

Having solved the capsid tagging problem, also tagged tegument proteins might be employed to generate viruses labeled at the capsid, the tegument and the envelope as it was done for HSV (22, 72, 103). Altogether, these mutants can be now used to analyze the functions of viral and cellular proteins in virus morphogenesis. Especially the combination with different deletions of viral proteins might be of great interest to analyze their role in capsid transport.

Perhaps the MHV-68 SCP-FP mutants can be applied in *in vivo* studies, as the used MHV-68-D2 is only deleted in the M1 gene. This gene is not essential for lytic replication nor latency establishment in B-lymphocytes until 40 dpi (pers. comm. A. Vidy). The MCMV S-GFP-SCP cassette, however, would have to be transferred to another backbone, as the MCMV- Δ 1-16

virus poorly replicates *in vivo*. The ectopic expression cassette can be easily transferred by Flp-mediated recombination, and suitable non-attenuated viruses with enough coding space and an FRT site are reported (11, 53, 90). Thus, *in vivo* imaging of MCMV seems possible. Moreover, due to the modular architecture of the expression cassette, viruses expressing specialized fluorescent proteins for two-photon-imaging like mPlum (97) can also be generated rapidly.

Altogether, by solving the capsid labeling problem we were able to generate the first viable recombinant beta- and gamma-herpesviruses that produce fluorescently labeled capsids. In comparison to the widely used HSV-1 and PRV capsid-tagged mutants (52, 72) the here described MCMV recombinant did not show any growth defect in cell culture and exhibited biological features comparable to their parental WT virus. All tested recombinants produced fluorescent virus capsids with an intensity sufficient to track single particles over extended periods in live cell microscopy. This allowed us to establish protocols to study the dynamics of beta-herpesvirus entry on cell protrusions for the first time. In addition, protocols for the analysis of intracellular particle transport during MCMV egress, for the first time with subpixel-spatial- and high temporal- resolution in the herpesvirus field, enabled us to characterize the cytoplasmic transport of a beta-herpesvirus with high detail.

In summary, the results described in this study will enable the comparative study of alpha-, beta- and gamma-virus capsid dynamics. Especially, conserved nuclear transport processes of HV capsids will be of great interest in future studies.

5 Primer Sequences

Table 1

Primer	Sequence ^{a,b}
MCMV-for	ATCATCCGTTGCATCTCGTTG
MCMV-rev	CGCCATCTGTATCCGTCCAT
M54-as	[FAM]-AACGTACATCGCTCTCTGCTGGCCG-6-carboxytetramethylrhodamine [TAMRA]
SCPPfor	GTGT <u>GATATCG</u> TGCTGCTGCGCGAGTCATCC
SCPPrev	GTGTCTTAAGACTAGTGGCGTAGTCGGGCACGTCGTAGGGGTAGCTGCTG CCGCCGCTTCTCC
SP- <i>Afl</i> III-FP- <i>Bsr</i> GI	GTGACTCTTAAGGCCACCATGGTGAGCAAGGGCGAGGA
ASP- <i>Afl</i> III-FP- <i>Bsr</i> GI	CACAGTTGTACAGCTCGTCCATGCCGCCGGTGG
SP-MCP-binding-negative	ATCGTG <u>CAGCTG</u> GACCTTTAAGACACACATACAGAAAAATAAA
ASP-MCP-binding-negative	AGTCACGGGCCCACATGTGCGAGGCC
attB1-S-GFP-SCP-attB2-SP	GGGGACAAGTTTGTACAAAAAAGCAGGCTTACTAGCTCTCTCTACTTTA
attB1-S-GFP-SCP-binding- neg-No-Stop-attB2-ASP	GGGGACCACTTTGTACAAGAAAGCTGGGTAAAGGTCCAGCTGGTAGGCG AG
Delta M1 for	TCGGGGGAGTCCAGGGTTTTCCCTAAGTATTACTGTTGGGATATCGCGCC CACCTTTATTGTAAGGG
Delta M1 rev	CATTCTGAGTGGCACGAGAATTATTTGCATGTGTGTGAGCAGCCTTCCGG CTCGTATGTTGTGTGG
ORF65for	GTGACTAATATTGAGAAACAGTTTAACATATG
ORF65rev	CACAGTTGATCAGCGAGCTCCTACTTTTCTTTCCATTTC
EGFP65for	GTGACTAGGCCCTGTGGTACGGACTGGGCGTGAGCAAGGGCGAGGAGCTG
EGFP65rev	CACTGAAGGGCCCCCCTTGTACAGCTCGTCCATGCC
mCherry65for	GTGACTAGCGCTGTGGTACGGACTGGGCGTGAGCAAGGGCGAGGAGGA
mCherry65rev	CACAGTGGGCCCCCCTTGTACAGCTCGTCCATGC

^a Underlined nucleotides: cleavage sites for restriction enzymes

^b Italic nucleotides: protein tags

6 List of Abbreviations

aa	amino acid
AIHV1	alcelaphine herpesvirus 1
AP	assembly protein
BAC	bacterial artificial chromosome
BHK	baby hamster kidney cells
BSA	bovine serum albumine
CCD	charged coupled device
CLSM	confocal laser scanning microscope
CPE	cytopathic effect
DBPS	Dulbecco's phosphate-buffered saline
DIC	differential interference contrast
dpi	days post infection
E	early
EBV	Epstein-Barr virus
EHV-1	equine herpesvirus 1
EM	electron microscopy
FCS	fluorescence correlation spectroscopy
FP	fluorescent protein
FRAP	fluorescence after photobleaching
GFP	green fluorescent protein
HA	hemagglutinin
HCMV	human cytomegalovirus
HHV-6	human herpesvirus 6
HHV-7	human herpesvirus 7
hpi	hours post infection
HSV-1	herpes simplex virus 1
HSV-2	herpes simplex virus 2
HV	herpesvirus
IE	immediate early
IF	immuno fluorescence
KSHV	Kaposi-sarcoma associated virus
L	late
MCMV	murine cytomegalovirus
MCP	major capsid protein
MEF	murine embryonic fibroblasts
MOI	multiplicity of infection
MSD	mean square displacement
NA	numerical aperture
ND10	nuclear domain 10
NLS	nuclear localization signal
ORF	open reading frame
OvHV1	ovine herpesvirus 1

PCR	polymerase chain reaction
PFA	paraformaldehyde
PFU	plaque forming units
PORT	portal protein
POX	peroxidase
PR	maturation protease
PRV	pseudorabies virus
PTLD	posttransplant associated lymphoid disease
SCP	small capsid protein
SDS	sodium dodecyl-sulfate
SPT	single particle tracking
TBS-T	TRIS-buffered saline with Tween
TRI1	triplex monomer 1
TRI2	triplex monomer 2
VZV	varicella zoster virus
Y2H	yeast two hybrid

7 References

1. **Abramoff, M. D., P. J. Magelhaes, and S. J. Ram.** 2004. Image Processing with ImageJ. *Biophotonics International* **11**:36-42.
2. **Adler, H., M. Messerle, M. Wagner, and U. H. Koszinowski.** 2000. Cloning and mutagenesis of the murine gammaherpesvirus 68 genome as an infectious bacterial artificial chromosome. *J Virol* **74**:6964-6974.
3. **Antinone, S. E., and G. A. Smith.** 2010. Retrograde Axon Transport of Herpes Simplex Virus and Pseudorabies Virus: a Live-Cell Comparative Analysis. *Journal of Virology* **84**:1504-1512.
4. **Baker, M. L., W. Jiang, F. J. Rixon, and W. Chiu.** 2005. Common Ancestry of Herpesviruses and Tailed DNA Bacteriophages. *Journal of Virology* **79**:14967-14970.
5. **Barylko, B., G. Jung, and J. P. Albanesi.** 2005. Structure, function, and regulation of myosin 1C. *Acta Biochim Pol* **52**:373-380.
6. **Blaskovic, D., M. Stancekova, J. Svobodova, and J. Mistrikova.** 1980. Isolation of five strains of herpesviruses from two species of free living small rodents. *Acta Virologica* **24**:468.
7. **Borst, E. M., G. Hahn, U. H. Koszinowski, and M. Messerle.** 1999. Cloning of the human cytomegalovirus (HCMV) genome as an infectious bacterial artificial chromosome in *Escherichia coli*: a new approach for construction of HCMV mutants. *J Virol* **73**:8320-8329.
8. **Borst, E. M., S. Mathys, M. Wagner, W. Muranyi, and M. Messerle.** 2001. Genetic evidence of an essential role for cytomegalovirus small capsid protein in viral growth. *Journal of Virology* **75**:1450-1458.
9. **Bubeck, A., M. Wagner, Z. Ruzsics, M. Lotzerich, M. Iglesias, I. R. Singh, and U. H. Koszinowski.** 2004. Comprehensive mutational analysis of a herpesvirus gene in the viral genome context reveals a region essential for virus replication. *Journal of Virology* **78**:8026-8035.
10. **Bubeck, A., M. Wagner, Z. Ruzsics, M. Lötzerich, M. Iglesias, I. R. Singh, and U. H. Koszinowski.** 2004. Comprehensive mutational analysis of a herpesvirus gene in the viral genome context reveals a region essential for virus replication. *J Virol* **78**:8026-8035.
11. **Bubić, I., M. Wagner, A. Krmpotić, T. Saulig, S. Kim, W. M. Yokoyama, S. Jonjić, and U. H. Koszinowski.** 2004. Gain of virulence caused by loss of a gene in murine cytomegalovirus. *J Virol* **78**:7536-7544.
12. **Buser, C., P. Walther, T. Mertens, and D. Michel.** 2007. Cytomegalovirus Primary Envelopment Occurs at Large Infoldings of the Inner Nuclear Membrane. *Journal of Virology* **81**:3042-3048.
13. **Chalfie, M., Y. Tu, G. Euskirchen, W. W. Ward, and D. C. Prasher.** 1994. Green fluorescent protein as a marker for gene expression. *Science* **263**:802-805.
14. **Chaudhuri, V., M. Sommer, J. Rajamani, L. Zerboni, and A. M. Arvin.** 2008. Functions of Varicella-zoster virus ORF23 capsid protein in viral replication and the pathogenesis of skin infection. *J Virol* **82**:10231-10246.
15. **Cockrell, S. K., J. B. Huffman, K. Toropova, J. F. Conway, and F. L. Homa.** 2011. Residues of the UL25 Protein of Herpes Simplex Virus That Are Required for Its Stable Interaction with Capsids. *Journal of Virology* **85**:4875-4887.

16. **Conway, J. F., S. K. Cockrell, A. M. Copeland, W. W. Newcomb, J. C. Brown, and F. L. Homa.** 2010. Labeling and Localization of the Herpes Simplex Virus Capsid Protein UL25 and Its Interaction with the Two Triplexes Closest to the Penton. *Journal of Molecular Biology* **397**:575-586.
17. **Coons, A.** 1961. The beginnings of immunofluorescence. *J Immunol* **87**:499-503.
18. **Coons, A. H., H. Creech, R. Jones, and E. Berliner.** 1942. The demonstration of pneumococcal antigen in tissues by the use of fluorescent antibody. *Journal Of Immunology* **45**:159-170.
19. **Das, S. C., D. Nayak, Y. Zhou, and A. K. Pattnaik.** 2006. Visualization of Intracellular Transport of Vesicular Stomatitis Virus Nucleocapsids in Living Cells. *J Virol* **80**:6368-6377.
20. **Datsenko, K. A., and B. L. Wanner.** 2000. One-step inactivation of chromosomal genes in *Escherichia coli* K-12 using PCR products. *Proceedings of the National Academy of Sciences of the United States of America* **97**:6640-6645.
21. **Davison, A. J., R. Eberle, B. Ehlers, G. S. Hayward, D. J. McGeoch, A. C. Minson, P. E. Pellett, B. Roizman, M. J. Studdert, and E. Thiry.** 2009. The order Herpesvirales. *Arch Virol* **154**:171-177.
22. **de Oliveira, A. P., D. L. Glauser, A. S. Laimbacher, R. Strasser, E. M. Schraner, P. Wild, U. Ziegler, X. O. Breakefield, M. Ackermann, and C. Fraefel.** 2008. Live visualization of herpes simplex virus type 1 compartment dynamics. *Journal of Virology* **82**:4974-4990.
23. **Desai, P., N. A. DeLuca, and S. Person.** 1998. Herpes simplex virus type 1 VP26 is not essential for replication in cell culture but influences production of infectious virus in the nervous system of infected mice. *Virology* **247**:115-124.
24. **Desai, P., and S. Person.** 1998. Incorporation of the green fluorescent protein into the herpes simplex virus type 1 capsid. *Journal of Virology* **72**:7563-7568.
25. **Diaspro, A.** 2010. *Nanoscopy and multidimensional optical fluorescence microscopy.* CRC Press/Taylor & Francis Group, Boca Raton.
26. **Dixit, R., V. Tiwari, and D. Shukla.** 2008. Herpes simplex virus type 1 induces filopodia in differentiated P19 neural cells to facilitate viral spread. *Neuroscience letters* **440**:113-118.
27. **Dohner, K.** 2006. Eclipse Phase of Herpes Simplex Virus Type 1 Infection: Efficient Dynein-Mediated Capsid Transport without the Small Capsid Protein VP26. *J Virol* **80**:8211-8224.
28. **Dolan, A., C. Cunningham, R. D. Hector, A. F. Hassan-Walker, L. Lee, C. Addison, D. J. Dargan, D. J. McGeoch, D. Gatherer, V. C. Emery, P. D. Griffiths, C. Sinzger, B. P. McSharry, G. W. G. Wilkinson, and A. J. Davison.** 2004. Genetic content of wild-type human cytomegalovirus. *J Gen Virol* **85**:1301-1312.
29. **Donnelly, M., and G. Elliott.** 2001. Fluorescent Tagging of Herpes Simplex Virus Tegument Protein VP13/14 in Virus Infection. *Journal of Virology* **75**:2575-2583.
30. **Drew, W. L.** 1992. Nonpulmonary manifestations of cytomegalovirus infection in immunocompromised patients. *Clinical microbiology reviews* **5**:204-210.
31. **Elliott, G., and P. O' Hare.** 1998. Herpes Simplex Virus Type 1 Tegument Protein VP22 Induces the Stabilization and Hyperacetylation of Microtubules. *Journal of Virology* **72**:6448.
32. **Endress, T., M. Lampe, J. a. G. Briggs, H.-G. Kräusslich, C. Bräuchle, B. Müller, and D. C. Lamb.** 2008. HIV-1-cellular interactions analyzed by single virus tracing. *European biophysics journal : EBJ* **37**:1291-1301.
33. **Feierbach, B., S. Piccinotti, M. Bisher, W. Denk, and L. W. Enquist.** 2006. Alpha-Herpesvirus Infection Induces the Formation of Nuclear Actin Filaments. *PLoS Pathog* **2**:e85.

34. **Finke, S., K. Brzózka, and K.-K. Conzelmann.** 2004. Tracking fluorescence-labeled rabies virus: enhanced green fluorescent protein-tagged phosphoprotein P supports virus gene expression and formation of infectious particles. *J Virol* **78**:12333-12343.
35. **Flach, B., B. Steer, N. N. Thakur, J. Haas, and H. Adler.** 2009. The M10 Locus of Murine Gammaherpesvirus 68 Contributes to both the Lytic and the Latent Phases of Infection. *J Virol* **83**:8163-8172.
36. **Forest, T., S. Barnard, and J. D. Baines.** 2005. Active intranuclear movement of herpesvirus capsids. *Nature cell biology* **7**:429-431.
37. **Fossum, E., C. C. Friedel, S. V. Rajagopala, B. Titz, A. Baiker, T. Schmidt, T. Kraus, T. Stellberger, C. Rutenberg, S. Suthram, S. Bandyopadhyay, D. Rose, A. von Brunn, M. Uhlmann, C. Zeretzke, Y.-A. Dong, H. Boulet, M. Koegl, S. M. Bailer, U. Koszinowski, T. Ideker, P. Uetz, R. Zimmer, and J. Haas.** 2009. Evolutionarily conserved herpesviral protein interaction networks. *PLoS pathogens* **5**:e1000570.
38. **Frampton, A. R., H. Uchida, J. von Einem, W. F. Goins, P. Grandi, J. B. Cohen, N. Osterrieder, and J. C. Glorioso.** 2010. Equine herpesvirus type 1 (EHV-1) utilizes microtubules, dynein, and ROCK1 to productively infect cells. *Vet Microbiol* **141**:12-21.
39. **François, S., S. Vidick, M. Sarlet, J. Michaux, P. Koteja, D. Desmecht, P. G. Stevenson, A. Vanderplassen, and L. Gillet.** 2010. Comparative study of murid gammaherpesvirus 4 infection in mice and in a natural host, bank voles. *The Journal of general virology* **91**:2553-2563.
40. **Fred, E. B.** 1933. Antony van Leeuwenhoek: On the Three-hundredth Anniversary of his Birth. *J Bacteriol* **25**:iv.2-18.
41. **Geada, M. M., I. Galindo, M. M. Lorenzo, B. Perdiguero, and R. Blasco.** 2001. Movements of vaccinia virus intracellular enveloped virions with GFP tagged to the F13L envelope protein. *J Gen Virol* **82**:2747-2760.
42. **Gill, M. B., R. Edgar, J. S. May, and P. G. Stevenson.** 2008. A gamma-herpesvirus glycoprotein complex manipulates actin to promote viral spread. *PloS one* **3**:e1808.
43. **Gillet, L., M. B. Gill, S. Colaco, C. M. Smith, and P. G. Stevenson.** 2006. Murine gammaherpesvirus-68 glycoprotein B presents a difficult neutralization target to monoclonal antibodies derived from infected mice. *J Gen Virol* **87**:3515-3527.
44. **Glotzer, J. B., A. I. Michou, A. Baker, M. Saltik, and M. Cotten.** 2001. Microtubule-Independent Motility and Nuclear Targeting of Adenoviruses with Fluorescently Labeled Genomes. *Journal of Virology* **75**:2421-2434.
45. **Gram, H.** 1884. Über die isolierte Färbung der Schizomyceten in Schnitt- und Trockenpräparaten. *Fortschritte der Medizin* **2**:185-189.
46. **Grosse, S. D., D. S. Ross, and S. C. Dollard.** 2008. Congenital cytomegalovirus (CMV) infection as a cause of permanent bilateral hearing loss: a quantitative assessment. *Journal of clinical virology : the official publication of the Pan American Society for Clinical Virology* **41**:57-62.
47. **Hazelton, P. R., and H. R. Gelderblom.** 2003. Electron microscopy for rapid diagnosis of infectious agents in emergent situations. *Emerging infectious diseases* **9**:294-303.
48. **Henson, B. W., E. M. Perkins, J. E. Cothran, and P. Desai.** 2009. Self-Assembly of Epstein-Barr Virus Capsids *J Virol* **83**:3877-3890.
49. **Jung, C.** 2007. Single Molecule Traffic in Mesoporous Materials and New Photostable Water-Soluble Terrylenediimide Derivatives. Dissertation. LMU Munich, Munich.
50. **Kalejta, R. F.** 2008. Tegument Proteins of Human Cytomegalovirus. *Microbiology and Molecular Biology Reviews* **72**:249-265.

51. **Kirstein, J., C. Jung, and C. Hellriegel.** 2005. Single Molecule Spectroscopy: Translational and Rotational Diffusion of Single Fluorescent Dyes in Nano-Structured Porous Materials. *Diffusion Fundamentals*:94.91-94.92.
52. **Krautwald, M., C. Maresch, B. G. Klupp, W. Fuchs, and T. C. Mettenleiter.** 2008. Deletion or green fluorescent protein tagging of the pUL35 capsid component of pseudorabies virus impairs virus replication in cell culture and neuroinvasion in mice. *The Journal of general virology* **89**:1346-1351.
53. **Kulesza, C. A., and T. Shenk.** 2006. Murine cytomegalovirus encodes a stable intron that facilitates persistent replication in the mouse. *Proceedings of the National Academy of Sciences of the United States of America* **103**:18302-18307.
54. **Lai, L., and W. J. Britt.** 2003. The interaction between the major capsid protein and the smallest capsid protein of human cytomegalovirus is dependent on two linear sequences in the smallest capsid protein. *J Virol* **77**:2730-2735.
55. **Lampe, M., J. a. G. Briggs, T. Endress, B. Glass, S. Riegelsberger, H.-G. Kräusslich, D. C. Lamb, C. Bräuchle, and B. Müller.** 2007. Double-labelled HIV-1 particles for study of virus-cell interaction. *Virology* **360**:92-104.
56. **Lehmann, M. J., N. M. Sherer, C. B. Marks, M. Pypaert, and W. Mothes.** 2005. Actin- and myosin-driven movement of viruses along filopodia precedes their entry into cells. *J Cell Biol* **170**:317-325.
57. **Lichtman, J. W., and J.-A. Conchello.** 2005. Fluorescence microscopy. *Nature Methods* **2**:910-919.
58. **Lötzerich, M., Z. Ruzsics, and U. H. Koszinowski.** 2006. Functional domains of murine cytomegalovirus nuclear egress protein M53/p38. *J Virol* **80**:73-84.
59. **Lux, K., N. Goerlitz, S. Schlemminger, L. Perabo, D. Goldnau, J. Endell, K. Leike, D. M. Kofler, S. Finke, M. Hallek, and H. Büning.** 2005. Green fluorescent protein-tagged adeno-associated virus particles allow the study of cytosolic and nuclear trafficking. *J Virol* **79**:11776-11787.
60. **Luxton, G. W. G., J. I.-H. Lee, S. Haverlock-Moyns, J. M. Schober, and G. A. Smith.** 2006. The pseudorabies virus VP1/2 tegument protein is required for intracellular capsid transport. *J Virol* **80**:201-209.
61. **Lyman, M. G., and L. W. Enquist.** 2008. Herpesvirus Interactions with the Host Cytoskeleton. *J Virol* **83**:2058-2066.
62. **Maninger, S., J. B. Bosse, F. Lemnitzer, M. Pogoda, C. A. Mohr, J. Von Einem, P. Walther, U. H. Koszinowski, and Z. Ruzsics.** 2011. M94 is essential for the secondary envelopment of murine cytomegalovirus. *Journal of Virology*.
63. **Maurer, U. E., B. Sodeik, and K. Grünewald.** 2008. Native 3D intermediates of membrane fusion in herpes simplex virus 1 entry. *Proc Natl Acad Sci USA* **105**:10559-10564.
64. **McGeoch, D. J., F. J. Rixon, and A. J. Davison.** 2006. Topics in herpesvirus genomics and evolution. *Virus research* **117**:90-104.
65. **Menard, C., M. Wagner, Z. Ruzsics, K. Holak, W. Brune, A. E. Campbell, and U. H. Koszinowski.** 2003. Role of murine cytomegalovirus US22 gene family members in replication in macrophages. *J Virol* **77**:5557-5570.
66. **Messerle, M., I. Crnković, W. Hammerschmidt, H. Ziegler, and U. H. Koszinowski.** 1997. Cloning and mutagenesis of a herpesvirus genome as an infectious bacterial artificial chromosome. *Proc Natl Acad Sci USA* **94**:14759-14763.
67. **Mettenleiter, T. C., B. G. Klupp, and H. Granzow.** 2009. Herpesvirus assembly: an update. *Virus research* **143**:222-234.
68. **Mocarski, E.** 2007. Chapter 1, Human Herpesviruses: Biology, Therapy, and Immunoprophylaxis, 1st ed. Cambridge University Press, Cambridge.

69. **Monier, K., J. C. Armas, S. Etteldorf, P. Ghazal, and K. F. Sullivan.** 2000. Annexation of the interchromosomal space during viral infection. *Nat Cell Biol* **2**:661-665.
70. **Muranyi, W., J. Haas, M. Wagner, G. Krohne, and U. H. Koszinowski.** 2002. Cytomegalovirus recruitment of cellular kinases to dissolve the nuclear lamina. *Science* **297**:854-857.
71. **Murphy, D. B.** 2001. *Fundamentals of light microscopy and electronic imaging.* Wiley-Liss, New York.
72. **Nagel, C.-H., K. Dohner, M. Fathollahy, T. Strive, E. M. Borst, M. Messerle, and B. Sodeik.** 2008. Nuclear Egress and Envelopment of Herpes Simplex Virus Capsids Analyzed with Dual-Color Fluorescence HSV1(17+). *J Virol* **82**:3109-3124.
73. **Nash, A. A., B. M. Dutia, J. P. Stewart, A. J. Davison, P. Trans, and R. S. Lond.** 2001. Natural history of murine gamma-herpesvirus infection. *Philosophical transactions of the Royal Society of London. Series B, Biological sciences* **356**:569-579.
74. **Nil, S., C. Morgan, and H. M. Rose.** 1968. Electron Microscopy of Herpes Simplex Virus II . Sequence of Development. *Microbiology* **2**:517-536.
75. **Oh, M.-J., J. Akhtar, P. Desai, and D. Shukla.** 2010. A role for heparan sulfate in viral surfing. *Biochemical and biophysical research communications* **391**:176-181.
76. **Pellet, P., and B. Roizman.** 2006. The Family Herpesviridae: A Brief Introduction. *In* D. M. Knipe, P. M. Howley, and D. M. Griffin (ed.), *Fields Virology*, 5th ed, vol. 5. Lippincott Williams & Wilkins.
77. **Pemberton, L. F., and B. M. Paschal.** 2005. Mechanisms of Receptor-Mediated Nuclear Import and Nuclear Export. *Traffic* **6**:187-198.
78. **Perkins, E. M., D. Anacker, A. Davis, V. Sankar, R. F. Ambinder, and P. Desai.** 2008. Small capsid protein pORF65 is essential for assembly of Kaposi's sarcoma-associated herpesvirus capsids. *Journal of Virology* **82**:7201-7211.
79. **Potel, C., K. Kaelin, I. Gautier, P. Lebon, J. Coppey, and F. Rozenberg.** 2002. Incorporation of green fluorescent protein into the essential envelope glycoprotein B of herpes simplex virus type 1. *Journal of Virological Methods* **105**:13-23.
80. **Radtke, K., K. Döhner, and B. Sodeik.** 2006. Viral interactions with the cytoskeleton: a hitchhikers guide to the cell. *Cell Microbiol* **8**:387-400.
81. **Reddehase, M. J., F. Weiland, K. Münch, S. Jonjić, A. Luske, and U. H. Koszinowski.** 1985. Interstitial murine cytomegalovirus pneumonia after irradiation: characterization of cells that limit viral replication during established infection of the lungs. *Journal of Virology* **55**:264-273.
82. **Rieder, M., K. Brzozka, C. K. Pfaller, J. H. Cox, L. Stitz, and K. K. Conzelmann.** 2010. Genetic Dissection of Interferon-Antagonistic Functions of Rabies Virus Phosphoprotein: Inhibition of Interferon Regulatory Factor 3 Activation Is Important for Pathogenicity. *Journal of Virology* **85**:842-852.
83. **Rietdorf, J., A. Ploubidou, I. Reckmann, A. Holmström, F. Frischknecht, M. Zettl, T. Zimmermann, and M. Way.** 2001. Kinesin-dependent movement on microtubules precedes actin-based motility of vaccinia virus. *Nat Cell Biol* **3**:992-1000.
84. **Roberts, K. L., and J. D. Baines.** 2010. Myosin Va enhances secretion of herpes simplex virus 1 virions and cell surface expression of viral glycoproteins. *J Virol.*
85. **Robinson, J. P.** 2001. Principles of confocal microscopy. *Methods Cell Biol* **63**:89-106.
86. **Roizman, B., D. M. Knipe, and W. Richard.** 2006. Herpes Simplex Viruses. *In* D. M. Knipe, P. M. Howley, and D. M. Griffin (ed.), *Fields Virology*, vol. 5. Lippincott Williams & Wilkins.

87. **Rost, F. W. D.** 1995. 18 - The history of fluorescence microscopy, p. 473, Fluorescence microscopy. Cambridge Univ Pr.
88. **Rupp, B., Z. Ruzsics, T. Sacher, and U. H. Koszinowski.** 2005. Conditional cytomegalovirus replication in vitro and in vivo. *J Virol* **79**:486-494.
89. **Ruzsics, Z., and U. H. Koszinowski.** 2008. Mutagenesis of the cytomegalovirus genome. *Current topics in microbiology and immunology* **325**:41-61.
90. **Sacher, T., J. Podlech, C. A. Mohr, S. Jordan, Z. Ruzsics, M. J. Reddehase, and U. H. Koszinowski.** 2008. The major virus-producing cell type during murine cytomegalovirus infection, the hepatocyte, is not the source of virus dissemination in the host. *Cell host & microbe* **3**:263-272.
91. **Sampaio, K. L., Y. Cavignac, Y.-D. Stierhof, and C. Sinzger.** 2005. Human cytomegalovirus labeled with green fluorescent protein for live analysis of intracellular particle movements. *J Virol* **79**:2754-2767.
92. **Saxton, M. J., and K. Jacobson.** 1997. Single-particle tracking: applications to membrane dynamics. *Annual review of biophysics and biomolecular structure* **26**:373-399.
93. **Schaffer, P. A.** 1975. Temperature-sensitive mutants of herpesviruses. *Current topics in microbiology and immunology* **70**:51-100.
94. **Schelhaas, M., H. Ewers, M.-L. Rajamäki, P. M. Day, J. T. Schiller, and A. Helenius.** 2008. Human papillomavirus type 16 entry: retrograde cell surface transport along actin-rich protrusions. *PLoS pathogens* **4**:e1000148.
95. **Scrivano, L., J. Esterlechner, H. Mühlbach, N. Ettischer, C. Hagen, K. Grünewald, C. A. Mohr, Z. Ruzsics, U. Koszinowski, and B. Adler.** 2010. The m74 gene product of murine cytomegalovirus (MCMV) is a functional homolog of human CMV gO and determines the entry pathway of MCMV. *Journal of Virology* **84**:4469-4480.
96. **Shaner, N., P. Steinbach, and R. Y. Tsien.** 2005. A guide to choosing fluorescent proteins. *Nat Methods* **2**:905-909.
97. **Shaner, N. C., R. E. Campbell, P. A. Steinbach, B. N. G. Giepmans, A. E. Palmer, and R. Y. Tsien.** 2004. Improved monomeric red, orange and yellow fluorescent proteins derived from *Discosoma* sp. red fluorescent protein. *Nat Biotechnol* **22**:1567-1572.
98. **Shimomura, O., F. H. Johnson, and Y. Saiga.** 1962. Extraction, purification and properties of aequorin, a bioluminescent protein from the luminous hydromedusan, *Aequorea*. *Journal of cellular and comparative physiology* **59**:223-239.
99. **Smith, G. A., S. P. Gross, and L. W. Enquist.** 2001. Herpesviruses use bidirectional fast-axonal transport to spread in sensory neurons. *Proc Natl Acad Sci USA* **98**:3466-3470.
100. **Sodeik, B.** 2000. Mechanisms of viral transport in the cytoplasm. *Trends in microbiology* **8**:465-472.
101. **Steer, B., B. Adler, S. Jonjić, J. P. Stewart, and H. Adler.** 2010. A gammaherpesvirus complement regulatory protein promotes initiation of infection by activation of protein kinase Akt/PKB. *PloS one* **5**:e11672.
102. **Stellberger, T., R. Häuser, A. Baiker, V. R. Pothineni, J. Haas, and P. Uetz.** 2010. Improving the yeast two-hybrid system with permuted fusions proteins: the Varicella Zoster Virus interactome. *Proteome science* **8**:8.
103. **Sugimoto, K., M. Uema, H. Sagara, M. Tanaka, T. Sata, Y. Hashimoto, and Y. Kawaguchi.** 2008. Simultaneous Tracking of Capsid, Tegument and Envelope Protein Localization in Living Cells Infected with Triple Fluorescent Herpes Simplex Virus 1. *J Virol*.

104. **Trus, B. L., J. B. Heymann, K. Nealon, N. Cheng, W. W. Newcomb, J. C. Brown, D. H. Kedes, and A. C. Steven.** 2001. Capsid structure of Kaposi sarcoma-associated herpesvirus, a gammaherpesvirus, compared to those of an alphaherpesvirus, herpes simplex virus type 1, and a betaherpesvirus, cytomegalovirus. *J Virol* **75**:2879-2890.
105. **Tsien, R. Y.** 1998. The green fluorescent protein. *Annu Rev Biochem* **67**:509-544.
106. **Valeur, B., and M. r. N. Berberan-Santos.** 2011. A Brief History of Fluorescence and Phosphorescence before the Emergence of Quantum Theory. *Journal of Chemical Education* **88**:731-738.
107. **Walther, P., and A. Ziegler.** 2002. Freeze substitution of high-pressure frozen samples: the visibility of biological membranes is improved when the substitution medium contains water. *Journal of microscopy* **208**:3-10.
108. **Ward, B. M., and B. Moss.** 2001. Visualization of Intracellular Movement of Vaccinia Virus Virions Containing a Green Fluorescent Protein-B5R Membrane Protein Chimera. *Journal of Virology* **75**:4802.
109. **Wu, T.-T., H.-I. Liao, L. Tong, R. S. Leang, G. Smith, and R. Sun.** 2011. Construction and characterization of an infectious murine gammaherpesvirus-68 bacterial artificial chromosome. *Journal of biomedicine & biotechnology* **2011**:926258.
110. **Yang, F., L. G. Moss, and G. N. Phillips.** 1996. The molecular structure of green fluorescent protein. *Nature biotechnology* **14**:1246-1251.
111. **Yu, X., S. Shah, I. Atanasov, P. Lo, F. Liu, W. J. Britt, and Z. H. Zhou.** 2005. Three-dimensional localization of the smallest capsid protein in the human cytomegalovirus capsid. *J Virol* **79**:1327-1332.

8 List of Figures and Tables

Figure 1-1: Conjugated field planes in a simple compound microscope	2
Figure 1-2: Rayleigh criterion for spatial resolution.....	3
Figure 1-3: Physics of fluorescence	4
Figure 1-4: Molecular structure of wildtype GFP	5
Figure 1-5: Basic beam path in a fluorescence microscope	6
Figure 1-6: Basic features of widefield and confocal fluorescence microscopes	7
Figure 1-7: Schematic drawing of a live imaging setup.....	8
Figure 1-8: Herpesvirus Particle.....	12
Figure 1-9: General herpesvirus lifecycle	14
Figure 3-1: Alignment of beta-herpesvirus SCPs sequences	33
Figure 3-2: Construction of MCMV S-FP-SCP fusion proteins.....	34
Figure 3-3: Plaque-phenotype of tagged MCMV mutants.....	35
Figure 3-4: Tagged MCMV mutants are viable.....	36
Figure 3-5 Alignment of gamma-herpesvirus SCP sequences with ClustalW (REF).....	37
Figure 3-6: Construction of MHV-68 ORF65-FP fusion proteins.....	38
Figure 3-7: Plaque phenotype of GFP-tagged MHV-68 mutant.....	39
Figure 3-8: Tagged MHV-68 mutants are viable.....	40
Figure 3-9: S-GFP-SCP produces a high percentage of labeled virus particles.....	41
Figure 3-10: ORF-65-GFP labeled MHV-68 produces a high percentage of GFP labeled virus particles.....	42
Figure 3-11: GFP-labeled SCP is incorporated into MCMV S-GFP-SCP virus particles.....	43
Figure 3-12: GFP-labeled SCP is incorporated into MHV-68 virus particles	44
Figure 3-13: S-GFP-SCP nuclear transport is MCP dependent.....	45
Figure 3-14: Viruses carrying labeled SCP mutants are genetically stable.....	47
Figure 3-15: Capsid-tagged MHV-68 mutants express only one ORF-65-FP isoform.....	48
Figure 3-16: Ultrastructural assessment of S-GFP-SCP infected cells.....	50
Figure 3-17: MCMV fluorescent virus particles are spread-competent.....	51
Figure 3-18: MHV-68 fluorescent particles are spread-competent.....	52
Figure 3-19: ORF65-GFP can be detected throughout the infection cycle by its fluorescence.....	53
Figure 3-20: Tracing of extracellular particle trafficking.....	55
Figure 3-21: Nocodazole treatment leaves no detectable Microtubule filaments after 1 h.....	57
Figure 3-22: Nocodazole blocks MCMV fluorescent particle mobility.....	57
Figure 3-23: Quantification of particle tracks.....	58
Figure 4-1: Comparison of hexon morphologies for KSHV, SCMV and HSV-1	62

9 Danksagung

Allen voran gilt mein Dank Herrn Prof. Dr. Dr. Ulrich Koszinowski für dieses Projekt. Insbesondere möchte ich mich dafür bedanken, dass er mich mit allen seinen Kräften gefordert, gefördert und großzügig unterstützt hat.

Dr. Zsolt Ruzsics, alias „Mr. Vector NTI“, möchte ich für seine immerwährende Unterstützung vom ersten Moment an danken. Ohne ihn wäre diese Arbeit sicher nicht entstanden.

Weiterhin möchte ich mich bei allen meinen Kollegen bedanken, allen voran Lisa Marcinowski, Bernd Rädle und Martina Rieder, die das „Harmonie-Labor“ a.k.a. „Elba“ zur bestbeschallten „Labor-Insel“ im ganzen Genzentrum gemacht haben.

Allen meinen jetzigen und früheren Kollegen möchte ich ganz herzlich für die viele Hilfe danken. Besonders Lisa Marcinowski für ihre Hilfe bei quantitativer PCR, Sigrid Seelmeier und Simone Boos für die tolle technische Unterstützung und Frederik Lemnitzer für viele interessante Diskussionen und Hilfe bei den Gradientenaufreinigungen.

Auch bei den „Conzelmännern“ möchte ich mich für die schöne Zeit bedanken. Martina für die Western-Blot Unterstützung in letzter Minute, Laetitia für den französischen Flair und natürlich allen zusammen für die generelle Einsicht, dass RNA-Viren gar nicht „so langweilig“ sind.

Ein ganz großer Dank gilt meinen vielen tollen, selbständigen PraktikantInnen. Thomas Riffelmacher, der das erste getaggte MHV-68 kloniert hat, Leonhard Popilka, der mir bei der Etablierung des cytoplasmatischen Trackings eine große Hilfe war, Jessica Steinbacher, die sich an exotischen Myosinen fast die Zähne ausgebissen hätte und Christian Albig, der mir geholfen hat, die MHV-68 Mutanten zu charakterisieren.

Ganz besonders möchte ich mich auch bei allen unseren Kooperationspartnern bedanken, ohne die kein einziger Schritt dieser Arbeit möglich gewesen wäre:

Dr. Harald Wodrich für seine ansteckende Begeisterung für die Wissenschaft, für stundenlange Mikroskopierabende und einen tollen Monat in Bordeaux.

Prof. Dr. Heiko Adler für seine Hilfe und Unterstützung im MHV-68 Projekt und viele anregende Diskussionen. Durch seine Konstruktion des MHV-68 BACs bin ich auf das Koszinowski-Labor aufmerksam geworden.

Dr. Jens von Einem, Prof. Dr. Paul Walther, Eberhard Schmid sowie Prof. Thomas Mertens für mehr als drei Monate in Ulm, in denen ich wahnsinnig viel gelernt habe, und auch für aufbauende Worte, wenn nach der Hochdruck-Gefrierung von den Saphir-Plättchen mal nicht viel übrig blieb und das mCherry-spezifische Serum.

Dr. Rudolf Bauerfeind und Prof. Dr. Beate Sodeik für zwei sehr, sehr schöne und produktive Wochen in Hannover, in denen ich das Live-Imaging lernen konnte und viele interessante Diskussionen.

Dr. Christophe Jung, Martina Täglich und Prof. Dr. Ulrike Gaul möchte ich für die geduldige Einführung in das Single Particle Tracking, das zur Verfügung-stellen der Tracking-Software und umfangreiche Hilfe bei Auswertungen in letzter Minute danken.

Dr. Philip Stevenson for the kind gift of capsid-specific antibodies.

Der Studienstiftung des deutschen Volkes danke ich für die großzügige finanzielle und ideelle Förderung.

Zu guter Letzt möchte ich meiner Familie danken:

Meinen Großeltern, die die Fertigstellung dieser Arbeit leider nicht mehr erleben konnten und besonders meinem Opa, der mich immer so unterstützt hat.

Den besten Eltern der Welt, die immer an mich glauben und die mir so viel Kraft gegeben haben.

Meinem „kleinen“ Bruder, der in Japan „Ersatzteile verkauft“. Du bist der Beste!

Meiner Frau Kerstin, die mir das größte Geschenk der Welt gemacht hat.

10 Curriculum Vitae

Personal Data

Full name: Jens-Bernhard Bosse (born as Jens-Bernhard Lösing)
Date of birth: 22.09.1981
Place of birth: Vreden, NRW, Germany
Citizenship: German

Education

PhD program in Virology

LMU Munich; 01/2008 – 08/2011
Title: Herpesvirus Capsid Dynamics in Living Cells.
Laboratory of Prof. Dr. Dr. Ulrich Koszinowski.

Master of Science in Biotechnology

RWTH Aachen; 10/2005 - 01/2008
Thesis title: Molecular characterization of the Epstein-Barr virus encoded gene BDLF2.
Laboratory of Prof. Dr. Klaus Ritter.

Bachelor of Science in Biotechnology

RWTH Aachen; 10/2002 - 06/2005
Thesis title: Relevance of the Epstein-Barr virus encoded gene BDLF2 for the expression of important genes of the lytic cycle and viral latency.
Laboratory of Prof. Dr. Klaus Ritter.

Additional Extracurricular Studies in Medicine

RWTH Aachen; 10/2005-07/2007
Medical Physiology, Biology, Cell Biology, Physics and Medical Terminology

High School Diploma (German Abitur)

Gymnasium Georgianum Vreden; 06/2001

International Research Experience

Internship at the Division of Virology, University of Cambridge, UK

10/2006 - 04/2007

Title: Immune Evasion of persistent herpes viruses.

Laboratory of Dr. Philip Stevenson

Honors and Awards

Studentship awarded by the German National Academic Foundation

03/2009 - present

Studentship granted for the course of graduation

Studentship awarded by the German National Academic Foundation

11/2006 - 12/2007

Studentship granted during the Masters program.

Visiting scholar of the Heinrich-Hertz Foundation

10/2006 - 04/2007

Laboratory of Dr. Philip Stevenson, University of Cambridge, UK

Society Memberships

German Society for Virology (GfV)

Poster Presentations at scientific meetings

Meeting of the European Society of Virology 2010 in Como/Italy.

Oral Presentations at Scientific Meetings

Annual Meeting of the German Society for Virology (GfV) in 2008/2009/2011

Cell Biology of Viral Infections, 2009 in Deidesheim/Germany

Mini-Herpes Workshop 2009 in Berlin/Germany

Beta-herpesvirus satellite workshop at the IHW in 2009/2011

International Herpes Workshop (IHW) 2010 in Salt Lake City/USA

Publications

For an updated list go to: <http://www.researcherid.com/rid/D-7336-2011>

Maninger S.*, Bosse J.B.*, Lemnitzer F., Pogoda M., Mohr C., von Einem J., Walther P., Koszinowski U., Ruzsics Z., 2011

M94 is essential for secondary envelopment of murine cytomegalovirus.
Journal of Virology

Loesing J.B.*, Di Fiore S.*, Ritter K., Fischer R., Kleines M., 2009
Epstein-Barr virus BDLF2-BMRF2 complex affects cellular morphology.
Journal of General Virology

Gaspar M., Gill M.B., Lösing J.B., May J.S., Stevenson P.G., 2008.
Multiple functions for ORF75c in Murid Herpesvirus-4 infection.
Plos One

*contributed equally